9-2010

Structure-property Evolution During Polymer Crystallization

Deepak Arora
University of Massachusetts Amherst, deepakarora04@gmail.com

STRUCTURE-PROPERTY EVOLUTION DURING POLYMER CRYSTALLIZATION

A Dissertation Presented

by

DEEPAK ARORA

Submitted to the Graduate School of the
University of Massachusetts Amherst in partial fulfillment
of the requirements for the degree of

DOCTOR OF PHILOSOPHY

September 2010

Polymer Science and Engineering

STRUCTURE-PROPERTY EVOLUTION DURING POLYMER CRYSTALLIZATION

A Dissertation Presented

by

DEEPAK ARORA

Approved as to style and content by:

_____
H. Henning Winter, Chair

_____
Alfred J. Crosby, Member

_____
Jonathan P. Rothstein, Member

_____
David A. Hoagland, Department Head
Polymer Science and Engineering

DEDICATION

To my Grandpa and my middle school principal Mrs. Parveen Khanna who taught me that the goals are important and the approach, towards them, is even more important.

&

To my Mom and Dad who taught me patience and handling tough times.

ACKNOWLEDGMENTS

First and foremost, I am thankful to my research advisor Professor Henning Winter. Today I consider myself a well balanced scientist who is capable of imagining wild while keeping in touch with the reality solely due to the training I had with him. He provided me with the opportunities to interact with a diverse group of researchers in form of conferences, workshops, industry funded projects and the mentoring projects that made me an independent scholar and a careful researcher. He taught me to be fearless while asking questions. The Gordon Research Conferences that I attended with him possibly opened up few more memory slots in my brain due to the combination of scrumptious food and indulging science. His significant other-half Mrs. Karen Winter made sure that we get a few breaks from research while still being around Henning. Those breaks which were full of delicious cooking introduced me to a whole new side of yogurt, see figure A. Thank you very much Henning for all the shaping. I proudly carry the signatures that you have left.

Figure A: (left) Raspberries in the backyard of Henning's beach house in RI, (right) same raspberries on a crisp waffle with yogurt in between

I am grateful to Professor Al Crosby and Professor Jonathan Rothstein. The organizational skills of Professor Crosby along with his teaching style always inspired me

to perform and those are the traits I am going to adhere to. I was fortunate enough to have a few courses with him. Professor Rothstein has been an inspiring researcher and a mentor, and his composure is admirable.

Thank you very much professor Alan Lesser, Professor Gido, Professor Bryan Coughlin, Professor Hsu, Professor Emrick, Professor Dicks Stein and Professor Alex for the recommendations and suggestions.

I am thankful to Professor Jim Capistran for all the guidance for a successful debut to the industrial world.

I am also thankful to Professor Patrick Mather from Syracuse University. The discussion that I had with him during the SoR conference in Maine proved to be very valuable.

Thanks a lot Souvik! Your suggestions and active help from cradle to grave were invaluable. Consistent composure is what I learn from you.

I appreciate all the assistance from Alyssa, Sekar, Andre, Maria, Greg, Lisa, Vivien, Ramla, Susan, Lulu, Joe, Don, John and all the PSE and Chemical Engineering staff. Thanks a lot, Lisa and Vivien, I would have never managed to keep track of the requirements for my Ph.D. without your support.

Thanks a lot Gary for helping me out with fixing machines in the lab and out of the lab. I have learnt to look for simple solutions and tricks from you.

I am indebted to my middle school principal Mrs. Parveen Khanna for molding my career during the early stages. Next time when you see me, I will be a refined construction with a solid foundation that was rendered by you.

My cultural roots make me hesitant thanking my family, since it is taken as a gesture of detachment in a closely knitted family, I belong to. I stood where I am due to all the resilience and values that I gained early on. Thank you Baba (Grandpa), Amma (Grandma), Daddy, Mummy, Bade Uncle, Badi Aunti, Chote Uncle, Chote Aunti, Santosh Didi and Bharat Jiju, Sangee and Babbal, Sonu and Bhabhi, Hema and Manoj, Sanju, Babbi and Vishal, Jyoti, Jitu, Vicky, Ilu, Raja, Dheeraj, Babali and Bhabhi, My Mamoos and Mamis, especially Sacchu Mama, Raju Mama and Alka Mami, Johny, Rahul, Vicky, Jitu, Gudiya, Ravi, Naru, Rekha, and all the change, that includes Vinni, our sweet hearts Kishmish and Pari, Junior Pari, Krish and Jr. Krish, Sarthu – the Hero and Vedi – the Model. I am also thankful to Jay who has been a friend and a family for me here in US.

The stay that I had here in Amherst is a significant portion of my life. Thanks Nilu, Manu, Saugata and Somdutta, Chandu, Jelly, Rahul and Pranali, Sri, Mai-ya, Ashish, Gunjan, Kate, Ajay, Vivek (Mouse), Arjun and Vivek (Tomar). Thank you, Shilpi, Sinan, Malvika, Vikram and Naveen for your suggestions. They were valuable and helped me a lot with my presentation skills. Thanks a lot, Nilu.

I would also like to thank Prashant, Jay, Mohit, Siva, Manoj, Souvik, Natalia, Marco, Fei, Xiaoliang, Dhuwaihi, Craig, Ankit, Katie, Niva and Audrey. They are/ were my colleagues during these years. Thanks Prashant, for your advice and help. Thank you, Liz, Greg, Scott, Lisa, Max and Loie for the good times.

Arnie, Akki, Amit, Anup, Jaswant, Animesh and Sajal, thanks a lot for being with me during the good times as well as the bad times. We still have long way to go.

I am also thankful to Ms. Elisa Campbell from OIT for the thesis writing sessions. My sincere gratitude goes to University of Massachusetts Amherst, Department of Polymer Science and Engineering, the International Programs Office, National Science Foundation and MRSEC for this opportunity and all the help.

Everything you can imagine is real.

- Pablo Picasso

ABSTRACT

STRUCTURE-PROPERTY EVOLUTION DURING POLYMER CRYSTALLIZATION

SEPTEMBER 2010

DEEPAK ARORA, B.TECH., INDIAN INSTITUTE OF TECHNOLOGY MADRAS

M.TECH., INDIAN INSTITUTE OF TECHNOLOGY MADRAS

M.S., UNIVERSITY OF MASSACHUSETTS AMHERST

Ph.D., UNIVERSITY OF MASSACHUSETTS AMHERST

Directed by: Professor H. Henning Winter

The main theme of this research is to understand the structure-property evolution during crystallization of a semicrystalline thermoplastic polymer. A combination of techniques including rheology, small angle light scattering, differential scanning calorimetry and optical microscopy are applied to follow the mechanical and optical properties along with crystallinity and the morphology.

Isothermal crystallization experiments on isotactic poly-1-butene at early stages of spherulite growth provide quantitative information about nucleation density, volume fraction of spherulites and their crystallinity, and the mechanism of connecting into a sample spanning structure. Optical microscopy near the fluid-to-solid transition suggests that the transition, as determined by time-resolved mechanical spectroscopy, is not caused by packing/jamming of spherulites but by the formation of a percolating network structure.

The effect of strain, Weissenberg number ($We = \dot{\gamma}\lambda_{mat}$) and specific mechanical work ($w = \eta\dot{\gamma}^2 t_s$) on rate of crystallization (nucleation followed by growth) and on

growth of anisotropy was studied for shear-induced crystallization of isotactic poly-1-butene. The samples were sheared for a finite strain at the beginning of the experiment and then crystallized without further flow (Janeschitz-Kriegl protocol). Strain requirements to attain steady state/ leveling off of the rate of crystallization were found to be much larger than the strain needed to achieve steady state of flow. The large strain and *We* >1 criteria were also observed for morphological transition from spherulitic growth to oriented growth.

An apparatus for small angle light scattering (SALS) and light transmission measurements under shear was built and tested at the University of Massachusetts Amherst. As a new development, the polarization direction can be rotated by a liquid crystal polarization rotator (LCPR) with a short response time of 20 ms. The experiments were controlled and analyzed with a LabVIEW^{TM} based code (LabVIEW^{TM} 7.1) in real time. The SALS apparatus was custom built for ExxonMobil Research in Clinton NJ.

TABLE OF CONTENTS

Page

LIST OF TABLES

LIST OF FIGURES

CHAPTER 1

INTRODUCTION

Some of the earliest work on polymer crystallization was carried out via solution crystallization [1]. Much of the research was focused on establishing the structure of polymer crystals and the state of a chain in a crystal. A key break through was to confirm the presence of chain folding during polymer crystallization [1, 2]. The results were definitive due to the direct visualization of solution grown single crystals by electron microscopy. On the contrary, melt crystallization always provides aggregates of crystals in form of micro or macroscopic spherulites for isotropically crystallized melts and it is difficult to obtain conclusive real-time images with many details as for solution grown crystals. Now it is well accepted that chain-folding is an inherent feature of polymer crystallization from the solutions as well as from the melts. It is also recognized that adjacent reentry of a chain is a common feature for solution grown crystals, though it is just one of the contributions to overall folding for melt grown crystals [3]. The molecular path of a chain in a melt grown crystal resemblances a random coil when observed from distance [4]. In this chapter, we have reviewed some of the aspects of polymer melt crystallization, especially for flexible polymers (polyethylene, polypropylene, polyethylene oxide, poly-1-butene etc.) that are isotropically crystallized including the proposed mechanisms for crystal growth and structural features of melt grown crystals. Findings from solution crystallization are invoked for comparison purpose.

1.1 Polymer Crystallization

Crystallization in polymers is described by the process of nucleation (primary nucleation) and the crystal growth. The event of primary nucleation is termed as

heterogeneous nucleation when the nucleation sites are foreign substances (dust, impurities, nucleating agents, residual catalyst and any existing surfaces). Homogeneous nucleation involves the aggregation of polymer chains/ chain segments of parent material to certain size and order. Usually during melt crystallization, nucleation is a combination of heterogeneous and homogeneous nucleation and it is hard to separate the two contributions due to the lack of any definitive techniques for direct visualization of nucleation sites. It is well-known that nucleation is a time-dependent process and takes place as a rate even under isothermal conditions [4].

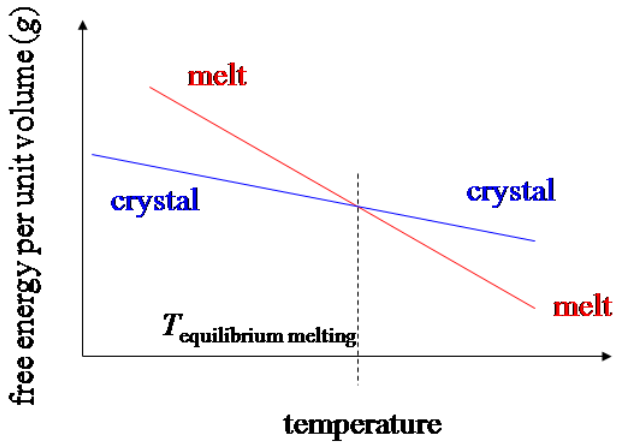

Figure 1.1 Schematic of the free energies for a melt and corresponding crystal [18].

At a temperature below equilibrium melting point, a crystal structure has lower free energy than the melt, and the crystallization is favored thermodynamically, figure 1.1. Though there is a critical size requirement for the primary nucleation that depends on the degree of undercooling. During the event of primary homogeneous nucleation new surfaces are formed in a melt resulting in an increment of system's free energy. Crystallization is an exothermic process and thus lowers the overall free energy of the system. These two opposing phenomena give rise to the critical smallest size of the aggregate that is required for a nucleus to grow. Thus any aggregate that is equal or larger

than this critical size acts as a nucleation site for primary nucleation, figure 1.2. The process of crystal growth further lowers the free energy of a crystallizing system. The crystal growth process is explained by two theories – surface nucleation theory by Hoffman and Lauritzen [5-7] and the surface roughing theory by Sadler and Gilmer [8, 9].

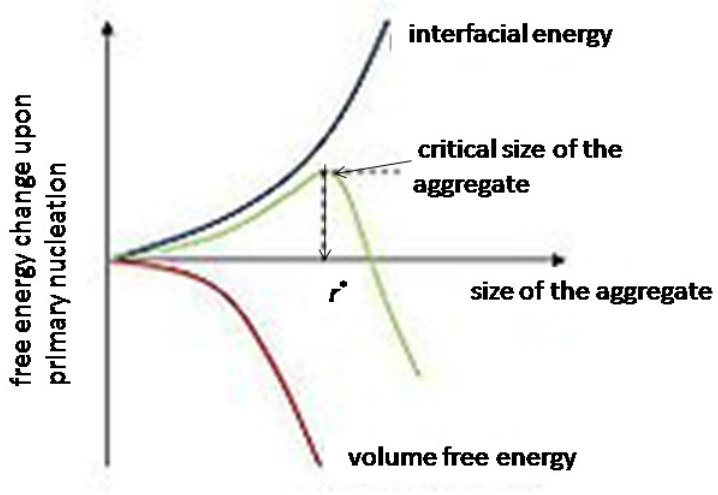

Figure 1.2 Free energy change during nucleation - Interfacial energy grows due to the formation of new surfaces during crystallization where as the free energy of melting has a negative contribution [1, 6].

1.1.1 Surface Nucleation Theory

The earliest theories, the secondary nucleation theories, to explain the crystal growth process for polymers were adopted from the well established models for the crystallization of small molecules [10] and at the very onset it was realized that such theories can explain the temperature dependence of the crystal growth rate for polymers. The spherulitic growth rate for polymers shows a bell-shaped dependence on crystallization temperature if crystallization can be followed for a wide enough temperature range. Figure 1.3 shows the spherulitic growth rate variation with

crystallization temperature for isotactic PS [1], Nylon 6 [1] and PET [11]. Such a bell-shaped curve is typical of the processes that are nucleation controlled at high temperatures and diffusion/ mobility controlled at the low temperatures.

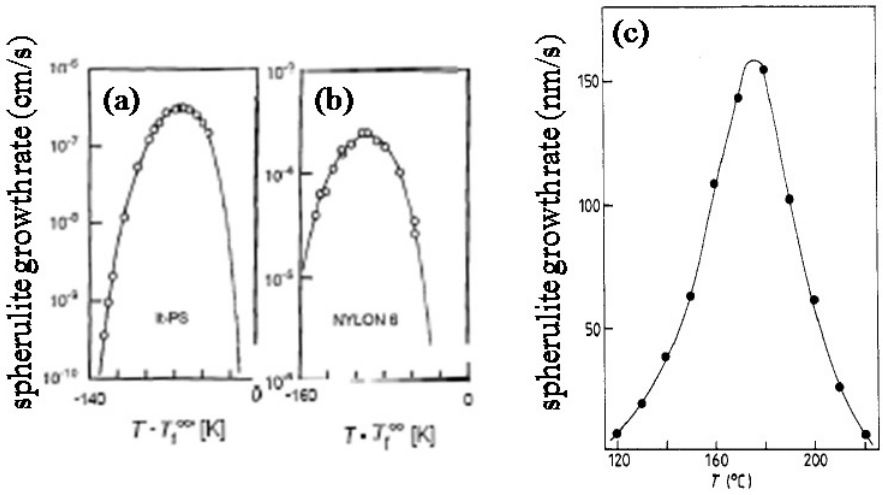

Figure 1.3 Temperature dependence of the radial growth rate of spherulites in (a) isotactic polystyrene [1] (b) polyamide 6 [1] (c) poly(ethyleneterephthalate) [11].

Surface nucleation theory by Hoffman and Lauritzen [5-7] is the most-developed theory to explain the crystal growth process for polymers. It describes the process of crystal growth by surface nucleation events – secondary and tertiary nucleation. Primary nucleation can be seen as a process of formation of six new surfaces as shown in figure 1.4. Secondary and tertiary nucleation events, which are used to describe the crystal growth process, involve the formation of four and two new surfaces, respectively, see figure 1.4. The theory assumes the presence of adjacent re-entry for chain folding, which has been observed for polyethylene melts for low undercoolings. A fast mode of mobility is required to have adjacent re-entry during melt crystallization so that polymer chains can be withdrawn quickly enough from an entangled melt. Chain reptation, which is the

fastest known mode available to a polymer chain, is introduced in the model to incorporate the adjacent re-entry folding.

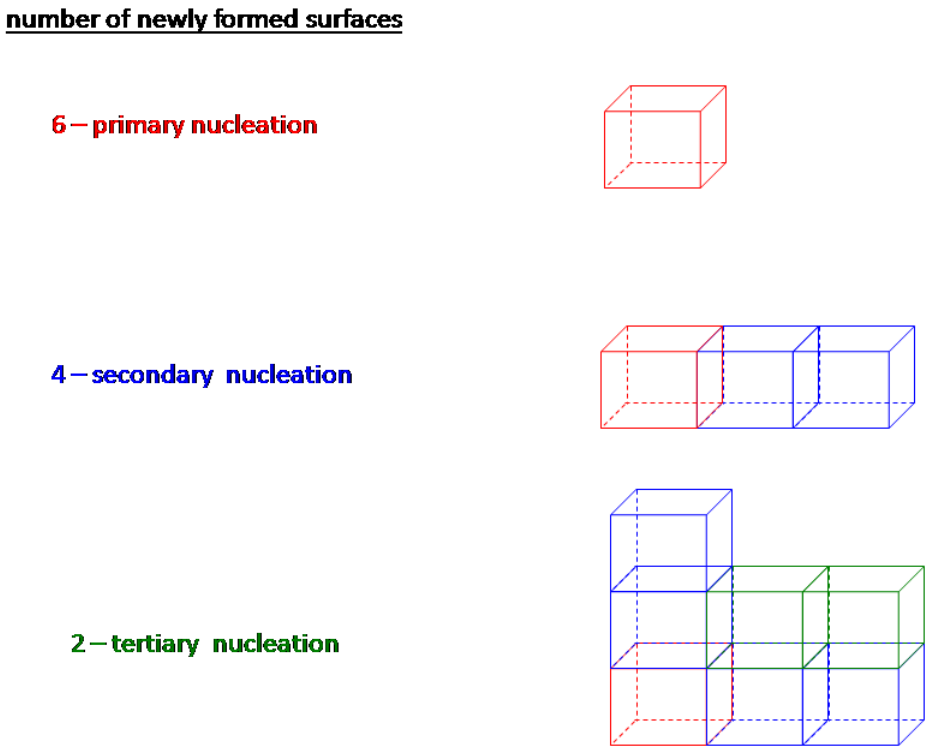

Figure 1.4 Schematic of primary, secondary and tertiary nucleation events [6].

The model describes the crystal growth process as a combination of secondary nucleation rate '*i*' and the substrate completion rate '*g*'. The substrate completion rate (*g*) is the rate of lateral spreading involving tertiary nucleation. In the classical secondary nucleation theory, the nucleation rate (*i*) is taken as the rate determining step for crystal growth where the '*g*' is very fast compared to '*i*'. In the Hoffman and Lauritzen theory for polymers the crystal growth process is described via three regimes so far depending on the relative values of the nucleation (*i*) and the substrate completion (*g*) rates [6]. Reptation is coupled with the substrate completion rate. Regime I is from the classical secondary nucleation theory where the rate of spreading (*g*) is much faster than rate of

secondary nucleation (*i*). In regime II, both the rates are comparable and in regime III, the rate of secondary nucleation (*i*) is very high compared to rate of spreading (*g*). These three regimes are shown schematically in figure 1.5 along with a diagram for the crystal growth rate with temperature. Low molecular weight polyethylenes showed only regime I where as high molecular weights had only regime II. A transition from regime I to II was observed for intermediate molecular weights upon decreasing the crystallization temperature [12]. All the three regimes were seen for cis-polyisoprene [13], poly(3,3-dimethyl thietane) [14] and polyethyleneoxide . In all the experiments, higher molecular weight fractions showed higher regime for the crystal growth. A transition from regime I to regime II was also reported during the growth of polyethylene single crystals from solution [15]. These regime transitions are controlled by the rate of secondary nucleation and the rate of substrate completion. Molecular weight, branching, degree of crosslinking etc. affect the rate of secondary nucleation and the chain mobility and so will affect the temperatures at which these transitions occur. The model by Hoffman and Lauritzen also assumes the single stem nucleation i.e. deposition of a single stem on a surface (a primary nucleus) starts the crystal growth process.

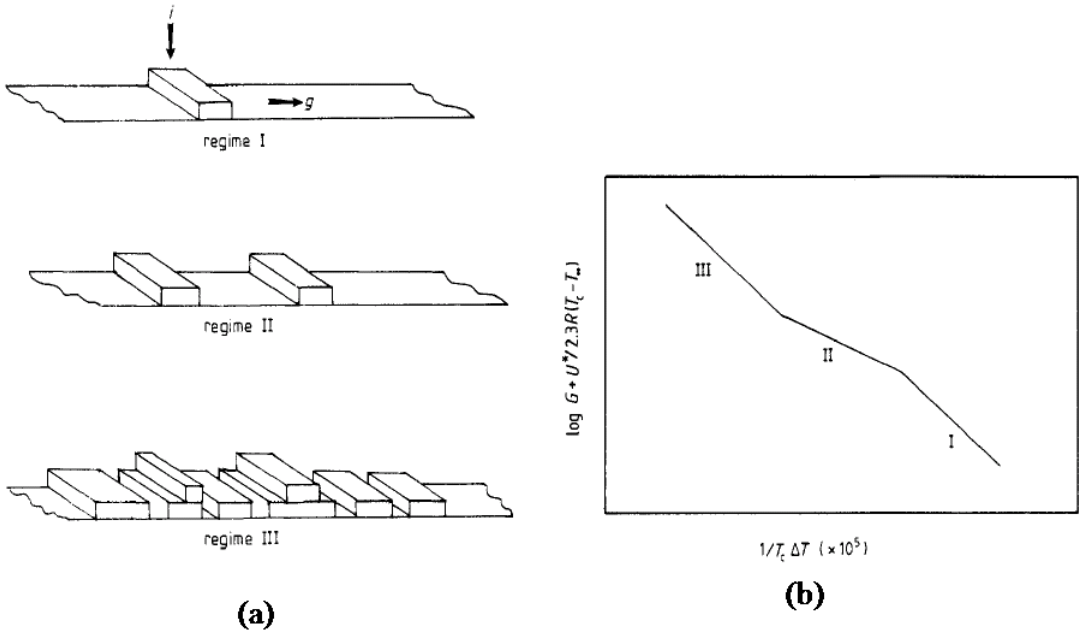

Figure 1.5 (a) Schematic for crystal growth regimes for polymers according to Hoffman and Lauritzen, *i* is the rate of secondary nucleation and the *g* is the substrate completion rate (b) Schematic showing the dependence of crystal growth rate with temperature for three regimes [6].

1.1.2 Surface Roughening Theory

The polymer crystals hardly contain well developed facets. The surface nucleation theory by Hoffman and Lauritzen assumes the presence of flat growth facet, where as curved surfaces are frequently observed for the solution grown single crystals. This was the key observation for Sadler and Gilmer to develop a theory that is based on the surface roughening at atomic length scales [8, 9, 16, 17]. The theory is able to predict the regime transition as well as the curved growth surfaces of crystals. A secondary nucleation step is not required according to this theory, though surface roughening can lead to secondary nucleation.

1.2 Polymer Crystals in Bulk Crystalline Polymers

Crystallization from melt hardly renders single polymer crystals. Aggregates of crystals are observed invariably, spherulites being one of the most commonly observed aggregates from isotropically crystallized melts. Spherulites consist of ribbon-like crystals that are arranged in an approximately radial array. Figure 1.6 shows the spherulites for polyisoprene [4] and isotactic PS [18]. The sheaf-like lamellar crystals are visible for polyisoprene due to the staining by OsO_4, which is discarded in the dark region among bright crystallites. Impingement of these spherulites gives rise to polyhedron structures with grain boundaries as shown schematically in figure 6 (c) [19]. Such polyhedrons are also observed in polycrystalline metals, but unlike polymers, these polyhedrons are single crystals in metals instead of crystal aggregates. The sheaf-like crystallites that are observed under electron microscope might be the cluster of single crystalline lamellae as shown in the schematic 6 (c). Formation of spherical aggregates from such ribbon-like crystallites is explained by the presence of crystals defects leading to the splaying of growing lamellae. Figure 1.7 shows such an initial sheaf for nylon 6 [1]. In many cases these crystalline lamellae are not linear but exhibit some sort of twisting and if such a twisting is regular, it gives rise to banded spherulites, see figure 1.8 [18].

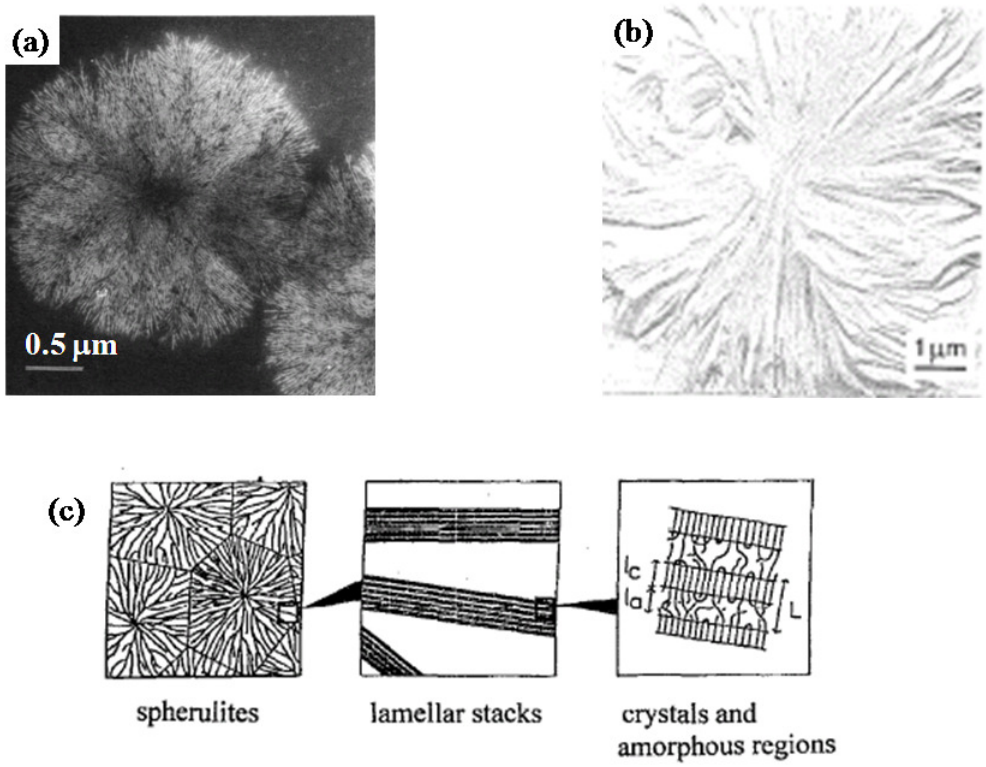

Figure 1.6 (a) A spherulite growing in a film of cis-polyisoprene. The crystal growth has been terminated prior to completion, through reaction of the film with osmium tetra oxide vapor, thereby permitting resolution of the individual lamellar crystals [4]. (b) Electron micrograph of the central sheaf-like part observed at an early stage of development of a spherulite of isotactic-PS [18]. (c) Schematic representation of the spherulitic structure and the arrangement of the crystals and the amorphous regions in the lamellar stacks forming the spherulites in polymers [19].

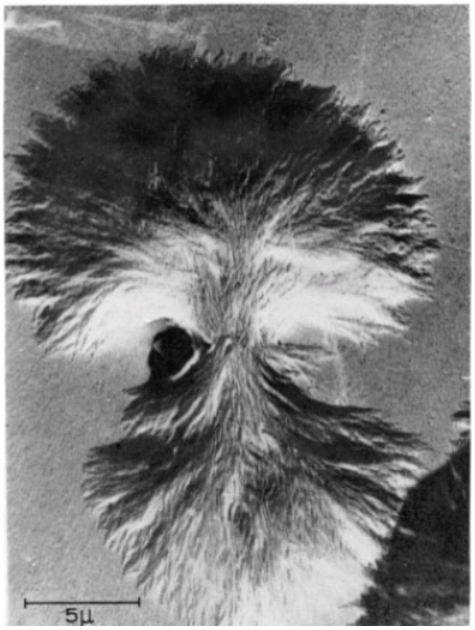

Figure 1.7 Initial sheaves in nylon 6 [1].

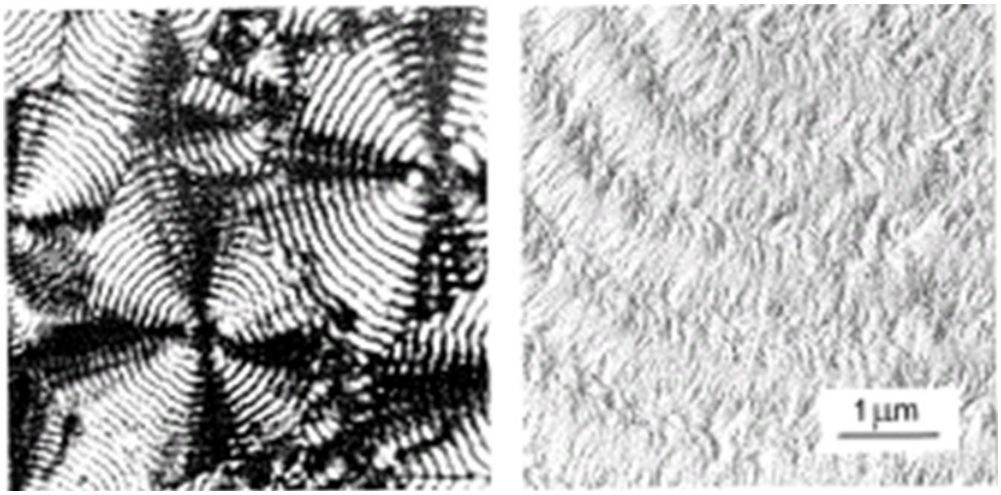

Figure 1.8 Banded spherulites of PE (a) Cross-polar optical micrograph showing the regular sequence of concentrating rings (b) electron micrograph of the surface which cuts through a spherulite [18].

In certain cases, non-spherical aggregates referred to as axialites are observed. These crystalline species are closer in appearance to single crystals grown from solutions and do not form uniform textured aggregates. Usually axialites are observed for low molecular weight polymers at low undercoolings [12]. Crystallization of polymers under

sufficient strain generates rod-like crystalline aggregates as shown in figure 1.9. Application of flow orients the polymer chains in the flow direction and gives rise to row-nucleated structures, also referred to as shish-kebabs [4].

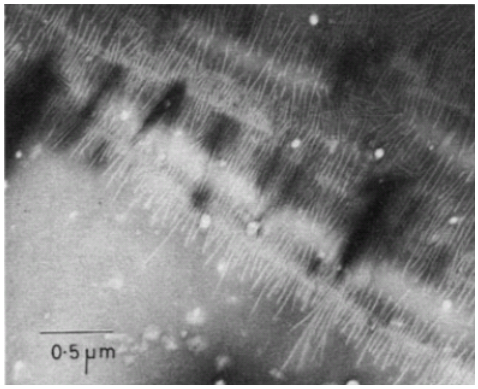

Figure 1.9 Row-nucleated (shish-kebabs) growth in cis-polyisoprene [4].

1.3 Dissertation Overview

Structure-property relations for thermoplastic semicrystalline polymers are not only critical in terms of establishing them for the final product, but it is important to understand the relationship between properties (mechanical, optical, electrical) and the underlying structure during their development. Film blowing of semicrystalline thermoplastics is an appropriate example, where polymer melt is blown as it passes through the frost line. Application of shear and elongational flows is one of the frequently encountered approach to change the underlying structure and hence the final properties. In case of blown films of semicrystalline polymers, these properties are primarily the mechanical strength and the optical clarity. The process of film blowing can be looked at in three stages. After the frost line where material is solid, before the frost line where it is fluid and somewhere in between while passing through the frost line it crystallizes and goes through a fluid-to-solid transition. In the molten state, it is easy to change the

structure, but the flow effects are forgotten due to the quick melt relaxation and once the material is solidified, it is difficult to manipulate the properties. It is advantageous to apply mild enough flow (low energy cost) and have the desired impact on the structure. In order for the flow to be most effective, the structure of the film should be soft enough to alter, and it should have enough strength and connectivity so that it can sustain its weight once it is blown beyond the frost line. Thus the flow will be most effective, in terms of changing the structure, when the material is still soft and has a longer relaxation time i.e. around the fluid-to-solid transition. The material should also be networked before it is blown for structural integrity. This makes it necessary to estimate the time for fluid-to-solid transition, the properties at this transition and the mechanism by which material goes from fluid-to-solid. We have reported these aspects in Chapter 2 for isotropically crystallizing isotactic poly-1-butene under isothermal conditions. Crystallinity using DSC and the morphology using cross-polar microscopy are followed as structural parameters. Evolution in mechanical and optical properties is measured by rheometry, and simultaneous transmission and scattering experiments, respectively. The objective is to understand the mechanism of fluid-to-solid transition and the properties at this transition. An attempt is made to understand the nucleation kinetics experimentally and to obtain an analytical expression for growing volume fraction of spherulites for the early stages of crystallization. A very small amount of crystal 7-8 % by volume results in fluid-to-solid transition. Connectivity among spherulites and the crystal lamellae by bridge molecules is proposed as the possible mechanisms for fluid-to-solid transition.

Chapter 3 deals with the flow effects on rate of crystallization and the morphology for the same polymer. Effect of shear strain, Weissenberg number (*We*) and

specific mechanical work is examined in an effort to search for criteria that govern the shear-induced crystallization. Transmission intensity and the light scattering experiments provide us with a measure for characteristic crystallization time scales. A leveling off in the rate of crystallization (inverse of characteristic crystallization time) is found for a critical value of shear strain. The critical strains are Weissenberg number dependent and are larger compared to the strains needed to reach steady state for the shear flow. The morphological transition from spherulitic growth to oriented growth is attained at smaller strains for larger *We*.

In Chapter 4, we present the detailed description and the validation of a house-built optical train. The train combines the transmission and the scattering measurements, and incorporates automated control, data acquisition and analysis in real time. A liquid crystal based device is the most novel addition to the instrument. The voltage controlled device controls the polarization direction of the outgoing linearly polarized laser beam and has a response time of about 25-30 ms. The device substitutes a bulky quarter wave plate which is a mechanical component with significantly larger response time.

Lastly Chapter 5 presents the final comments and a few suggestions for the future experiments.

1.4 References

[1] Keller A: Polymer crystals, Reports on Progress in Physics 31 (1968) 623-704.

[2] Sadler DM: New explanation for chain folding in polymers, Nature 326 (1987) 174-177.

[3] Sadler DM, Keller A: Neutron-scattering studies on molecular trajectory in polyethylene crystallized from solution and melt, Macromolecules 10 (1977) 1128-1140.

[4] Phillips PJ: Polymer crystals, Reports on Progress in Physics 53 (1990) 549-604.

[5] Lauritzen JI, Hoffman JD: Theory of formation of polymer crystals with folded chains in dilute solution, Journal of Research of the National Bureau of Standards Section a-Physics and Chemistry 64 (1960) 73-102.

[6] Hoffman JD, Miller RL: Kinetics of crystallization from the melt and chain folding in polyethylene fractions revisited: Theory and experiment, Polymer 38 (1997) 3151-3212.

[7] Hoffman JD, Lauritzen JI: Crystallization of bulk polymers with chain folding - theory of growth of lamellar spherulites, Journal of Research of the National Bureau of Standards A 65 (1961) 297-336.

[8] Sadler DM, Gilmer GH: A model for chain folding in polymer crystals - rough growth faces are consistent with the observed growth-rates, Polymer 25 (1984) 1446-1452.

[9] Sadler DM, Gilmer GH: Rate-theory model of polymer crystallization, Physical Review Letters 56 (1986) 2708-2711.

[10] Turnbull D, Fisher JC: Rate of nucleation in condensed systems, Journal of Chemical Physics 17 (1949) 71-73.

[11] Phillips PJ, Tseng HT: Influence of pressure on crystallization in poly(ethylene-terephthalate), Macromolecules 22 (1989) 1649-1655.

[12] Hoffman JD, Frolen LJ, Ross GS, Lauritzen JI: Growth-rate of spherulites and axialites from melt in polyethylene fractions - regime-1 and regime-2 crystallization, Journal of Research of the National Bureau of Standards Section a-Physics and Chemistry 79 (1975) 671-699.

[13] Phillips PJ, Vatansever N: Regime transitions in fractions of cis-polyisoprene, Macromolecules 20 (1987) 2138-2146.

[14] Lazcano S, Fatou JG, Marco C, Bello A: Crystallization regimes in poly(3,3-dimethylthietane) fractions, Polymer 29 (1988) 2076-2080.

[15] Organ SJ, Keller A: Fast growth-rates of polyethylene single-crystals grown at high-temperatures and their relevance to crystallization theories, Journal of Polymer Science Part B-Polymer Physics 24 (1986) 2319-2335.

[16] Sadler DM, Spells SJ: A neutron-scattering study of slowly crystallized bulk polyethylene, Polymer 25 (1984) 1219-1226.

[17] Sadler DM, Gilmer GH: Selection of lamellar thickness in polymer crystal-growth - a rate-theory model, Physical Review B 38 (1988) 5684-5693.

[18] Strobl GR: Metastable partially crystalline states, The physics of polymers, Berlin (1997).

[19] Wutz C, Bark M, Cronauer J, Dohrmann R, Zachmann HG: Simultaneous measurements of small-angle x-ray-scattering, wide-angle x-ray-scattering, and light-scattering during phase-transitions in polymers, Review of Scientific Instruments 66 (1995) 1303-1307.

CHAPTER 2

NETWORK FORMATION IN A SEMICRYSTALLINE POLYMER AT THE EARLY CRYSTALLIZATION STAGES: FROM NUCLEATION TO PERCOLATION

2.1 Abstract

Isothermal crystallization experiments on isotactic poly-1-butene at early stages of spherulite growth provide quantitative information about nucleation density, volume fraction of spherulites and their crystallinity, and the mechanism of connecting into a sample spanning structure. An attempt is made to relate the crystal fraction inside spherulites, which is very small initially, to the overall crystallinity in the sample. Experiments include optical microscopy, DSC, SALS, and rheology. Optical microscopy near the fluid-to-solid transition suggests that the transition, as determined by time-resolved mechanical spectroscopy, is not caused by packing/jamming of spherulites but by the formation of a percolating network structure. Impingement of pairs of spherulites starts to occur long before percolation. This makes it difficult to predict crystal growth and define spherulitic impingement for the whole sample. At percolation, the absolute crystallinity is about 7-8 vol%. The transition material can be understood as a soft physical gel with an out-of-equilibrium structure.

2.2 Introduction

The spherulitic growth of crystals in a semicrystalline polymer is initiated by lowering the temperature from the melt stage. Below a polymer-specific temperature level, nuclei begin to appear. On these nuclei, lamellar crystals grow to form spherulitic structures [1-5]. Early stages of crystal growth serve as templates for further growth and

thus control the processing behavior as well as the final morphology, which determines mechanical and optical end-use properties of semicrystalline polymers. This experimental study focuses on the post-nucleation, early stages of crystallization. Our aim is to understand the kinetics of early crystal growth and the nature of the fluid-to-solid transition during crystallization.

Crystallization processes have been argued to start long before the appearance of nuclei. SAXS and WAXD experiments at the early stages in polymer crystallization pinpoint the presence of preorder in the melt before nucleation [6-11]. The observations of these pre-nucleation studies have been explained with the presence of a long-range order and liquid-liquid phase separation before nucleation. However, many questions remain which require detailed experiments before further conclusions can be drawn. More accessible to experimentation are the early stages after nucleation. A deeper understanding of the structure-property evolution during such post-nucleation stages is expected to lead to a better predictive model for polymer melt crystallization [12-14].

A crystal nucleus is envisioned as an ordered aggregate of polymer chain segments. A critical aggregate size is required to make the nucleus stable by locally lowering the free energy $\Delta E = -\Delta e V_{nuc} + \Sigma A_i \sigma_i$ [15]. ΔE, Δe, V_{nuc}, σ_i and A_i are the free energy change during nucleation, free energy of melting for a unit volume (e_{melt}-e_{cryt}), volume of the nucleus, surface energy, and area of newly formed surfaces, respectively. Chain-folded lamellae grow from the spatially distributed nuclei to form supramolecular structures in the shape of spherulites, in the absence of flow, and with radial gradients in crystallinity and density [3, 4, 16, 17]. These semicrystalline spherulites can be viewed as suspended particles that grow in an amorphous fluid (polymer melt). Kinetic crystal

growth theories of Lauritzen-Hoffmann [1] and Sadler-Gilmer [2] for polymers predict a constant growth rate for spherulites under isothermal conditions as, $\dot{R} \propto \exp\left(-K/T_{cry}\Delta T\right)$, where $\dot{R}$, K, T_{cry}, and ΔT are the spherulite radial growth rate, growth rate constant, crystallization temperature, and degree of undercooling, respectively. These models were developed for the isolated growth of a single spherulite and do not describe the sample volume filling by multiple spherulites.

The empirical Weibull function, $y(t) = 1 - \exp\left\{-\left(t/t_W\right)^{\beta}\right\}$, has often been employed to describe the volume fraction of spherulites, $\phi_{sph}(t)$, and/or the total relative crystallinity, $\phi_{cry}(t)/\phi_{cry}(\infty)$, during crystal growth (Avarami and Ozawa type functions) [15, 18] . The sigmoidal Weibull function features an incubation time followed by an accelerated growth and the final saturation (for $t \to \infty$). It contains two fitting parameters, a characteristic crystallization time, t_W, and an exponent, β. The characteristic time corresponds to $y(t = t_W) = 0.63$. It is expected that the fitting parameters will depend on experimental conditions.

As a consequence of crystallization, the material undergoes a liquid-to-solid transition, which can be captured by rheological gel point measurements. Dynamic mechanical spectroscopy (DMS) is a very sensitive tool to locate the gel point which expresses itself in a self-similar relaxation modulus, $G(t) = St^{-n}$ for $t > 1/\omega_c$ [19-24]. In case of dynamic mechanical measurements, the gel point structure results in complex moduli $G' = G''/\tan\delta = S\Gamma(1-n)\cos(n\pi/2)\omega^n$ for $\omega < \omega_c$, and a frequency independent loss tangent, $\tan\delta = \tan(n\pi/2) \neq f(\omega)$ for $\omega < \omega_c$, in the terminal region. S is the gel-stiffness and n is the relaxation exponent for the critical gel. For crystallizing

homopolymers, the mechanism that causes the fluid-to-solid transition is not well-understood [25-28]. One of the objectives of this work is to identify the connectivity mechanism and, specifically, to identify the structure at the gel point.

Another objective is to describe the sample volume filling by spherulites in an analytical expression that is based on experimental information such as growth rate and birth time of spherulites [29-31]. A fundamental experimental study was needed to generate the data that can answer the above questions.

2.3 Experimental

2.3.1 Material and Sample Preparation

Isotactic poly-1-butene (iPB), from Basell, with M_w = 176000 g/mol and M_w/M_n of 5.7, served as test material. Pellets of iPB (as obtained from Basell) were compression molded into thick sheets, from which samples were cut for Differential Scanning Calorimetry (DSC), rheometry and optical measurements. The iPB was used without a nucleating agent.

Differential scanning calorimetry (DSC) was carried out under nitrogen in a DSC Q1000 (TA Instruments) using standard aluminum pans (from TA instruments) 6 mm in diameter and weighing about 24 mg. A thin sample (about 12 mg) was pressed into a DSC pan and heated above melting temperature to establish uniform contact between polymer and pan. For the DSC measurements, samples were heated as well as cooled at 10K/min. First melting, second melting, and crystallization peaks were observed at 120 ^oC (100-130 ^oC), 110 ^oC (100-120 ^oC), and 54 ^oC, respectively (Fig. 2.1). First melting belongs to the crystal FormI of iPB, which has a density of 950 Kg/m^3 and is a

thermodynamically stable form. Second melting belongs to FormII that is less dense (907 Kg/m^3) than FormI and is a kinetically favored crystal form. FormII transforms into FormI within 7-12 days at room temperature and atmospheric pressure [32-35].

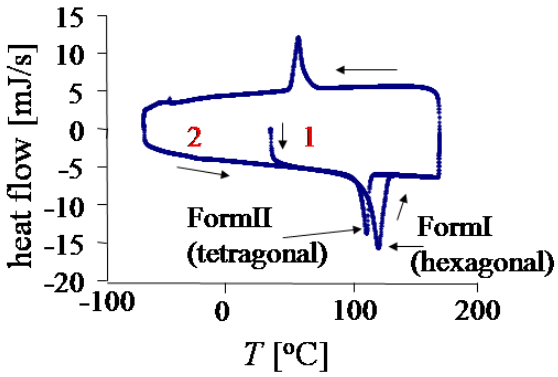

1 – first heating cycle

2 – second heating cycle

$T_{m\text{-}I}$=120.0 ºC (100-130 ºC)
$T_{m\text{-}II}$=110.7 ºC (100-120 ºC)
T_c=54.7 ºC (70-50 ºC) at 10 K/min

Figure 2.1 Differential scanning calorimetry for iPB for heating and cooling rates of 10 K/min. Two polymorphs of iPB, FormI and FormII, were observed during first and second heating, respectively.

For rheology, a 2mm thick disk-shaped sample was inserted between the parallel disk fixtures (diameter 25 mm) of a torque-controlled rheometer (Stresstech of ATS Rheosystems). It was heated above melting point and then compressed to a thickness of about 0.9 mm to establish uniform contact between the sample and rheometer plates. *G'-G''* data from isothermal frequency sweeps at T = 88.9, 100.8, 110.9, 121.4, 131.5, 141.5, 151.8, and 174 ^{o}C were merged into a set of master curves at 88.9 ^{o}C (Fig. 2.2). The shear measurements were performed in the linear viscoelastic region.

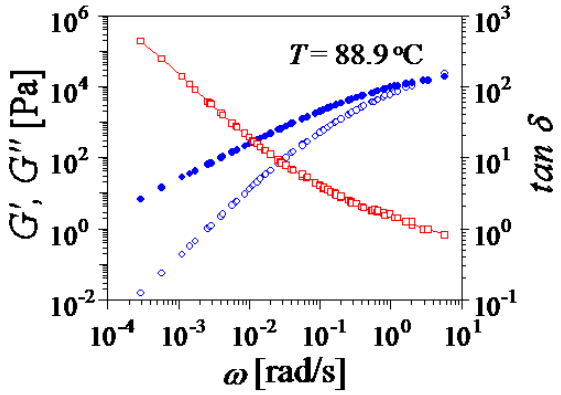

Figure 2.2 Master curve of iPB melt at crystallization temperature 88.9 °C (from isothermal frequency sweeps at T = 88.9, 100.8, 110.9, 121.4, 131.5, 141.5, 151.8, and 174 °C).

For optical measurements, a 2 mm thick disk shaped sample was placed between the parallel plates of an optical device (CSS 450 from Linkam Scientific). There, it was heated above melting and then compressed to a thickness of about 300 μm. The parallel disk optical device (R = 15 mm), with quartz windows, was alternatively mounted in an optical train for light scattering and transmission intensity measurements and in an optical microscope (Carl Zeiss Universal (ZPU01) under transmission mode) with cross-polars. For a detailed description of the device and the instrument, refer to the publications by Pogodina et al.

For small angle light scattering (SALS) and transmission intensity measurements, a 5 mW, linearly polarized, He-Ne (632.8 nm) LASER beam (around 1 mm in diameter) was sent through the sample. Scattered and transmitted intensities under parallel and cross polars were measured simultaneously using an analyzer sheet and photodiodes, respectively.

The transmission intensity under parallel-polars (I_{HH}) defines the evolving turbidity, $\mu = -(1/h)\ln(I_{HH}/I_0)$, of the sample due to crystallization. h and I_0 are sample thickness and laser source intensity, respectively [12, 13].

Two-dimensional light scattering invariants were calculated from intensity measurements according to Stein-Wilson theory for random orientation correlations [36],

$$Q_\delta = \int_{q_1}^{q_2} I_{HV}(q) q^2 dq \propto \left\langle \delta^2 \right\rangle, Q_\eta = \int_{q_1}^{q_2} \left(I_{VV}(q) - \frac{4}{3} I_{HV}(q) \right) q^2 dq \propto \left\langle \eta^2 \right\rangle \text{ and } q = \frac{4\pi}{\lambda} \sin\frac{\theta}{2} \quad (1).$$

Q_δ, Q_η, q, δ, η, θ, and λ are the orientation fluctuation invariant, density fluctuation invariant, wave vector, orientation fluctuations, density fluctuations, scattering angle and wavelength of the light source, respectively. These invariants are the measure of mean square fluctuations.

Mean square density fluctuations, $\left\langle \eta^2 \right\rangle$, are related to the volume fraction of anisotropic aggregates (ϕ_A) as,

$$\left\langle \eta^2 \right\rangle = \phi_A (1 - \phi_A)(\bar{\alpha}_A - \alpha_s)^2 \qquad (2).$$

$\bar{\alpha}_A$ and α_s are the average polarizability of the aggregate and the surrounding, respectively. For a crystallizing polymer, spherulites can be treated as anisotropic aggregates of crystals in an isotropic melt. Mean square orientation fluctuations, $\left\langle \delta^2 \right\rangle$, offer an estimate of the crystal volume fraction in the sample.

$$\left\langle \delta^2 \right\rangle = \phi_A \delta_A^{\,2} + (1 - \phi_A)\delta_s^{\,2} \qquad (3)$$

δ_A and δ_s define the anisotropy of the aggregate and surrounding, respectively. For a melt, δ_s can be assumed to be zero. For semicrystalline aggregates, their anisotropy can be expressed as a function of their crystal content, eq. 4.

$$\delta_A = \phi_{cry,A}\delta^0_{cry} f_{cry,A} + (1-\phi_{cry,A})\delta^0_{amo} f_{amo,A} + \delta_F \qquad (4)$$

$\phi_{cry,A}, \delta^0_{cry}, \delta^0_{amo}, \delta_F, f_{cry,A}$, and $f_{amo,A}$, are the volume fraction of the crystal in the aggregate, intrinsic anisotropy of the crystal, anisotropy of the amorphous region, form anisotropy, orientation function for the crystals in aggregate and orientation function for the amorphous regions in the aggregate, respectively. The assumptions are that all crystals reside within the aggregates,

$$\phi_{cry} = \phi_A \phi_{cry,A} \qquad (5),$$

, and that form and amorphous anisotropies can be neglected. Then, eqs. 3, 4 and 5 combined predict the mean square anisotropy for a volume-filling sample,

$$\left\langle \delta^2 \right\rangle = {\phi_{cry}}^2 {\delta^0_{cry}}^2 {f_{cry,A}}^2 \propto Q_\delta \qquad (6).$$

The crystal volume fraction in the sample is predicted to be proportional to the square root of the mean square orientation fluctuation invariant

$$\phi_{cry}(t) \propto \sqrt{Q_\delta(t)} \qquad (7)$$

under the assumption that δ^0_{cry} and $f_{cry,A}$ remain constant during crystallization.

2.3.2 Experimental Protocol

For all the experiments, samples were heated to 174.5 ^{o}C, kept there for about 15 minutes. Such a high temperature (about 50 K above melting) was used to erase the thermo-mechanical history and to melt all the crystallites present in the sample as recommended by Hadinata et al. [37]. Then the sample was cooled down to T_x = 88.9 ^{o}C, the temperature for isothermal crystallization. Time t = 0 was assigned to the instant at which the experimental temperature T_x was reached. Optical measurements were

performed in air unlike thermal and mechanical measurements, which were done under dry heated nitrogen. Temperature calibration was performed for all the devices including optical cell, rheometer, and DSC; see the Appendix for details.

2.4 Results

2.4.1 Rheology

The purpose of the rheological experiments is to find the gel point so that the structural properties can be measured at that transition. Figure 2.3 shows the respective development of the storage (G') and loss (G'') moduli. Both moduli grow with time and level off at longer times. It was surprising to observe the frequency independence of plateau values at longer times for both the moduli. However, this trend is not unique, glassy materials demonstrate similar behavior [38].

The gel point as marked by a loss tangent that is independent of frequency [39, 40] can be measured with time-resolved oscillatory shear [41] at frequencies between 0.1 and 0.8 rad/s. The loss tangent was found to intersect at t_{gel} =1180-1192 s (Fig. 2.3). Gel stiffness and relaxation exponent are S=1.85-2.54 *10^4 Pa s^n and n=0.5-0.54, respectively. A low mutation number, N_{mu} =d log(G')/d log t, is a measure of the quality of the data [41]. The highest mutation number N_{mu} (for the smallest frequency 0.1 rad/s) was 0.105, establishing the quasi-stable nature of the crystallizing sample. [22, 42]. The knowledge of the gel point, in combination with structural observations, allows us to answer questions about the structural state that causes the transition. The structure will be characterized in the following.

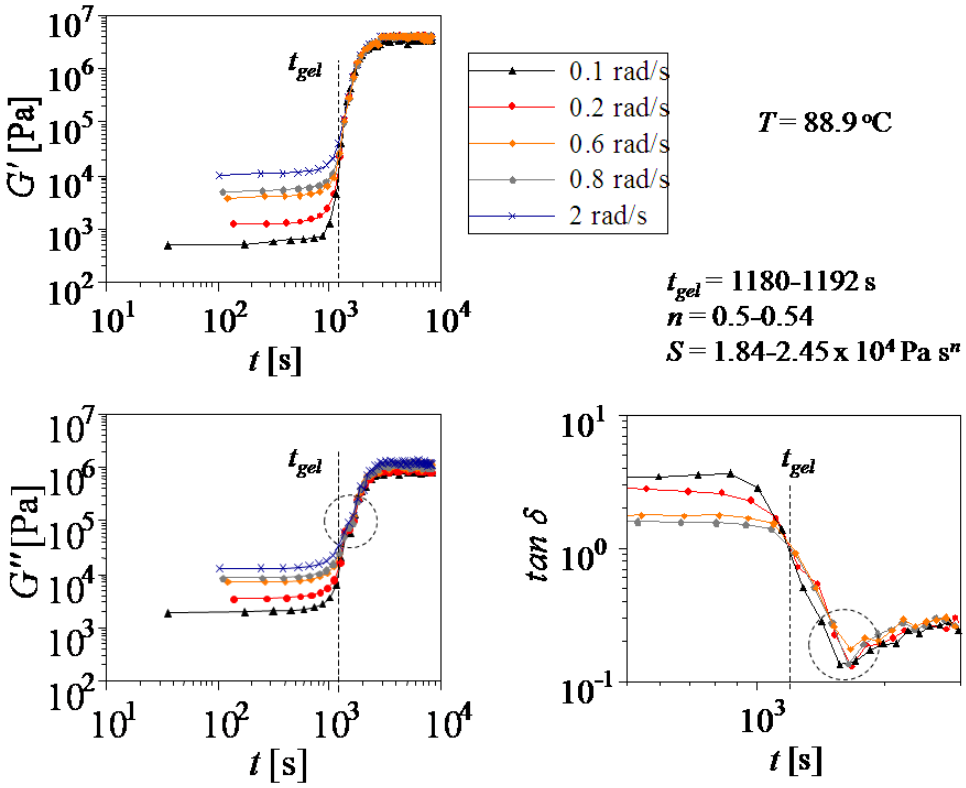

Figure 2.3 Growth of *G'*(*t*) and *G''*(*t*) during crystallization of iPB at 88.9°C. The fluid-to-solid transition is marked by the frequency-independent loss tangent. At long times, the loss tangent becomes less accurate when *G'* and *G''* differ by too much, after the gel point (lack of sensitivity). The dip in the loss tangent after the gel point is due to the noisy *G''* data, region marked by a circle.

2.2 Differential Scanning Calorimetry (DSC)

Samples were crystallized isothermally at 88.9 °C and the evolved heat served as a measure of developing crystallinity. A single baseline was not able to describe the heat evolution during crystallization, so multiple baselines were used to obtain running integrals of evolved heat. The absolute crystal weight fraction was calculated as $w_{cry}(t) = H(t) / H_{ideal\ crystal}$, where $H(t)$ and $H_{ideal\ crystal}$ are the specific heat evolved up to time '*t*' for a crystallizing sample and the specific heat required to melt an ideal crystal. We used 146 J/g as heat of melting for an ideal crystal of FormII [32]. It is reasonable to

assume that the initial crystallization always leads to FormII, since polymorphic transformations from FormII to FormI take 7-12 days [35].

In order to compare amorphous and crystalline domains in the sample, we convert DSC crystal weight fractions (w_{cry}) into crystal volume fractions, $\phi_{cry} = w_{cry}.\rho_{sam} / \rho_{cry}$. We approximate the average sample density, $\rho_{sam} = (\rho_{cry} - \rho_{amo})w_{cry} + \rho_{amo}$, *as* linear function of the crystal fraction; ρ_{cry} (907 Kg/m^3) and ρ_{amo} (868 Kg/m^3) are densities of the ideal crystal and the amorphous melt, respectively. The crystal weight fraction (w_{cry}) of iPB is slightly higher than the corresponding crystal volume fraction (ϕ_{cry}), see Fig. 2.15 in the Appendix.

The crystal volume fraction (Fig. 2.4) increases quickly in the first 2500 s, followed by a much slower growth at longer times. The absolute crystallinity (ϕ_{cry}) is normalized with its maximum value ($\phi_{cry,\infty}$). The crystal fraction reaches a value of about 18 vol% at the end of 2500s and further grows slowly to 20 vol%. The Weibull time ($t_{W-\phi_{cry}}$) obtained from these measurements is 1500 s, corresponding to a relative crystallinity of 63 vol% (inset in Fig. 2.4). The absolute crystal volume fraction at the gel point is 7-8 % which is about 1/3 of final crystallinity. It should be noted that the Avrami-type stretched exponential function is not able to describe the growing crystal fraction ($\phi_{cry}/\phi_{cry,\infty}$) in the sample for the first 500 s, Fig. 2.16 in the Appendix.

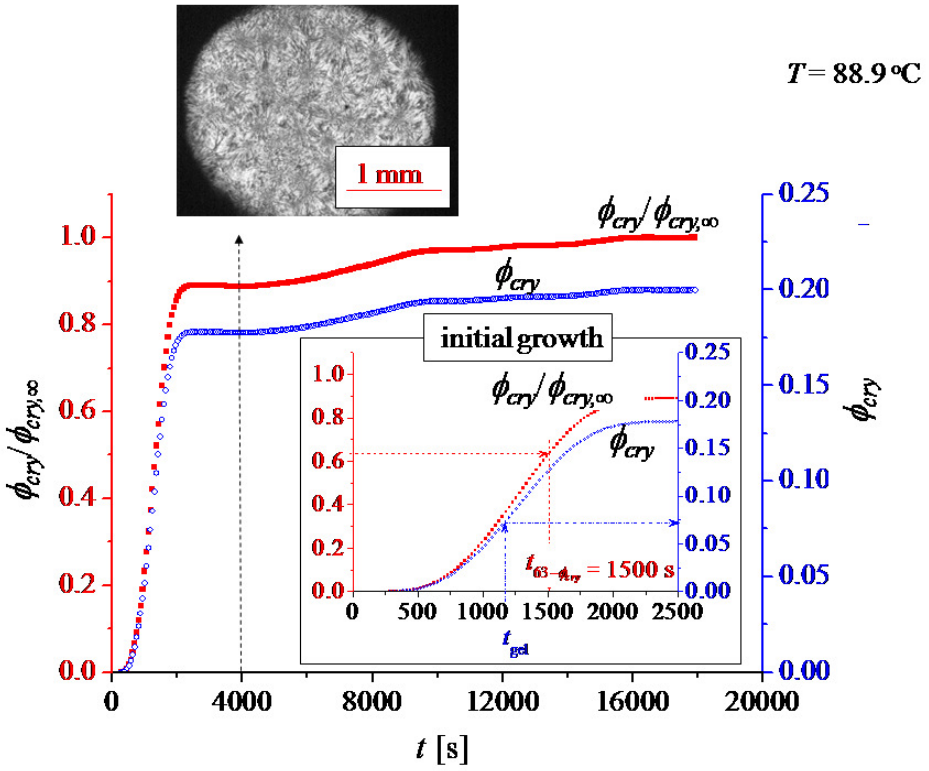

Figure 2.4 Relative ($\phi_{cry}/\phi_{cry,\infty}$) and absolute ($\phi_{cry}$) crystal volume fraction in the entire sample from DSC for isothermal crystallization of iPB at 88.9 °C. The micrograph shows that the sample is already completely filled with spherulites at t=4000 s and that further crystal growth has to occur within the primary crystal structure.

2.4.3 Optical Microscopy

2.4.3.1 Fluid-to-Solid Transition

The optical micrograph, Fig. 2.5, at the gel point shows spherulites of different sizes that are not jammed or packed. Most of them have already impinged whereas others are still away from impingement. In the micrograph, we observe impingement between pairs of spherulites, though it is hard to define an instant of spherulitic impingement for the whole sample. We find that a percolated structure gives rise to the fluid-to-solid transition rather than jamming or close packing of spherulites. Crystal volume fraction at this instant, from DSC, is 7-8 vol% indicating the amorphous nature of spherulites.

2.4.3.2 Kinetics of Nucleation

The distribution in size implies that the spherulites are born at different times. With optical microscopy (Fig. 2.5) we observed that most spherulites appear early after cooling followed by a small number of gradually appearing new spherulites.

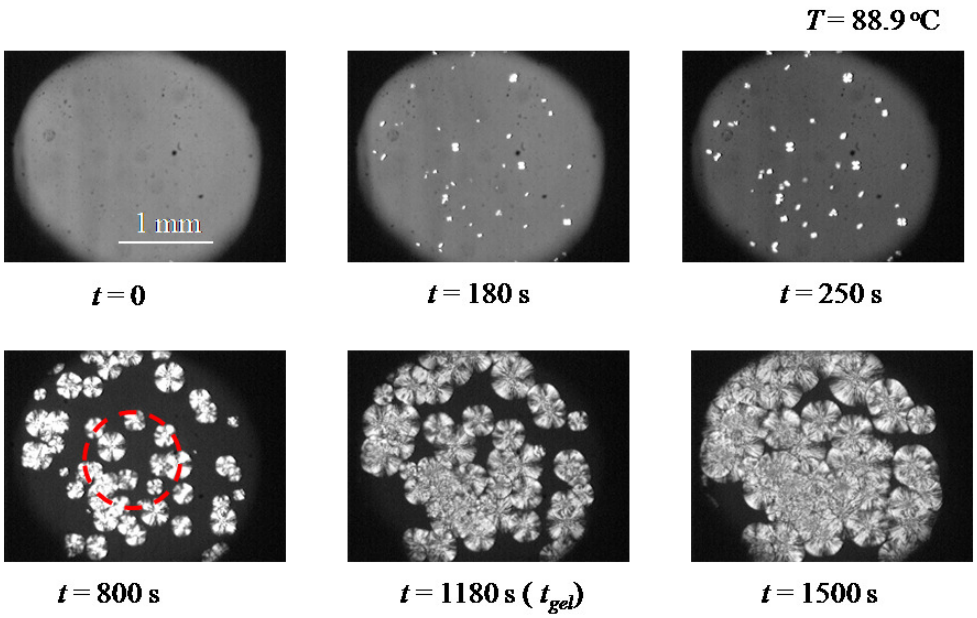

Figure 2.5 Cross-polar micrographs for crystallizing iPB at 88.9°C (observation window is not perfectly circular). The dotted circle in the optical micrograph at 800 s is 1 mm in diameter and represents the size and location of the laser beam used for scattering and transmission measurements of Fig. 2.10 and 2.11.

- **Size Tracking of Spherulites**

An optical tracking procedure is used to follow the radial growth of individual spherulites, $R(t)$, as plotted in Fig. 2.6. The linear $R(t)$ data are extrapolated backwards to R=0 for estimating the "time of birth", t_{birth}, at which lamellae begin to grow radially from a nucleus. In this way, the data define the instant of nucleation and the spherulite growth rate, $\dot{R}$. All spherulites, present in the observation window, were labeled and tracked. For example, R_1, R_{12} and R_{19} refer to the (arbitrarily chosen) spherulites labeled

1, 12 and 19; see the cross-polar micrograph in Fig. 2.6. It is assumed that each imaged area is the cross sectional area of a spherulite equaling πR^2. The extrapolation procedure also includes spherulites that were already "born" during cooling i.e. before having reached the experimental temperature, T_x. Spherulites entering from outside into the field of view were not counted and radius tracking was continued as long as a spherulite remained in the observation window.

Noticeable is the upper time limit for microscopy experiments. In the beginning, spherulites grow freely in all three dimensions but, once their size exceeds the sample thickness, they continue to grow two dimensionally. Since the sample thickness is about 300 μm, spherulites were tracked until they had reached a size of 300 μm in diameter or until they impinged with neighboring spherulites. It should be noted that, apart from the sample thickness, the 3D to 2D transition in growth pattern depends on the nucleation density in the neighborhood of individual spherulites.

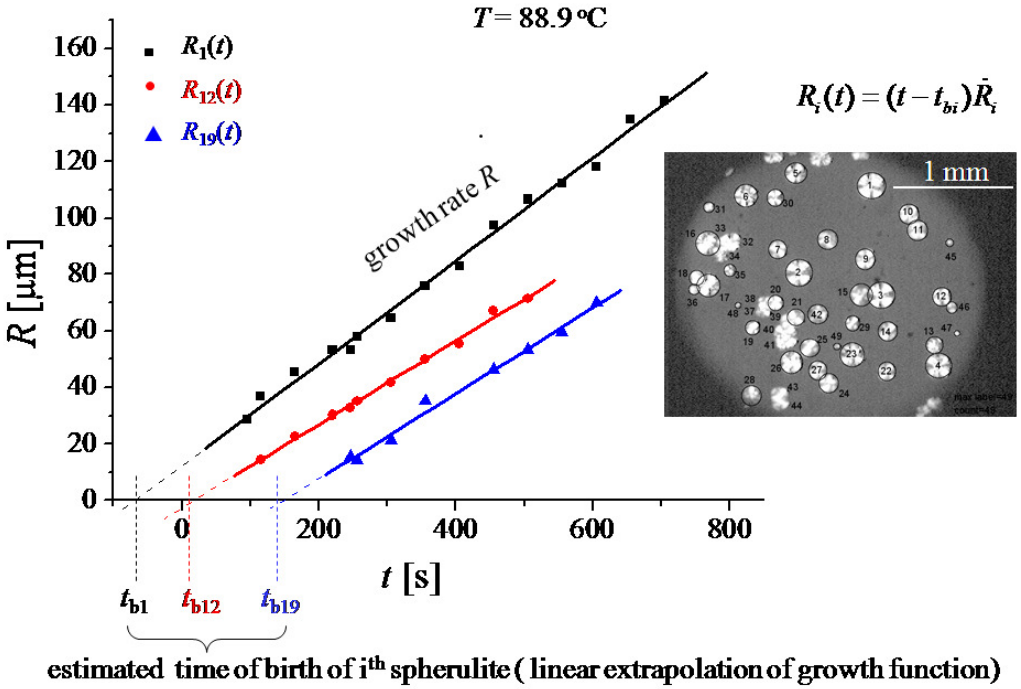

Figure 2.6 Spherulite tracking by marking individual spherulites, measuring their size *R*(*t*), and extrapolating backwards in time. *R*(*t*) plots are linearly fitted and shown for arbitrarily chosen spherulites, labeled 1, 12 and 19. Insert: cross-polar image of early crystallization with labeled spherulites.

Spherulites grow by 0.1- 0.35 μm/s as shown in Fig. 2.7(a). This results in a number average growth rate $\dot{R}_n = \sum N_i \dot{R}_i / \sum N_i$ of about 0.16 μm/s and a volume average growth rate $\dot{R}_v = \left(\sum N_i R_i^3 / \sum N_i \right)^{1/3}$ of about 0.22 μm/s. In search of a more meaningful average growth rate, we also looked at the time-averaged growth rate $\dot{R}_t = \left(\sum R_i^3 (t - t_i)^3 / \sum (t - t_i)^3 \right)^{1/3}$. $\dot{R}_t$ varies with time and interestingly, reaches a steady value that is close to the volume average growth rate, 0.22 μm/s, see Fig. 2.17 in the Appendix. Most of the spherulites grow at a rate between 0.1 and 0.2 μm/s. Here we take notice that Ostwald ripening studies frequently use a volume-average growth rate to

describe growing droplet radius [43] and we would employ this growth rate to model volume fraction of spherulites in the sample.

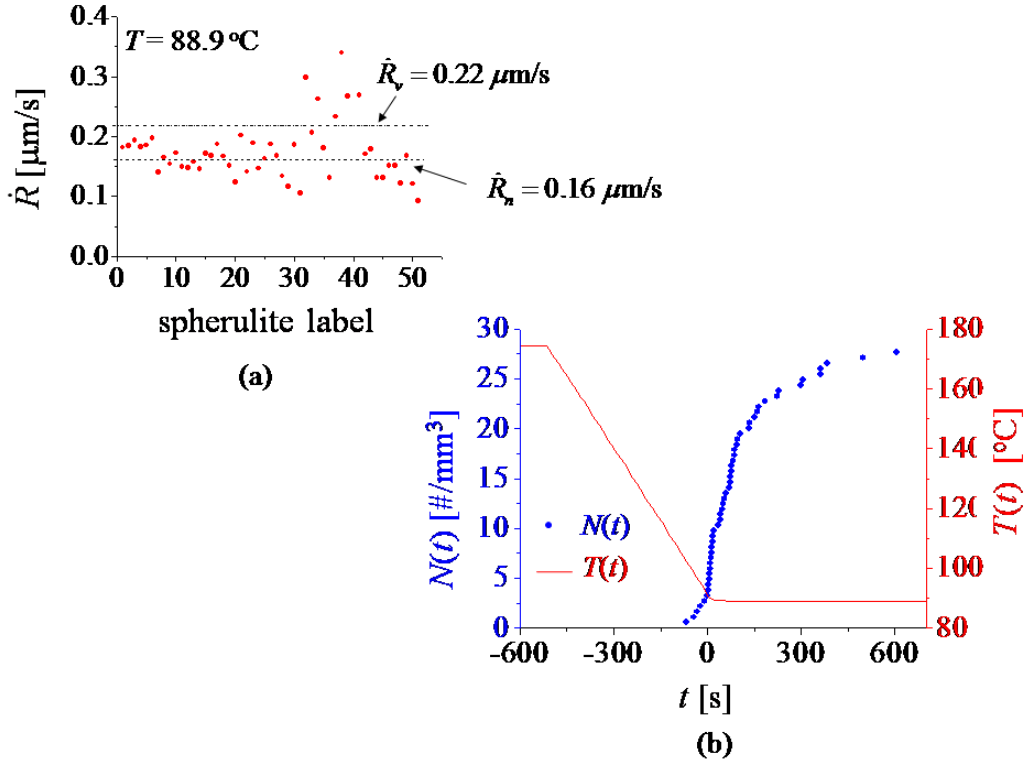

Figure 2.7 (a) Measured growth rates of all spherulites along with number and volume average growth rates. (b) Temperature protocol and measured population of nuclei using the protocol in Fig. 2.6. The nucleation density, $N(t)$, is defined as the number of nuclei per unit volume of sample. t=0 refers to the instant during cooling when the sample has reached the temperature for isothermal crystallization (T_x).

Figure 2.7 (b) shows the calculated nucleation density along with the applied temperature protocol. Nuclei already appear during cooling before having reached the experimental temperature of T_x=88.9 °C. Further nucleation takes place under isothermal conditions, however, at decreasing rate. Because of this, we use two different regimes for modeling the appearance of nuclei, see Fig. 2.8: instantaneous nucleation during cooling ($t_r \le t \le 0$; t_r is the reference time when nucleation starts during cooling) and nucleation as a rate process under isothermal conditions ($t \ge 0$).

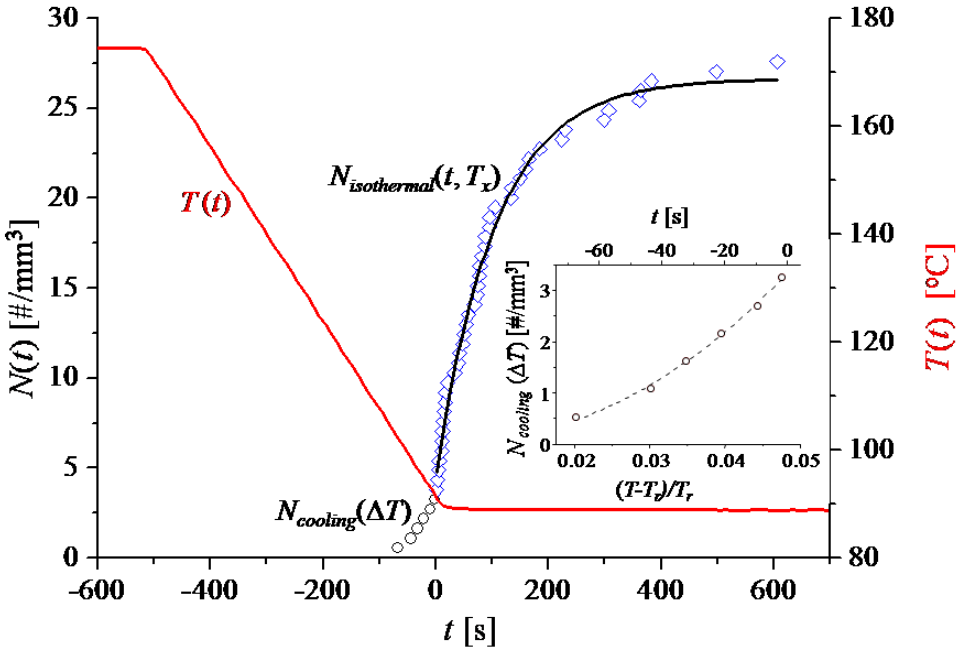

Figure 2.8 Different nucleation regimes: nucleation density during cooling, $N_{cooling}(\Delta T)$, is a function of the varying depth of undercooling, $\Delta T = T_r - T(t)$, and nucleation density at crystallization temperature (T_X), $N_{isothermal}(t, T_X)$, is a function of T_X and time, t. The solid line, on the nucleation data, is a fit for the nuclei appearing at T_X. The inset shows the fit for the nucleation during cooling as a function of dimensionless undercooling.

- **Appearance of Nuclei during Cooling**

Nuclei appear instantaneously when lowering the temperature. The nucleation density is assumed to depend on the increasing depth of undercooling, $\Delta T = T_r - T(t)$, T_r being the polymer characteristic reference temperature at which nucleation starts. Potentially, nuclei can grow at any temperature below the melting point. In this study, we take the DSC peak melting temperature (110 ^{o}C) as the reference temperature (T_r) for the nucleation to start.

Experimental data in the inset of Fig. 2.8 were found to follow a parabola,

$$N(T) = a\{(T - T_r)/T_r\}^2 \qquad (8)$$

with a = 2841.7 #/mm^3 . When cooling the sample at a constant rate, $\dot{T}$, each temperature 'T' is related to a corresponding time 't' by $T - T_r = \dot{T}(t - t_r)$. This assigns the reference temperature, T_r, to a corresponding reference time, t_r. It introduces a time-dependence into eq. 8, and transforms it into,

$$N(t) = a\{\dot{T}(t - t_r)/T_r\}^2 \qquad \text{for } t_r \le t \le 0 \qquad (9)$$

This can be expressed as a rate (as needed in the model further below)

$$\dot{N}(t) = 2a(\dot{T}/T_r)^2(t - t_r) \qquad \text{for } t_r \le t \le 0 \qquad (10)$$

with $\dot{T}$ =9.7 K/min, T_r = 383.1 K, and t_r = -120 s, see Fig. 2.18 in the Appendix for the cooling rate, which was obtained from temperature calibration. When reaching the experimental temperature at t=0, this accumulates in a density of already existing nuclei

$$N_0 = a\dot{T}^2 t_r^{\,2}/T_r^2 \qquad (11)$$

at the beginning of the isothermal crystallization process.

- **Isothermal Nucleation**

Many more nuclei appear after having reached T_x and while maintaining the crystallization temperature T_x over an extended period, $t \ge 0$. An exponential rate-function, eq. 12, describes the measured nucleation density for this isothermal nucleation process, see Fig. 2.8.

$$\dot{N}(t) = ke^{-t/\lambda} \qquad \text{for } t \ge 0 \qquad (12)$$

k $=0.21\pm0.01$ #/(mm^{3}s) and λ = 105.4 ± 4.2 s are the specific rate of nucleation (nucleation rate per unit volume) at t=0 and a characteristic time associated with the slow-down of the rate of nucleation, respectively.

Equation 12 integrates to the nucleation density at time 't',

$$N(t) = N_0 + k\lambda(1-e^{-t/\lambda}) \qquad \text{for } t \geq 0 \qquad (13),$$

with $N_0 = N(t=0)$ from eq. 11.

- **Volume Fraction of Spherulites at Early Stages of Crystallization**

Measurements of t_{birth} $(\equiv t_i)$ and individual growth rate, $\dot{R}_i$, of spherulites as shown above provide the volume fraction occupied by growing spherulites (ϕ_{sph}),

$$\phi_{sph} = \frac{V_{sph}}{V_{sample}} = \frac{1}{V_{sample}}\sum_{i=1}^{n} V_i = \frac{4\pi}{3V_{sample}}\sum_{i=1}^{n} R_i^3 \quad \text{with } R_i = \dot{R}_i(t-t_i) \qquad (14).$$

Equation 14 for the volume fraction of spherulites does not account for the spherulitic impingement and is valid only at the early stages of crystallization. Instead of summing over all individual spherulites, we can use the nucleation density as described by eq. 10 and 12 for $t_r \leq t \leq 0$ and $t \geq 0$, respectively.

The rate of nucleation and the crystal growth rate define the growing volume fraction that the spherulites occupy $\phi_{sph}(t)$. This can be expressed as time-integral over the crystallization history

$$\phi_{sph}(t) = \int_{t_r}^{t} dt' \frac{4}{3}\pi\dot{R}^3(t-t')^3\dot{N}(t') \qquad (15).$$

Based on the experimental observation, Fig. 2.7, the growth rate $(\dot{R})$ is expressed by its average value. A more general expression is shown in the Appendix. For our experiment, the time-integral gets split into two regions for which the nucleation rate had been determined earlier:

$$\phi_{sph}(t) = \int_{t_r}^{0} dt' \frac{4}{3}\pi \dot{R}^3 (t-t')^3 \dot{N}(t') + \int_{0}^{t} dt' \frac{4}{3}\pi \dot{R}^3 (t-t')^3 \dot{N}(t') \qquad (16)$$

Using eq. 10 and 12 for nucleation rate, eq. 16 integrates to

$$\phi_{sph}(t) = \frac{2}{15} a\pi \dot{R}^3 \left(\frac{\dot{T}}{T_r}\right)^2 \left[(t-t_r)^5 - t^4(t-5t_r)\right] + \frac{4}{3}\pi \dot{R}^3 k\lambda \left[t^3 - 3\lambda t^2 + 6\lambda^2 t - 6\lambda^3 (1-e^{-t/\lambda})\right] \qquad (17)$$

This analytical model expression for the volume fraction compares well with the numerically interpolated volume fraction, eq. 14, in Fig. 2.9. It should be noted that eq. 14 makes use of individually measured growth rates whereas eq. 17 employs an average growth rate. The volume-averaged growth rate gives a better agreement with eq. 14 than the number-averaged growth rate.

An Avrami-type stretched exponential function, the so called Weibull Function, eq. 18, can be used to fit the interpolated spherulite volume fraction (eq. 14) beyond the spherical growth. It agrees quite well with the analytical volume fraction for the early stages up to ≈ 800 s, Fig. 2.9.

$$\phi_{sph}(t) = 1 - \exp\left\{-\left(\frac{t}{t_{W-\phi_{sph}}}\right)^{\beta_{\phi_{sph}}}\right\} \qquad ; t_{W-\phi_{sph}} = 932.5 \text{ s}, \beta_{\phi_{sph}} = 3.78 \qquad (18)$$

In addition, the Weibull function introduces an upper limit to the growth. Whereas interpolated as well as analytical volume fractions, obtained from nucleation kinetics, over predict the volume fractions due to lack of impingement considerations and thus, fail at longer times. It should be noted that the Avrami-type stretched exponential function can be used to describe crystal volume fraction in the sample (ϕ_{cry}) as well as volume fraction of spherulites in the sample (ϕ_{sph}). In this study, we find that such a function does not describe the ϕ_{cry} very well (Fig. 2.16 in The Appendix), especially during the early stages of crystallization, but it works well for ϕ_{sph} (Fig. 2.9).

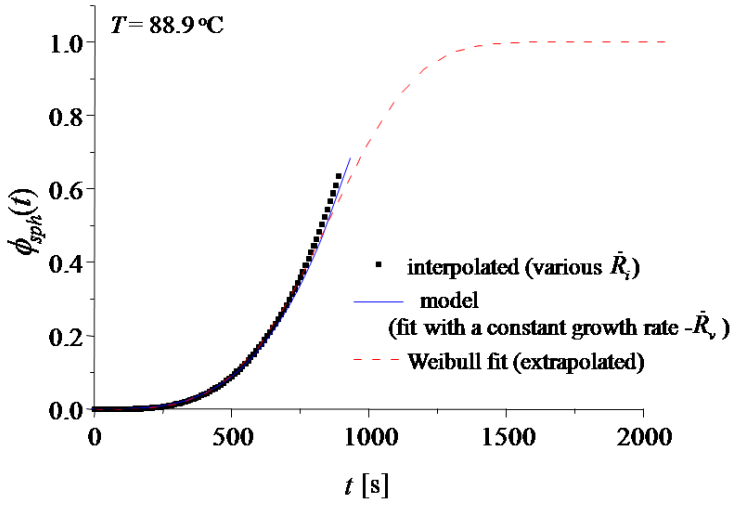

Figure 2.9 volume fraction of spherulites: dotted curve represents the volume fraction obtained from eq. 14. Smooth curve is the analytical expression, eq. 17, obtained using nucleation density information from Fig. 2.8. Dashed curve is the extrapolation on interpolated data using a Weibull function, eq. 18, with $t_{W-\phi_{sph}}$ = 932.5 s, $\beta_{\phi_{sph}}$ =3.78.

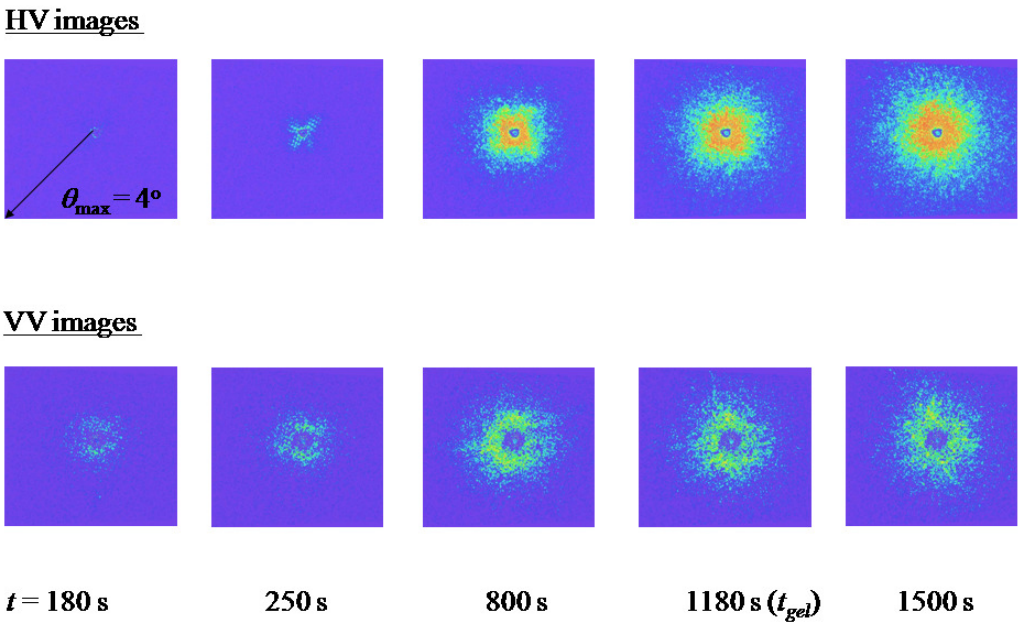

Figure 2.10 Small angle light scattering (SALS) images under cross-polars and parallel-polars for crystallizing isotactic poly-1-butene at 88.9 ^{o}C (beam size and position used for these measurements is shown in Fig. 2.5).

2.4.4 Light Transmission and SALS

The development of four-clover light scattering patterns (HV images), a characteristic of spherulitic morphology, is presented in Fig. 2.10. Scattering images under parallel-polars are shown as well. Images are corrected for the excess scattering (due to melt and stage windows) as well as the fluctuations in source intensity. The scattering and transmission measurements are done with a laser beam which is about 1 mm in diameter. The circular ring in Fig. 2.5 (optical micrograph at t = 800s) shows the relative size and the position of the laser beam with respect to the observation window and the spherulites. Such measurements are very sensitive to the location and count of the scatterers (spherulites) under the laser beam, in particular, when the nucleation density is not very high.

Light scattering invariants were calculated according to the areal integrals of eq. 1. The measured density fluctuation invariant goes through a maximum at about t = 250-400 s for six different measurements (Fig. 2.11). For a system consisting of anisotropic scatterers in an isotropic matrix with random orientation fluctuations, this maximum characterizes the instant when half of the sample volume is occupied by the scattering aggregates [36]. From optical microscopy, spherulites occupy about half of the sample volume at 800s, see Figs. 2.5 and 2.9. Spherulites are anisotropic aggregates of crystals in an isotropic melt, but orientation fluctuations in spherulites are nonrandom [36] due to the radial lamellar growth. This might be the origin of the mismatch between light scattering and optical microscopy measurements. Corresponding scattering images under cross-polar (Fig. 2.10) show a weak four clover pattern. Spherulites are far away from impingement at this characteristic time, see micrograph in Fig. 2.5. The four clover pattern diminishes as spherulites impinge and lose their spherical shape. The gel point comes much later when spherulites impinge more frequently. The cross-polar pattern further loses its four clover nature further confirming the significant impingement at the gel point. The normalized orientation fluctuation invariant ($Q_\delta(t)/Q_{\delta-\infty}$) grows with time and reaches a steady value within about 1600-2400 s. Due to growing inhomogeneities, the normalized parallel polar transmission intensity ($I_{HH}(t)/I_{HH-\infty}$) decreases and reaches a plateau in about 1600-1700 s. The HV pattern loses its four clover shape and becomes isotropic after this.

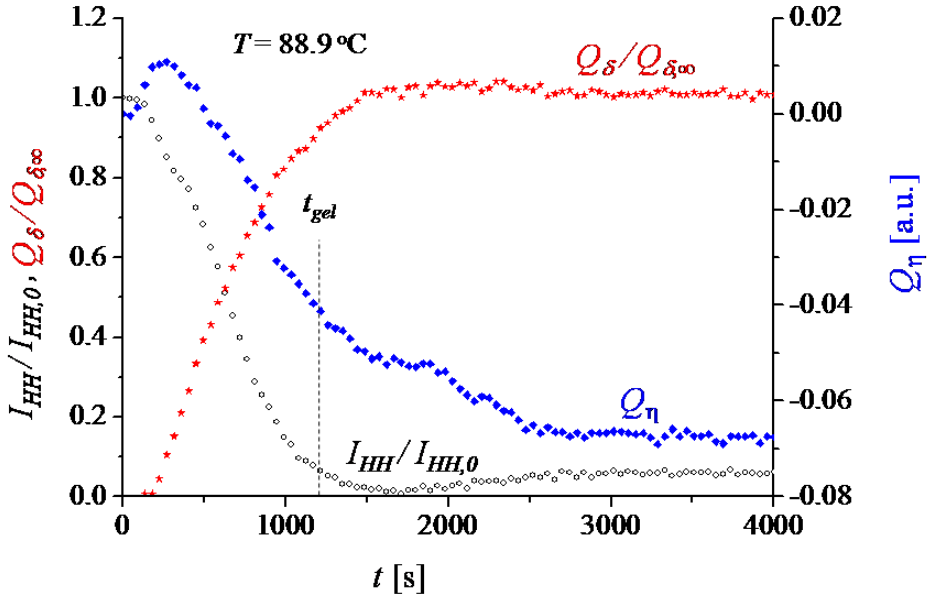

Figure 2.11 SALS and transmission measurements for crystallizing isotactic poly-1-butene and comparison to the instant of gelation. All measurements were performed at 88.9 °C. Invariants were calculated according to Stein-Wilson theory[36] for scattering from anisotropic aggregates with random orientation correlations.

A relative crystal volume fraction is calculated from SALS data as $0.886\sqrt{Q_\delta(t)/Q_{\delta-\infty}}$ and is compared with the relative crystal fraction obtain from DSC, Fig. 2.12 [36, 44]. Light scattering data is captured until 5000 s and relative crystallinity at that time, from DSC, is 0.886. Light scattering over-predicts the crystallinity for the early stages of crystallization. The formulation by Koberstein et al.[36] applies to ideal spherulites with perfect radial alignment of crystal optical axes and spherical boundaries. In real spherulites, the spherical boundaries are imperfect and crystal optical axes are not perfectly aligned. This might be the cause for the disagreement between crystallinity measurements by DSC and and by SALS, using the orientation fluctuation invariant.

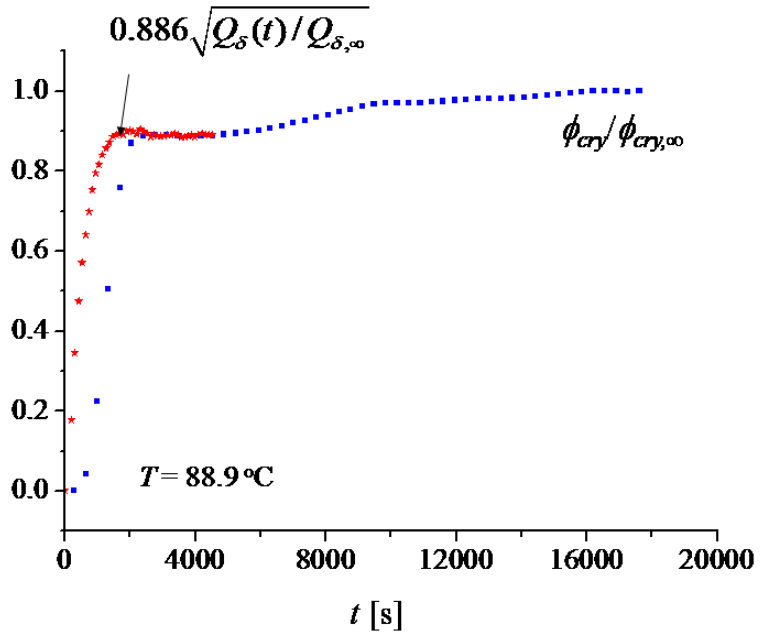

Figure 2.12 Relative crystal volume fraction from SALS (★) and DSC (■) for isothermal quiescent crystallization of iPB at 88.9 °C.

2.5 Discussion

2.5.1 Fluid-to-Solid Transition

Dynamic mechanical spectroscopy combined with optical microscopy and light scattering confirm the percolated nature of structure at fluid-to-solid transition for crystallizing isotactic poly-1-butene. At the microscopic level, the percolated structure is built by spherulites. The volume fraction of spherulites in the sample is clearly above 50% at the gel point, Fig. 2.5, though we only found 7-8 vol% crystal that gives rise to sample connectivity. Similar observations were made earlier for crystallizing polymers where fluid-to-solid transition was observed at very low crystal contents ranging from 1-5 vol% [21, 42, 45, 46]. This indicates that spherulites are certainly not equivalent to hard spheres and are mostly amorphous. In addition, due to their growth dynamics, spherulites are expected to be softer at the leading edge than in the interior. Secondary crystallization

within a growing spherulite furthers the crystallinity beyond primary crystallization. Thus spherulites are entities with a radial crystal gradient with highest crystallinity in the middle. Crystallization is an exothermic process. This might give rise to higher temperatures locally at the leading edge of spherulites and further softens the leading growth front.

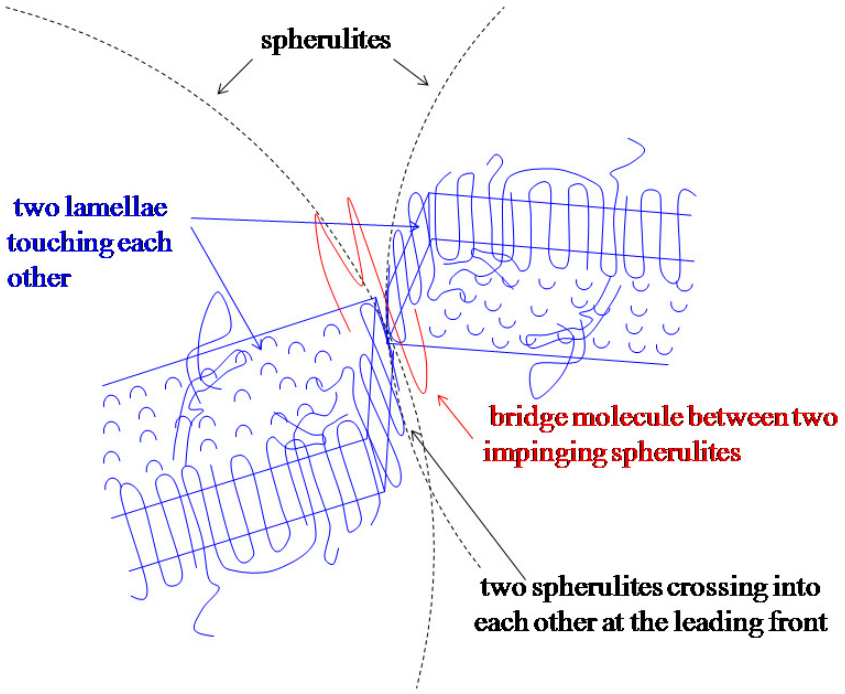

Figure 2.13 A schematic for a plausible mechanism for crystal connectivity at the interface between two impinging spherulites during crystallization of a semicrystalline polymer- contact and crossing among spherulites, network percolation by crystal lamellae and bridging by molecules.

Network percolation can also be viewed at the length scale of the spherulite-spherulites contact and its effect on the fluid-to-solid transition. When two neighboring spherulites are about to impinge, they compete for the same polymer chains and might end up sharing a macromolecular chain, thus forming a bridge molecule for network connectivity at molecular length scale, Fig. 2.13. Due to their soft nature at the leading growth front, chain-folded sheaf-like crystal lamellae, which are essentially 2D

nanosheets, might also cross into each other at the sperulite contact interface as shown schematically in Fig. 2.13. We anticipate that a combination of such phenomena, namely spherulite contact/ crossing, percolation among crystal lamellae and bridging molecules between spherulites, leads to network connectivity as required for solidification.

In comparison, a particle volume fraction of 3-4 % is sufficient to enable fluid-to-solid transition in aggregating suspensions [26]. It is interesting to find the same order of magnitude for the crystal volume fraction that enables the fluid-to-solid transition in the semicrystalline polymer.

It is worthwhile to notice the distinct behavior of $\tan\delta$, G' , and G'' before and after the gel point (Fig. 2.3). In the beginning, before having reached the gel point, $\tan\delta$ stays constant while G'' and G' are growing with time. As is typical for fluids, the measured $\tan\delta$ decreased at increased frequencies, but had values above unity due to the fluid (lossy) nature of the material. Small frequencies are probing the larger length scales, and for the mobile structure at this length scale, G'' is much higher than G'. The difference in G'' and G' reduces at higher frequencies, corresponding to the smaller length scales that govern the experiment.

At the gel point, where $\tan\delta$ becomes independent of frequency (at low probing frequencies), the $\tan\delta$ value is close to unity implying that material is as lossy as it is elastic. Having $\tan\delta$ near 1 at the gel point is exceptional, but it is a permitted value since $\delta = n\pi/2$ depends on the relaxation exponent n which might adopt values in the range $0<n<1$ (depending on the specific material of observation). Moduli are in the order of 10^4 Pa.

Across the gel point there is a drastic change in properties and soon after gel point (after t ~ 1300 s) G' and G'' become independent of frequency. Both the moduli increase and reach plateau values at t ~ 3000 s. Frequency independence of $G'(t)$ and $G''(t)$ suggests the presence of a structure that has the same response at all the length scales that are being probed. All these late-stage values of $tan\delta$ are < 1, which is typical for solids.

2.5.2 Crystallinity of Spherulites

The crystal volume fraction in the sample measured by DSC (ϕ_{cry}) and the volume fraction of spherulites in the sample (ϕ_{sph}), from optical microscopy, provide an estimate for the crystallinity inside spherulites, given by ϕ_{cry}/ϕ_{sph}. All the crystals are assumed to have formed inside the spherulites. Different expressions for the spherulite volume fraction (ϕ_{sph}) (eqs. 14, 17 and 18) are used to calculate the crystal volume fraction inside spherulites (ϕ_{cry}/ϕ_{sph}) and are compared in Fig. 2.14. There is a good agreement between calculated spherulite crystallinity values for interpolated, model and Weibull equations of volume fractions of spherulites, until $\approx$800 s. Interpolated and model values of ϕ_{sph} do not account for the impingement of spherulites and are expected to be suitable only at early stages.

Figure 2.14 compares the crystal volume fractions in sample (ϕ_{cry}) and in spherulites (ϕ_{cry}/ϕ_{sph}). Since all the crystals reside inside spherulites, the crystal fraction in spherulites is higher than the average crystal fraction in the entire sample before spherulites become volume filling. Once the whole sample is occupied by impinged spherulites, the average crystal fraction inside spherulites is the same as the sample crystallinity, Fig. 2.14.

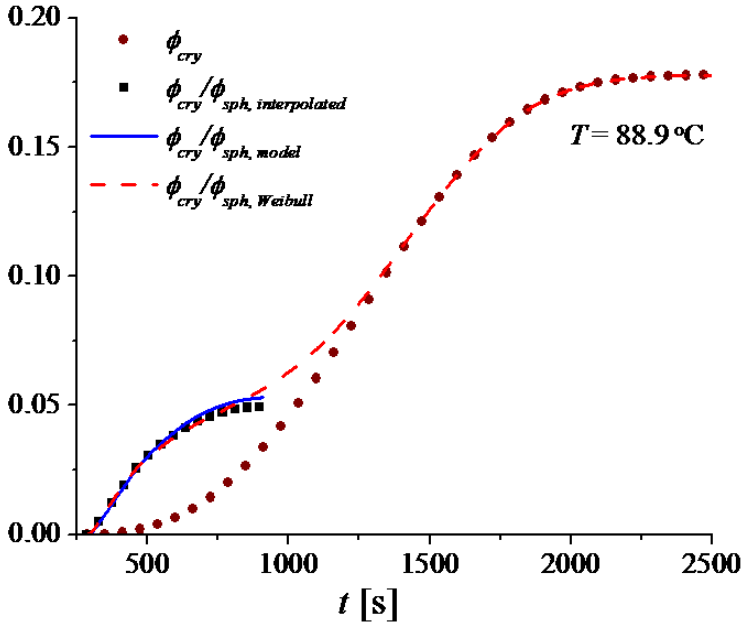

Figure 2.14 Crystal volume fraction inside spherulites (ϕ_{cry}/ϕ_{sph}) obtained from different expressions, dotted (▪) curve is from eq. 14, solid curve is from eq. 17 and the dashed line is from eq. 18. Crystal volume fraction (ϕ_{cry}) measured from DSC is also included for comparing sample crystallinity with spherulite crystallinity.

Crystal volume fraction in the sample (ϕ_{cry}) increases to 18% in the first 2500s and the entire sample fills with spherulites within 4000s, Fig. 2.4. Additional crystal growth beyond is due to the secondary crystallization [47, 48]. During the first 4000 s, crystal growth takes place by primary and secondary crystallization events [4, 44]. Such simple experiments combined with other structural tools such as X-ray scattering can provide us with knowledge to separate the effects of primary and secondary crystallization quantitatively.

It would be interesting to investigate the trends among various characteristic crystallization times obtained from rheology and optical measurements and correlate them with the corresponding morphologies. The correlation between crystallinity measurements from light scattering and DSC for quiescent crystallization at different

temperatures can provide a tool to measure insitu crystallinity for flow-induced crystallization.

2.6 Conclusions

Time-resolved mechanical and optical property measurements along with crystallinity and morphology help us understand the structure-property relations for crystallizing polymers. It was established that the fluid-to-solid transition takes place due to a percolating network structure, which is constituted of mostly amorphous spherulites. The crossing of crystal lamellae across spherulite interfaces and the presence of bridging chains between two spherulites is attributed to the network formation. An analytical expression for the growing volume fraction of spherulites was obtained from experimental measurements on nucleation density. The result agrees well with the empirical Avrami function for the early stages during crystallization.

2.7 Appendix

2.7.1 Time-Dependent Spherulite Growth

The spherulite growth rate is constant, at first, as shown by the isothermal crystallization experiments. However, nonisothermal conditions and variations between nuclei may cause the growth rate to vary, $\dot{R}(t,t')$, which needs to be accounted for in the spherulite volume fraction, ϕ_{sph}.

$$\phi_{sph}(t) = \int_{t_r}^{t} dt' \dot{N}(t') \frac{4\pi}{3} \left(\int_{t'}^{t} dt'' \dot{R}(t'',t') \right)^3$$

This expression can be simplified if the instantaneous growth rate depends on temperature only, $\dot{R}(t,t') = \dot{R}(T(t))$,

$$\phi_{sph}(t) = \int_{t_r}^{t} dt' \dot{N}(t') \frac{4\pi}{3} \left(\int_{t'}^{t} dt'' \dot{R}(T(t'')) \right)^3$$

with $\dot{R}$ =constant, this reduces to eq. 15 in the earlier analysis. The spherulitic growth ends when spherulites impinge and begin to lose their spherical symmetry.

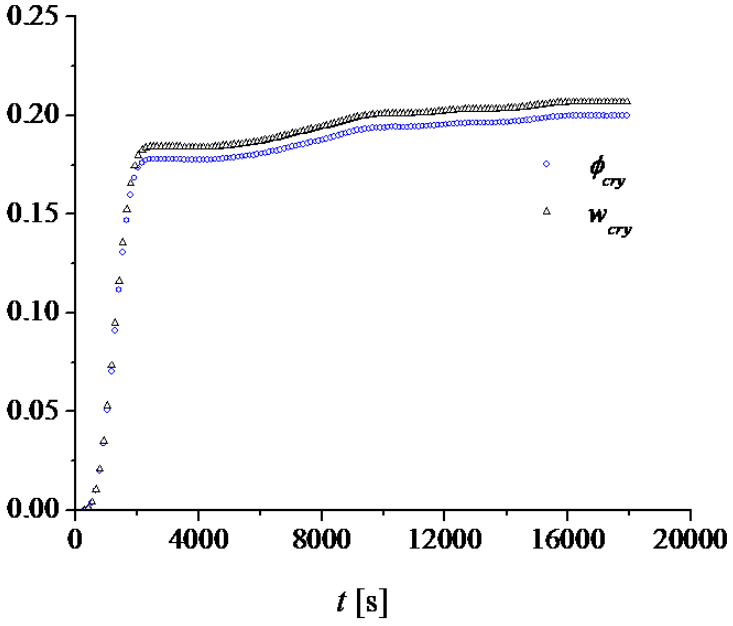

Figure 2.15 Crystal volume fraction (ϕ_{cry}) and crystal weight fraction (w_{cry}) in the sample from DSC for isothermal crystallization of iPB at 88.9 °C. Crystal weight fraction, $w_{cry}(t) = H(t)/H_{ideal\ crystal}$, was converted into crystal volume fraction in the sample (ϕ_{cry}), assuming a linear increase in sample density with crystal weight fraction, $\rho_{sam} = (\rho_{cry} - \rho_{amo}) w_{cry} + \rho_{amo}$.

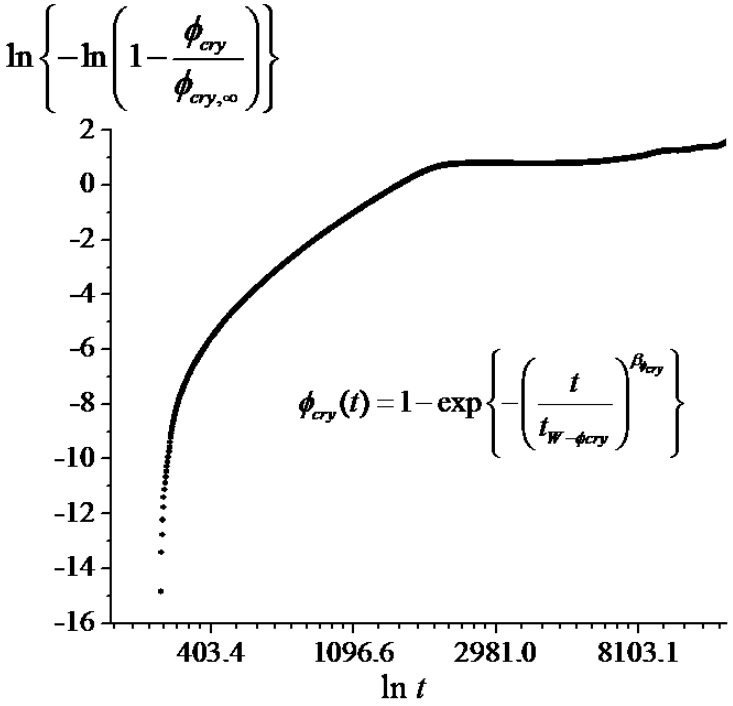

Figure 2.16 Crystal volume fraction (ϕ_{cry}) from DSC is replotted to confirm that the Avrami function can't describe the crystal growth for early stages (for first 500 s) for isothermal crystallization of iPB at 88.9 ^{o}C.

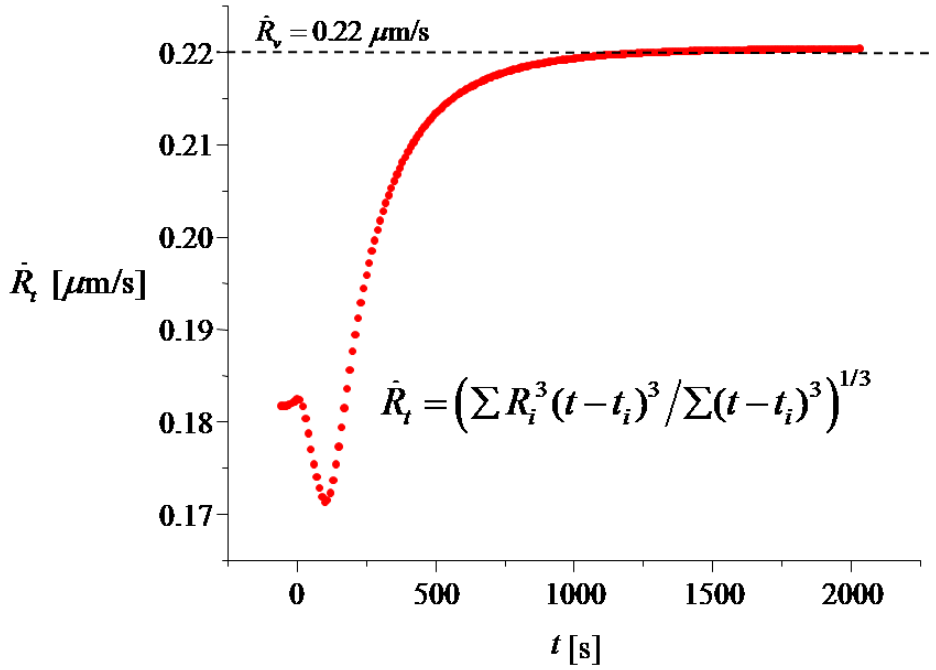

Figure 2.17 Time average growth rate for isothermal spherulitic growth of iPB at 88.9 °C. Interesting, $\dot{R}_t$ levels off at values that are close to the volume average growth rate, $\dot{R}_v = \left(\sum N_i R_i^3 / \sum N_i\right)^{1/3}$.

2.7.2 Temperature Calibration

Precalibrated K-type thermocouples (diameter 0.076 mm, length 0.92 m) were used to calibrate the optical unit as well as the rheometer for the experimental temperature profile. Thermocouple readings in Millipore ice water and boiling water were 0.2 °C and 100±0.2 °C, respectively.

- **Temperature Calibration for Optical Device**

Two 170 μm thick disks of isotactic poly-1-butene were prepared in optical cell, separately. One of them was reheated above melting point to position two thermocouples in it. One thermocouple was inserted close to the center (2.3 mm from center) and the other was close to the edge (11.4 mm from center), see Fig. 2.18 in The Appendix. Another disk was placed on the top of the first one. Final probe thickness was about 300

μm. Both the thermocouple wires were encircled within the sample few times before they were exposed to the air. The purpose was to minimize the heat transfer from wires to the atmosphere due to their fin-like effect. Temperature calibration curves along with the Linkam settings are shown in Fig. 2.18. As expected, the temperature close to the center of the geometry (dashed line with circles) was higher than the temperature at the edge (dotted line with triangles). Temperature at 7.5 mm (dash dot line with stars) from the center of parallel plate geometry, which is the center of the observation window, was obtained by assuming a linear variation in temperature with distance. A cooling rate of 9.7 K/min at 7.5 mm along with a gradient of 0.45 K/mm was found across the observation window.

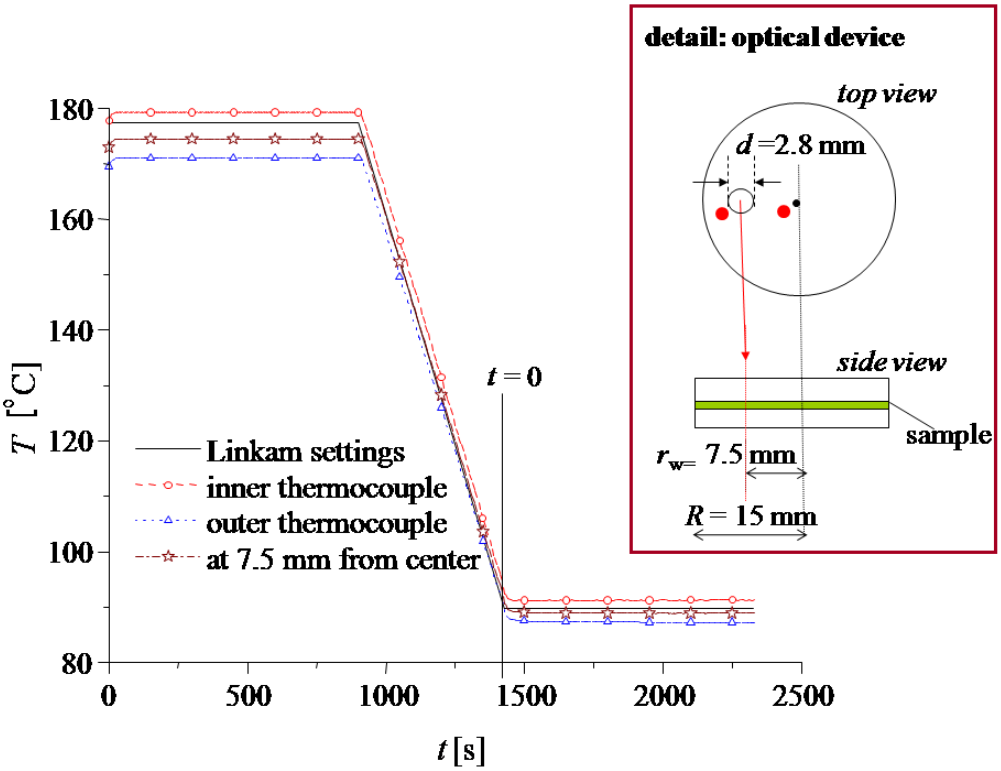

Figure 2.18 Temperature calibration for Linkam optical device (dots (•) in the detailed schematic of the optical device represent the thermocouple positions in the probe). Temperature at *r*=7.5 mm, center of the observation window, was obtained by linear interpolation of inner and outer thermocouple readings. Experimental time *t*=0 is shown in the plot.

- **Temperature Calibration for the Rheometer**

Calibration was performed with 25 mm parallel plate disks. The probe used for optical cell was cut to a size of 25 mm and was thickened to about 900 µm by adding two layers each of 300 µm on each side. Calibration is presented in Fig. 2.19 in the Appendix.

DSC was calibrated for the cooling and heating rates of 10K/min according to the procedure described by TA Instruments.

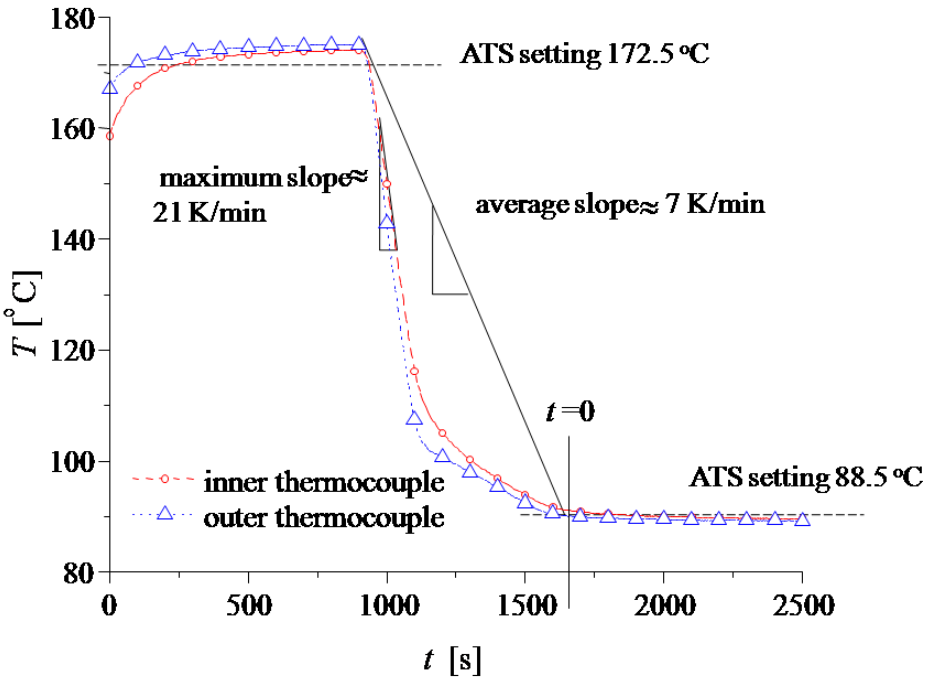

Figure 2.19 Temperature calibration for rheometer with 25 mm parallel plates. Inner and outer thermocouple readings are plotted and the rheometer settings are shown by dashed lines. Experimental time *t*=0 is shown in the plot.

2.8 References

[1] Hoffman JD, Miller RL: Kinetics of crystallization from the melt and chain folding in polyethylene fractions revisited: Theory and experiment, Polymer 38 (1997) 3151-3212.

[2] Sadler DM, Gilmer GH: A model for chain folding in polymer crystals - rough growth faces are consistent with the observed growth-rates, Polymer 25 (1984) 1446-1452.

[3] Gedde UW: Crystalline polymers, Polymer physics, London (1995).

[4] Strobl GR: Metastable partially crystalline states, The physics of polymers, Berlin (1997).

[5] Keller A: Polymer crystals, Reports on Progress in Physics 31 (1968) 623-704.

[6] Heeley EL, Maidens AV, Olmsted PD, Bras W, Dolbnya IP, Fairclough JPA, Terrill NJ, Ryan AJ: Early stages of crystallization in isotactic polypropylene, Macromolecules 36 (2003) 3656-3665.

[7] Wurm A, Soliman R, Schick C: Early stages of polymer crystallization - a dielectric study, Polymer 44 (2003) 7467-7476.

[8] Soccio M, Nogales A, Lotti N, Munari A, Ezquerra TA: Evidence of early stage precursors of polymer crystals by dielectric spectroscopy, Physical Review Letters 98 (2007) 1-4.

[9] Nishida K, Kaji K, Kanaya T, Matsuba G, Konishi T: Spinodal patterns indicating unstable regime of polymer crystallization, Journal of Polymer Science Part B-Polymer Physics 42 (2004) 1817-1822.

[10] Olmsted PD, Poon WCK, McLeish TCB, Terrill NJ, Ryan AJ: Spinodal-assisted crystallization in polymer melts, Physical Review Letters 81 (1998) 373-376.

[11] Panine P, Di Cola E, Sztucki M, Narayanan T: Early stages of polymer melt crystallization, Polymer 49 (2008) 676-680.

[12] Elmoumni A, Gonzalez-Ruiz RA, Coughlin EB, Winter HH: Isotactic poly(propylene) crystallization: Role of small fractions of high or low molecular weight polymer, Macromolecular Chemistry and Physics 206 (2005) 125-134.

[13] Pogodina NV, Lavrenko VP, Srinivas S, Winter HH: Rheology and structure of isotactic polypropylene near the gel point: Quiescent and shear-induced crystallization, Polymer 42 (2001) 9031-9043.

[14] Acierno S, Grizzuti N, Winter HH: Effects of molecular weight on the isothermal crystallization of poly(1-butene), Macromolecules 35 (2002) 5043-5048.

[15] Gedde UW: Crystallization kinetics, Polymer physics, London (1995).

[16] Keller A: Reminiscences on the discovery of chain folded single crystals, Polymer 41 (2000) 8751-8754.

[17] Hikosaka M, Amano K, Rastogi S, Keller A: Lamellar thickening growth of an extended chain single crystal of polyethylene .1. Pointers to a new crystallization mechanism of polymers, Macromolecules 30 (1997) 2067-2074.

[18] Shangguan YG, Song YH, Zheng Q: A query on crystallization temperature-dependent cooling function under nonisothermal condition, Journal of Polymer Science Part B-Polymer Physics 44 (2006) 795-800.

[19] Mours M, Winter HH: Relaxation patterns of nearly critical gels, Macromolecules 29 (1996) 7221-7229.

[20] Chen Q, Fan YR, Li WC, Zheng Q: Rheological properties of liquid-solid transition in isothermal crystallization for high-density polyethylene, Chemical Journal of Chinese Universities-Chinese 27 (2006) 365-368.

[21] Gelfer M, Horst RH, Winter HH, Heintz AM, Hsu SL: Physical gelation of crystallizing metallocene and ziegler-natta ethylene-hexene copolymers, Polymer 44 (2003) 2363-2371.

[22] Schwittay C, Mours M, Winter HH: Rheological expression of physical gelation in polymers, General Discussion on Gels (1995) 93-104.

[23] Winter HH: Polymer gels, materials that combine liquid and solid properties, MRS Bulletin 16 (1991) 44-47.

[24] Lin YG, Mallin DT, Chien JCW, Winter HH: Dynamic mechanical measurement of crystallization-induced gelation in thermoplastic elastomeric poly(propylene), Macromolecules 24 (1991) 850-854.

[25] Wilkins GMH, Spicer PT, Solomon MJ: Colloidal system to explore structural and dynamical transitions in rod networks, gels, and glasses, Langmuir 25 (2009) 8951-8959.

[26] Xu XM, Tao XL, Gao CH, Zheng Q: Studies on the steady and dynamic rheological properties of poly(dimethyl-siloxane) filled with calcium carbonate based on superposition of its relative functions, Journal of Applied Polymer Science 107 (2008) 1590-1597.

[27] Lima MD, Andrade MJ, Skakalova V, Bergmann CP, Roth S: Dynamic percolation of carbon nanotubes in liquid medium, Journal of Materials Chemistry 17 (2007) 4846-4853.

[28] Surve M, Pryamitsyn V, Ganesan V: Polymer-bridged gels of nanoparticles in solutions of adsorbing polymers, Journal of Chemical Physics 125 (2006) 1-12.

[29] Raimo M: "Kinematic" Analysis of growth and coalescence of spherulites for predictions on spherulitic morphology and on the crystallization mechanism, Progress in Polymer Science 32 (2007) 597-622.

[30] Wang ZG, Hsiao BS, Sirota EB, Agarwal P, Srinivas S: Probing the early stages of melt crystallization in polypropylene by simultaneous small- and wide-angle x-ray scattering and laser light scattering, Macromolecules 33 (2000) 978-989.

[31] Misra A, Prudhomm.Re, Stein RS: Distribution of spherulites in a polyethylene sample, Journal of Polymer Science Part B-Polymer Physics 12 (1974) 1235-1238.

[32] Kalay G, Kalay CR: Structure and physical property relationships in processed polybutene-1, Journal of Applied Polymer Science 88 (2003) 814-824.

[33] Kaszonyiova M, Rybnikar K, Geil PH: Polymorphism of isotactic poly(butene-1), Journal of Macromolecular Science-Physics B44 (2005) 377-396.

[34] Azzurri F, Gomez MA, Alfonso GC, Ellis G, Marco C: Time-resolved saxs/waxs studies of the polymorphic transformation of 1-butene/ethylene copolymers, Conference on Synchrotron Radiation in Polymer Science II (2002) 177-189.

[35] Azzurri F, Flores A, Alfonso GC, Calleja FJB: Polymorphism of isotactic poly(1-butene) as revealed by microindentation hardness. 1. Kinetics of the transformation, Macromolecules 35 (2002) 9069-9073.

[36] Koberstein J, Russell TP, Stein RS: Total integrated light-scattering intensity from polymeric solids, Journal of Polymer Science Part B-Polymer Physics 17 (1979) 1719-1730.

[37] Hadinata C, Gabriel C, Ruellman M, Laun HM: Comparison of shear-induced crystallization behavior of pb-1 samples with different molecular weight distribution, Journal of Rheology 49 (2005) 327-349.

[38] Bonn D, Coussot P, Huynh HT, Bertrand F, Debregeas G: Rheology of soft glassy materials, Europhysics Letters 59 (2002) 786-792.

[39] Winter HH, Mours M: Rheology of polymers near liquid-solid transitions, Neutron spin echo spectroscopy viscoelasticity rheology, Berlin (1997).

[40] Winter HH: Sharing the world's advanced rheology knowledge through rheo-hub, 15th International Congress on Rheology/80th Annual Meeting of the Society-of-Rheology (2008) 1387-1389.

[41] Mours M, Winter HH: Time-resolved rheometry, Rheologica Acta 33 (1994) 385-397.

[42] Pogodina NV, Winter HH: Polypropylene crystallization as a physical gelation process, Macromolecules 31 (1998) 8164-8172.

[43] Filippone G, Netti PA, Acierno D: Microstructural evolutions of ldpe/pa6 blends by rheological and rheo-optical analyses: Influence of flow and compatibilizer on break-up and coalescence processes, Polymer 48 (2007) 564-573.

[44] Akpalu Y, Kielhorn L, Hsiao BS, Stein RS, Russell TP, van Egmond J, Muthukumar M: Structure development during crystallization of homogeneous copolymers of ethene and 1-octene: Time-resolved synchrotron x-ray and sals measurements, Macromolecules 32 (1999) 765-770.

[45] Horst RH, Winter HH: Stable critical gels of a copolymer of ethene and 1-butene achieved by partial melting and recrystallization, Macromolecules 33 (2000) 7538-7543.

[46] Horst RH, Winter HH: Stable critical gels of a crystallizing copolymer of ethene and 1-butene, Macromolecules 33 (2000) 130-136.

[47] Wutz C, Bark M, Cronauer J, Dohrmann R, Zachmann HG: Simultaneous measurements of small-angle x-ray-scattering, wide-angle x-ray-scattering, and light-scattering during phase-transitions in polymers, Review of Scientific Instruments 66 (1995) 1303-1307.

[48] Kolb R, Wutz C, Stribeck N, von Krosigk G, Riekel C: Investigation of secondary crystallization of polymers by means of microbeam x-ray scattering, Polymer 42 (2001) 5257-5266.

CHAPTER 3

CRITERIA FOR SHEAR-INDUCED CRYSTALLIZATION: STRAIN AND WEISSENBERG NUMBER

3.1 Abstract

The effect of strain, Weissenberg number ($We = \dot{\gamma}\lambda_{mat}$) and specific mechanical work ($w = \eta\dot{\gamma}^2 t_s$) on rate of crystallization (nucleation followed by growth) and on growth of anisotropy was studied for shear-induced crystallization of isotactic poly-1-butene. Small angle light scattering (SALS), transmission intensity measurements and optical microscopy were the experimental techniques used. The samples were sheared for a finite strain at the beginning of the experiment and then crystallized without further flow (Janeschitz-Kriegl protocol). Shear conditions were varied as *We* = 0 to 12.5 and strains up to 200. Spherulitic growth was observed under quiescent conditions (*We* = 0) and at small strains and *We*. Strain requirements to attain steady state/ leveling off of the rate of crystallization were found to be much larger than the strain needed to achieve steady state of flow. Strain effects on nucleation density and so on the rate of crystallization were found to be tremendous even for few strain units, as far as shearing was performed with $We >> 1$. For $We \approx 1$, near the transition to shear thinning, even the large strains up to 180 could not enhance nucleation density significantly. The large strain and $We > 1$ criteria were also observed for morphological transition from spherulitic growth to oriented growth. The strain requirements for oriented growth and the steady value of rate of crystallization became less and less for higher *We* indicating a criterion based on specific mechanical work. *We* can be interpreted as the memorized strain by the

material with a relaxation time of λ_{mat}. It captures the interplay between rate of molecular relaxation ($1/\lambda_{mat}$) and rate of producing orientation ($\dot{\gamma}$).

3.2 Introduction

Flow-induced orientation in undercooled melts controls the optical and mechanical properties of a polymer product and is frequently encountered in polymer processes such as film blowing and injection molding. The processing of semicrystalline polymers would greatly be helped by a quantitative relation between shear flow parameters such as Weissenberg number (*We*), Deborah number (*De*), stress, strain, shear rate, mechanical work etc. and the microstructure length scales such as shish thickness, shish spacing, kebab spacing etc. that ultimately govern the final product properties. Flow effects on crystallization are frequently investigated in terms of the rate of crystallization (characteristic crystallization time) and the morphological changes. Our focus is to investigate the effect of strain, *We* and specific mechanical work on the rate of crystallization and the morphological transition to oriented growth.

Crystallization in semicrystalline polymers takes place by nucleation and growth. Thus rate of crystallization can be altered by affecting the nucleation density and/or the growth rate. Flow affects the nucleation density tremendously [1, 2] though its effect on growth rate, although not studied quite extensively, is presumably insignificant [3, 4]. The morphological transition to oriented growth is not a requirement to fasten rate of crystallization which can be enhanced solely by increasing the nucleation density. On the other hand the morphological transition to oriented growth is a consequence of material relaxation/ response to the prescribed flow conditions.

3.2.1 Rate of Crystallization

Application of flow aligns the polymer chain segments in the shear direction and brings them closer to their final lattice configuration in a crystalline state, where chains are extended compared to their random coil configuration in a melt. The most stable thermodynamic form of a crystal would be the one with chains completely extended and this has been observed for small molecular weight olefins [5, 6]. In case of crystals from polymer melts such complete chain extension has never been observed due to the kinetic nature of crystallization resulting in crystals with finite thickness which is significantly less than the fully extended chain [6, 7]. Crystal thickening in polymers upon annealing is an evidence that the chains prefer to be in fully extended form upon crystallization. The free energy change during crystallization is,

$$\Delta G = \Delta H - T\Delta S \,. \qquad (1)$$

Assuming that the melt is in thermodynamic equilibrium with the lowest energy crystal form with fully extended chains, the free energy change during crystallization will be zero just as it is zero for equilibrium melting. The crystallization temperature in this case would be equal to the equilibrium melting temperature ($T_m^{\,0}$) of the polymer. Thus the free energy change is,

$$G_{crystal} - G_{melt} = \left(H_{crystal} - H_{melt}\right) - T_m^{\,0}\left(S_{crystal} - S_{melt}\right) = 0 \,. \qquad (2)$$

The equilibrium melting temperature is,

$$T_m^{\,0} = \left(H_{melt} - H_{crystal}\right) \Big/ \left(S_{melt} - S_{crystal}\right) . \qquad (3)$$

The enthalpy change (H_{melt}-$H_{crystal}$) and the entropy change (S_{melt}-$S_{crystal}$) are positive terms. Flow produces orientation in the melt and thus reduces its entropy (S_{melt}) and so the entropy difference (S_{melt}-$S_{crystal}$). This in turn increases the equilibrium melting

temperature (T_m^0) of the polymer and so the driving force for crystallization resulting in higher nucleation density and the faster crystallization rates.

An enormous increase in nucleation density was observed by Janeschitz [1, 2, 8, 9] even at moderate strains and shearing conditions for iPP. Nucleation density increased by an order of decade for a mechanical work of 1 MPa at low undercooling. An extreme degree of undercooling was required in order to get similar increase in nucleation density for the same melt. For larger works of up to 6 MPa, an increase of up to six decades was observed while retaining the isotropic growth. It was also monitored that the rate of formation of primary nuclei was proportional to the work applied per unit volume (specific work). Also the increase in nucleation density, with mechanical loads or shearing times, was highly nonlinear.

It is well established that spherulitic growth rate (dR/dt) remains constant with time under isothermal conditions as far as spherulites are away from impingement [6]. Rate of spherulitic growth goes through a maximum with temperature [5, 10] for quiescent crystallization. However the flow effects on growth rate are presumably small. Large enough strains result in oriented row-nucleated structures. Recently Hsiao and coworkers [11] observed a diffusion controlled kebab growth for ultra high molecular weight polyethylene (UHMWPE) i. e. $G(t) \sim t^{-1/2}$ where $G(t)$ is growth rate of kebab, unlike spherulitic growth rate which remains constant with time. These studies were performed with a blend of UHMWPE (2 wt %) in a noncrystallizable polyethylene matrix. This type of growth rate dependence might appear due to the lack of crystallizable material as well.

3.2.2 Morphology and Crystal Growth Mechanism

Spherulites are formed by growth of crystal lamellae to point like nuclei under quiescent or mild flow conditions. Formation of a spherulitic object from a point like nucleus occurs due to the branching of a growing lamella that start to grow in different directions while retaining the radial growth [6, 12]. Application of shear affects the morphology. Strong enough shearing gives rise to highly oriented shish-kebab structures [6, 11, 13-16]. The mechanism of formation of these oriented structures is still an unresolved matter. It was proposed by Keller that application of flow orients the polymer chains in flow direction and bundles them together giving rise to linear nuclei (linear crystalline structures), also termed as shish. Growth phase involves folded-chain lamellar growth on these linear nuclei in form of kebabs that grow epitaxially on the shish [16].

How does the morphological transition take place from spherulitic to shish kebab growth? How do morphologies evolve for intermediate shearing? These are few of the questions that need to be addressed to understand structure development. Janeschitz observed elongated structures made from coalescence of growing spherulites [2]. He also noticed that isotropic growth can result from oblong precursors if they are far apart under mild shearing [2, 17].

Role of high molecular weight chains in forming row nucleated structures is crucial and still debatable. Kimata et at. [18, 19] observed that the fraction of long chains in the shish crystals was same as their bulk fraction stating that shish formation does not include only the long chains and the process of formation of elongated structures does not have any propensity for long chains. It is observed that increasing long chain content

increases the content of shish crystals as well as enhances the rate of formation of row nucleated structures [11, 16, 20].

Whether complete chain stretch is required for shish or not, is a topic requiring further research. Simulations by Dukovski et al. [21] indicate that a coil-stretch transition is essential for shish formation. These simulations show two different populations of chains even for monodisperse chains under elongation flow - stretched and coiled, contributing to the formation of shish and kebab respectively. According to Meerveld [22] stretching of high molecular weight chains is required for shish-kebab growth and chain orientation alone is not sufficient to produce elongated structures. The recoverable strain-based model by Peters et al. [23] suggests that the segmental orientation of high molecular weight tail is considered as the driving force for flow-induced crystallization.

Dimensions of shish-kebab morphology were measured by Hobbs and coworkers [13, 24] for a processed polyethylene using AFM. Shish thickness was around 9nm whereas kebabs were thicker (~ 50 nm). It was also observed that kebabs were not equally spaced on a backbone (shish). Presence of micro and macro shish kebab within a same stem is also observed [6]. From these measurements, one may speculate on the size of nuclei that should be a bundle of chains arranged in a cylindrical geometry with a dia of ~ 9nm and length of ~50 nm. It also suggests that flow-induced crystallization might be a good technique to measure size of nuclei or the critical size and orientation needed for nucleation to start.

3.2.3 Processing Parameters for Flow-induced Crystallization

Effect of stress (τ), shear rate ($\dot{\gamma}$), strain (γ), Weissenberg number (*We*), Deborah number (*De*) and mechanical work is frequently studied on rate of crystallization as well

as morphology. Weissenberg number, eq4, is the product of a material relaxation time (λ_{mat}) and the applied shear rate and can be interpreted as the memorized strain by the material.

$$We = \dot{\gamma}\lambda_{mat}$$
$$We \leq 1 \text{ steady shear viscosty} \qquad (4)$$
$$We > 1 \text{ shear thinning region}$$

For small memorized strains polymer melts exhibit linear viscoelastic behavior resulting in steady viscosity. Larger memorized strains correspond to nonlinear rheology. Thus the $We = 1$ captures the transition to nonlinearity which in case of most polyolefins is a transition to shear thinning region.

On the other hand, Deborah number, eq5, is the ratio of a material relaxation time (λ_{mat}) to the experimental time. Shearing duration (t_s) serves as the experimental time in case of preshearing experiments.

$$De = \lambda_{mat} / t_s$$
$$De > 1 \text{ start up of flow} \qquad (5)$$
$$De < 1 \text{ steady state for flow}$$

Deborah number characterizes the steady state of the flow and for $\lambda_{mat} > t_s$, flow is still in the start up phase due to material memory. Steady state is reached for $\lambda_{mat} << t_s$.

Shear strain for a constant shear rate experiment is,

$$\gamma = \dot{\gamma} t_s = \dot{\gamma}\lambda_{mat}\frac{t_s}{\lambda_{mat}} = \frac{We}{De} \qquad (6).$$

Specific mechanical work (work per unit volume) is,

$$w = \int_0^{t_s} d\gamma.\tau = \int_0^{t_s} d\gamma.\eta\dot{\gamma} = \int_0^{t_s} dt.\eta\dot{\gamma}^2 \qquad (7).$$

For constant shear rate and steady viscosity experiments,

$$w = \eta\dot{\gamma}^2 t_s = \eta\dot{\gamma}^2 \lambda_{mat}^2 \frac{t_s}{\lambda_{mat}^2} = \frac{\eta}{\lambda_{mat}} \frac{We^2}{De} \qquad (8).$$

It is interesting to notice how strain and specific mechanical work are related to the material properties and dimensionless numbers.

Vleeshouwers [25] and Hadinata [26] observed a shear rate criterion for rate of crystallization. Crystallization half time reaches a plateau value for iPP for a shearing duration of about 4s and wall stress of 0.06 MPa [27]. Kornfield needed a critical stress to observe threadlike precursors for a pressure driven flow. Meerveld used a criterion based on *We* to explain the state of a polymer chain under different flow regimes and morphological transition to oriented growth for flow-induced crystallization [22]. Two different *We* were defined associated with reptation and stretching of a chain. Janeschitz [28] observed oriented morphologies at large mechanical loads in the order of 25 MPa.

Large strains in the order of 1000 were needed to observe oriented growth in PE [29]. An underlying strain criterion was observed for iPP at *We* = 1 by Elmoumni et al [4] for the rate of crystallization. Crystallization rate leveled off for a very large value of strain of 600 at this *We*. It was suggested that for elongated growth *We* > 1. Here *We* was defined as the product of shear rate and cross over time from rheology [4, 30]. Importance of interplay between material relaxation time and shear rate is shown for poly-1-butene as well [26].

Here we extend this study to higher *We* and to another semicrystalline polymer, iPB. It is our objective to study the effect of strain, *We* and mechanical work on crystallization dynamics and identify the criteria for crystallization rate and morphological transition.

3.3 Experimental

3.3.1 Material and Sample Preparation

Isotactic poly-1-butene (iPB), from Basell, with M_w = 176000 g/mol and M_w/M_n of 5.7, served as test material. Pellets of iPB (as obtained from Basell) were compression molded into thick sheets, from which samples were cut for Differential Scanning Calorimetry (DSC), rheometry and optical measurements. The iPB was used without a nucleating agent.

Differential scanning calorimetry (DSC) was carried out under nitrogen in a DSC Q1000 (TA Instruments) using standard aluminum pans (from TA instruments) 6 mm in diameter and weighing about 24 mg. It was calibrated using Indium (T_m = 156.60, standard heat = 28.71 J/g) as a standard [31]. A thin sample (about 12 mg) was pressed into a DSC pan and heated above melting temperature to establish uniform contact between polymer and pan. For the DSC measurements, samples were heated as well as cooled at 10K/min. First melting, second melting, and crystallization peaks were observed at 123 ^oC (100-130 ^oC), 111 ^oC (100-120 ^oC), and 53 ^oC, respectively (Fig. 3.1). First melting belongs to the crystal FormI of iPB, which has a density of 950 Kg/m^3 and is a thermodynamically stable form. Second melting belongs to FormII that is less dense (907 Kg/m^3) than FormI and is a kinetically favored crystal form. FormII transforms into FormI within 7-12 days at room temperature and atmospheric pressure [32-35].

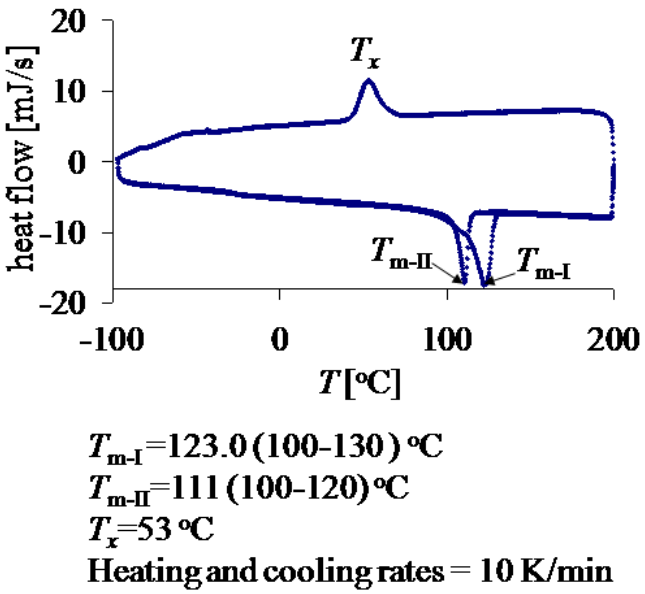

Figure 3.1 Differential scanning calorimetry of iPB. T_{m-I} and T_{m-II} are the peak melting temperatures for formI amd formII and are observed during first and second heating, respectively. T_x is the crystallization temperature during cooling. Heating and cooling rates are 10K/min.

For rheology, a 2mm thick disk-shaped sample was inserted between the parallel disk fixtures (diameter 25 mm) of a torque-controlled rheometer (Stresstech of ATS Rheosystems). It was calibrated for temperature using iPB, the polymer used in this study. For detailed description of the calibration refer to the Appendix in Arora et al. [36]. It was heated above melting point and then compressed to a thickness of about 1 mm to establish uniform contact between the sample and rheometer plates. *G'-G''* data from isothermal frequency sweeps at T = 85, 87.1, 89.1, 90.2, 95.2, 100.4, 110.5, 120.8, 131.2, 141.3, 151.7, and 161.5 °C were merged into a master curves at 98.9 °C (Fig. 3.2). The shear measurements were performed in the linear viscoelastic region. The master curve was used to obtain discrete relaxation modes and a continuous relaxation spectrum as described by Winter and Mours [37]. Figure 3.4 presents the steady viscosity Vs shear rate plot obtained using Cox-Merz [38]. Cross-over to shear-thinning takes place at a

shear rate of 0.8 s^{-1}. It is argued that the Cox-Merz works only in the linear viscoelastic region and it predicts the transition to shear-thinning quite well. The shear-thinning behavior usually is more pronounced from steady viscosity measurements. Carreau-Yasuda model, eq9, [39] describes the shear thinning behavior quite well. Corresponding Carreau-Yasuda parameters are shown in table3.1.

$$\eta(\dot{\gamma}) = A_1 + \frac{A_0 - A_1}{\left((1+(A_2\dot{\gamma})^{A_4}\right)^{A_3/A_4}} \qquad \text{Carreau-Yasuda model} \qquad (9)$$

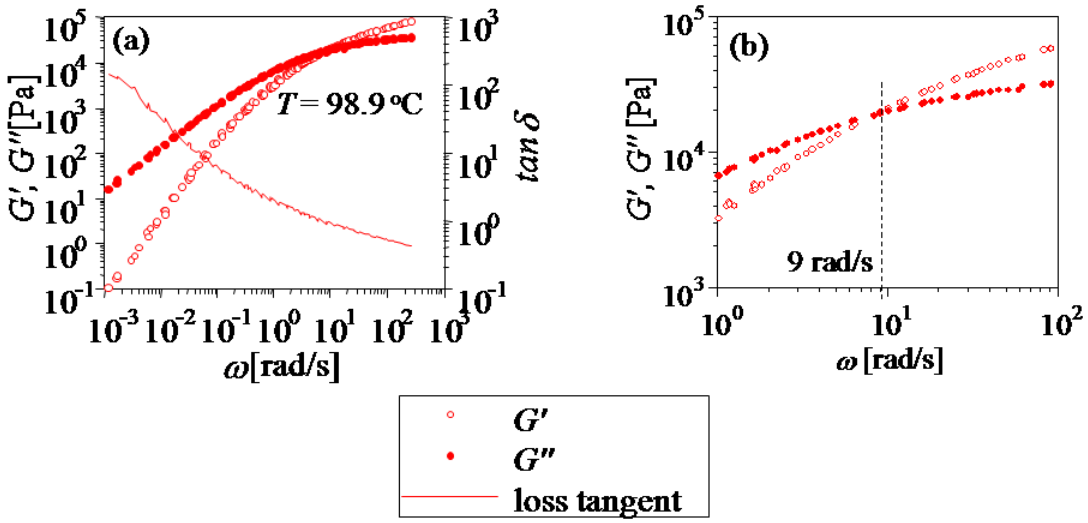

Figure 3.2 (a) Master curve for iPB melt at experimental temperature of 98.9 °C obtained by *t-T* superposition from isothermal frequency sweeps at *T* = 85, 87.1, 89.1, 90.2, 95.2, 100.4, 110.5, 120.8, 131.2, 141.3, 151.7 and 161.5 °C. (b) Cross-over between *G'* and *G''* at a frequency of 9 rad/s at 98.9 °C.

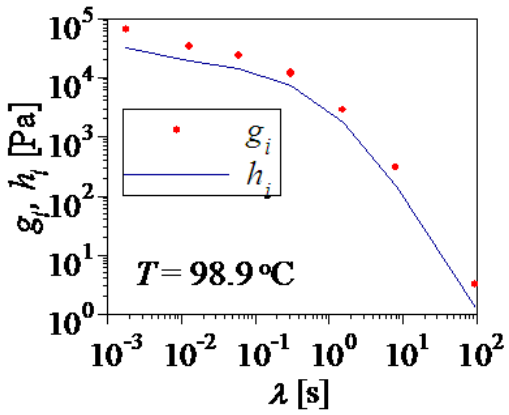

Figure 3.3 Discrete (g_i) and continuous relaxation (h_i) spectrums for iPB obtained from the master curve at 98.9 °C (seven relaxation modes were used to describe the $G'(\omega)$,$G''(\omega)$ behavior).

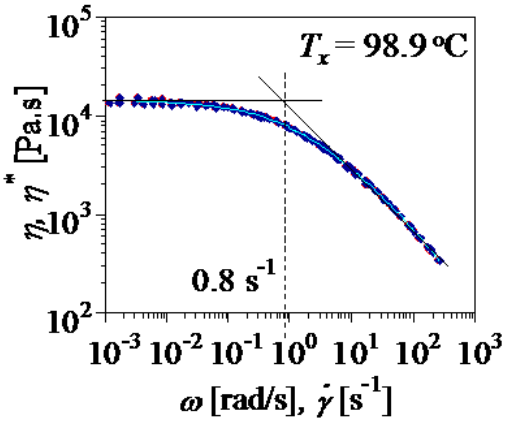

$$\lambda_{mat} = 1/0.8 = 1.25\ s$$

$\dot{\gamma}$ (s^{-1})	$We = \dot{\gamma}\lambda_{mat}$
1	1.25
7	8.75
10	12.5

Figure 3.4 Complex viscosity (η^*) Vs frequency (ω) plot for iPB at 98.9 °C obtained from the master curve. Cox-Merz relation provides the steady viscosity (η) Vs shear rate ($\dot{\gamma}$) curve from η^* Vs ωplot. Continuous line on the top of discrete points is the Carreau-Yasuda fit (parameters are shown in table3.1). The broken line shows the shear rate used to define a characteristic material relaxation time for the shear flow (λ_{mat}). Shear rates employed in this work and corresponding *We* are shown as well.

Table 3.1 Carreau-Yasuda parameters for iPB at 98.9 °C.

A0	1.4105×10^{4}
A1	-9.55×10^{1}
A2	7.66×10^{-1}
A3	6.56×10^{-1}
A4	6.31×10^{-1}

For optical measurements, a 2 mm thick disk shaped sample was placed between the parallel plates of an optical device (CSS 450 from Linkam Scientific). There, it was heated above melting and then compressed to a thickness of about 300 μm. The parallel disk optical device (R = 15 mm), with quartz windows, was alternatively mounted in an optical train for light scattering and transmission intensity measurements and in an optical microscope (Carl Zeiss Universal (ZPU01) under transmission mode) with cross-polars. For a detailed description of the device and the instrument, refer to the publication by Pogodina et al. [40]. Optical device was calibrated for the temperature using two thermocouples embedded in a 300 μm thick iPB sample.

3.3.2 Shearing and Temperature Protocol

For all the experiments, samples were heated to 174 °C, kept there for about 15 minutes. Such a high temperature (about 50 K above melting) was used to erase the thermo-mechanical history and to melt all the crystallites present in the sample as recommended by Hadinata *et al*. [26]. Then the sample was cooled down to T_x = 98.9 °C, the temperature for isothermal crystallization. Time t = 0 was assigned to the instant at which the experimental temperature T_x was reached. Sample was sheared for a duration of t_s from t=0 and then crystallized isothermally without any further shearing. Cooling was performed fast enough to avoid any crystallization during cooling. The main purpose

of adopting Janeschitz-Kriegl protocol [1, 8] was to isolate shearing action from crystal growth. This way dynamics of flow was governed by the melt dynamics instead of suspension dynamics (solid crystal suspended in melt). Optical measurements were performed in air unlike thermal and mechanical measurements, which were done under dry heated nitrogen.

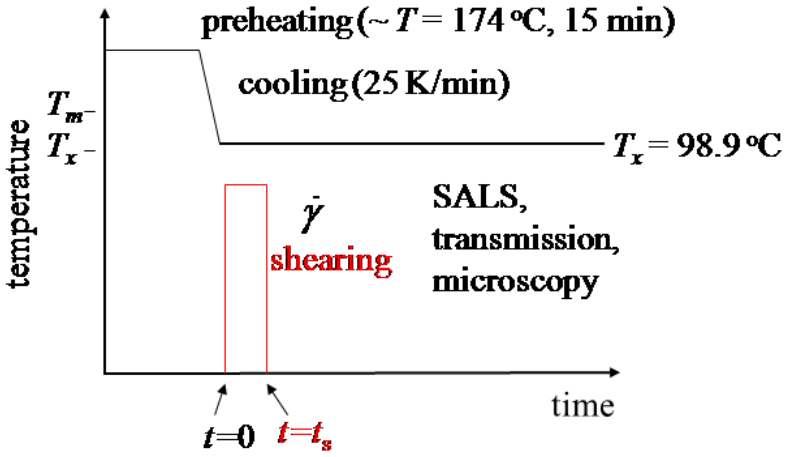

Figure 3.5 Shearing and temperature protocol: Sample is heated above melting temperature range from DSC, kept there for 15 minutes and cooled down to the experimental temperature. A short term shearing is provided while avoiding any crystal growth with shearing.

3.3.3 Optical Measurements and the Shearing Device

For small angle light scattering (SALS) and transmission intensity measurements, a 5 mW, linearly polarized, He-Ne (632.8 nm) LASER beam (diameter (d_l) ≈ 1 mm) was sent through the sample. Scattered and transmitted intensities under parallel and cross polars were measured simultaneously using an analyzer sheet and photodiodes, respectively.

The transmission intensity under parallel-polars (I_{HH}) defines the evolving turbidity (μ), eq10, of the sample due to crystallization. h and I_0 are sample thickness and laser source intensity, respectively [41, 42].

$$\mu = -(1/h)\ln(I_{HH}/I_0) \qquad (10)$$

Two-dimensional light scattering invariants were calculated from intensity measurements according to Stein-Wilson theory for random orientation correlations [43].

$$Q_\delta = \int_{q_1}^{q_2} I_{HV}(q) q^2 dq \propto \left\langle \delta^2 \right\rangle, Q_\eta = \int_{q_1}^{q_2} \left(I_{VV}(q) - \frac{4}{3} I_{HV}(q) \right) q^2 dq \propto \left\langle \eta^2 \right\rangle \quad \text{and} \quad q = \frac{4\pi}{\lambda} \sin\frac{\theta}{2}$$

(11)

Q_δ, Q_η, q, δ, η, θ, and λ are the orientation fluctuation invariant, density fluctuation invariant, wave vector, orientation fluctuations, density fluctuations, scattering angle and wavelength of the light source, respectively. These invariants are the measure of mean square fluctuations and can be used to estimate evolving crystal content [36, 40, 44].

A 30 mm parallel plate shearing device (fig.3.6) with quartz plates (CSS 450 from Linkam Scientific) was used for all optical measurements (optical microscopy as well as SALS). Top plate remains fixed and bottom plate is rotated to shear the polymer. Optical shear cell has a circular observation window (diameter (d_w) = 2.8 mm) at 7.5 mm (r_w) from the center. For detailed description of the device refer to the publication by Pogodina et al. [40].

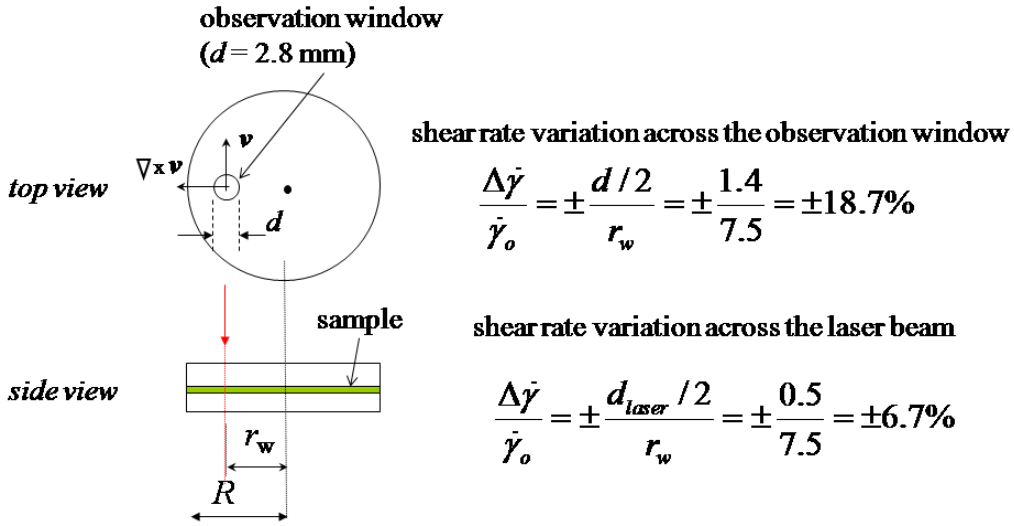

Figure 3.6 Schematic of a parallel plate (diameter =30 mm) optical shearing device (CSS 450 from Linkam Scientific). The observation window is about 2.8 mm in diameter and its center is 7.5 mm away from the center of parallel plate (diameter 30 mm) geometry. Laser beam used for SALS and transmission measurements is about 1 mm in diameter is sent through the center of the observation window (d_w = 2.8 mm).

The optical shearing device has a radial shear rate gradient due to the parallel plate geometry and shear rate increases linearly as,

$$\dot{\gamma} = \omega r / h \qquad (12)$$

where r is radial distance from center of plate and plate geometry, ω is rotational velocity and h is sample thickness. Due to the nature of shearing geometry, we also have shear rate variation across the window (d_w =2.8 mm), eq13, and the laser beam ($d_l \approx$ 1mm), eq14. The variation is from the prescribed values of shear rates that are for the center of the observation window i.e. at a distance of r_w from center of the shearing geometry.

$$\frac{\Delta\dot{\gamma}}{\dot{\gamma}_o} = \pm\frac{d_w/2}{r_w} = \pm\frac{1.4}{7.5} = \pm 18.7\% \qquad (13)$$

$$\frac{\Delta\dot{\gamma}}{\dot{\gamma}_o} = \pm\frac{d_l/2}{r_w} = \pm\frac{0.5}{7.5} = \pm 6.7\% \qquad (14)$$

Parallel plate geometry has a shear rate gradient associated with it. A point-like laser would be ideal to perform measurements for a single shear rate, however a thick beam is required to get a good average signal (signal averaging would be better with more scatterers). Considering these two opposing factors, a laser beam of about 1mm in diameter was chosen for an observation window of 2.8 mm in diameter.

3.4 Results

3.4.1 Quiescent Crystallization (*We* =0)

Growing spherulites were monitored under cross-polars at 98.9 ^{o}C for quiescent crystallization fig.3.7(a). Nucleation density was very small and spherulites of different sizes were observed. Variation in spherulite sizes indicated that they were nucleated at different times assuming that they would have same growth rate under isothermal conditions. Transmission intensity and SALS measurements were employed to follow the rate of crystallization. Size and position of the laser beam used for these measurements is presented in the optical micrograph at 7844 s by a circular dashed ring. Parallel-polar transmission intensity (I_{HH}) is a measure of growing turbidity in the sample due to growing crystallites. It diminished with time, fig.3.7(b) and reached a low steady value within 15000 s. Transmission intensity under cross-polars (I_{HV}) remained almost constant or increased a bit. Parallel-polar transmission intensity (I_{HH}) is normalized by its initial value ($I_{HH,0}$) and is plotted in fig.3.7(c). The parallel-polar transmission intensity reached half of its initial value at 9400s and this time served as a measure of characteristic crystallization time, $t_{1/2}$, i.e.

$$\text{at } t = t_{1/2} \quad \frac{I_{HH}}{I_{HH,0}} = 0.5 .$$

We term this time as transmission half-time. Simultaneous SALS measurements, fig.3.7(d), provided us the density fluctuation invariant (Q_η) and orientation fluctuation invariant (Q_δ). Density fluctuation invariant (Q_η) stayed constant for a while for melt, went through a maximum at t=6100 s and then declined to a low value. The time corresponding to the maximum in Q_η, $t_{Q_{\eta-\max}}$, is a characteristic of material and the crystallization process and served us as another measure for rate of crystallization. In the meanwhile, the Q_δ increased and reached a plateau. Square root of Q_δ can be used to follow the evolving crystal content in the sample [36, 43, 45].

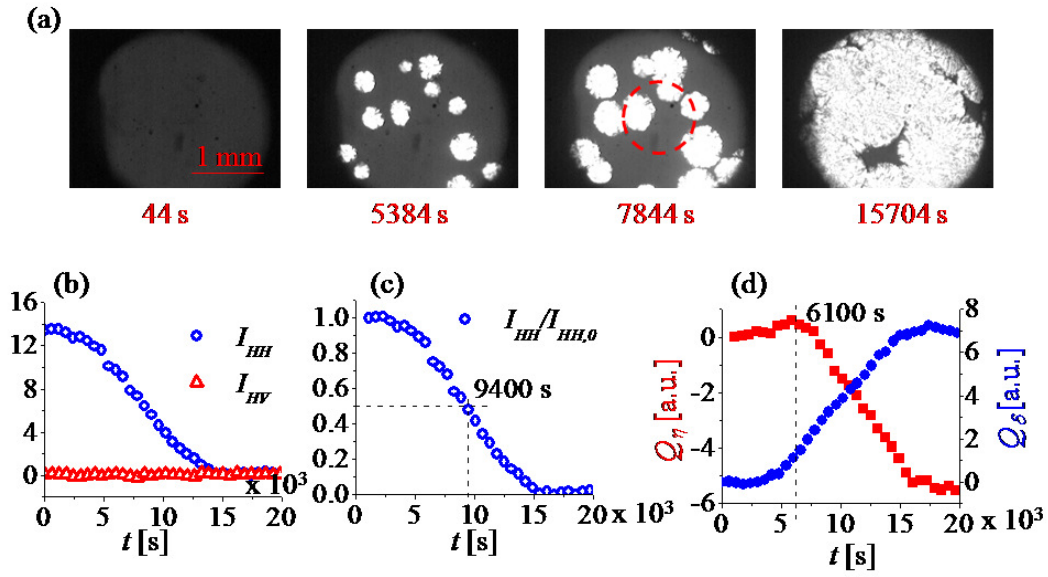

Figure 3.7 Quiescent crystallization of iPB at 98.9 °C (a) micrographs under cross-polars at different times. The observation window is not perfectly circular. The circular dashed ring in the micrograph shows the size and position of the laser beam used for transmission and SALS measurements. (b) Parallel-polar (I_{HH}) and cross-polar transmission (I_{HV}) intensity measurements (c) Normalized parallel-polar transmission intensity ($I_{HH}/I_{HH,0}$) provides us with a characteristic crystallization time (d) Density (Q_η) and orientation (Q_δ) fluctuation invariants from SALS. Maximum in density fluctuation invariant provides us another characteristic time for crystallization.

3.4.2 Shear-induced Crystallization near the Transition to Shear-thinning (near $We \approx 1$)

For flow-induced experiments three shear rates of 1, 7 and 10 s^{-1} were used. Strain was varied by varying shearing duration (t_s). The η *Vs* $\dot{\gamma}$ plot, fig.3.4, was considered as a guide to select the shear rates. Shear rate of 1 s^{-1} was close to the transition to shear-thinning whereas 7 and 10 s^{-1} were well into shear-thinning region. The same plot was used to define a characteristic material relaxation time (λ_{mat}) [46-52] which was 1.25 s for iPB melt at 98.9 °C . The λ_{mat} was obtained by the intersection of two tangents in steady viscosity plateau and the shear-thinning region, and was required for *We* ($We = \dot{\gamma}\lambda_{mat}$)

calculations. The shear rates of 1, 7 and 10 s^{-1} correspond to the dimensionless *We* of 1.25, 8.75 and 12.5, respectively.

Start up of shear flow for different shear rates was calculated using the master curve of material, fig.3.2, with Molecular Stress Function (MSF) of Wagner [53], see fig.3.8. The steady state for the flow was attained within 2-3 s of shearing. It is known that MSF works better for elongation than for shear flow.

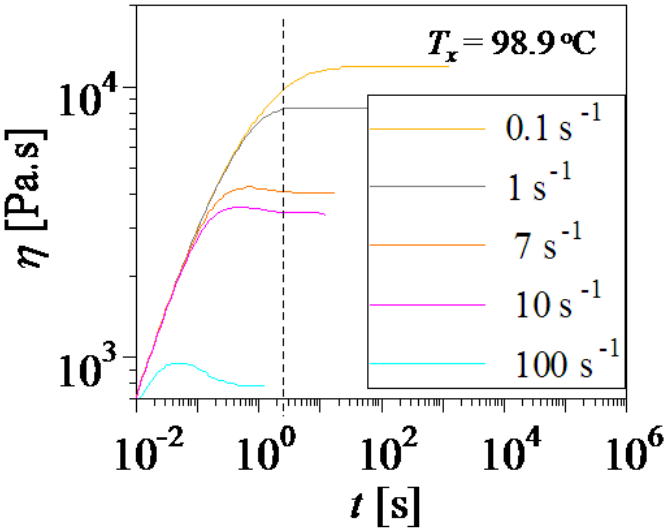

Figure 3.8 Start up of shear flow calculated using the master curve for iPB at 98.9 °C. Molecular stress function was used to obtain start up curves for different shear rates [53].

Figure 3.9 shows the cross-polar micrographs for a sample of iPB that was sheared for a duration of 180 s at *We* = 1.25 ($\dot{\gamma}=1\ s^{-1}$). Nucleation density increases compared to the quiescent case, but the increment is not striking even for the strains of 180 at this *We*. An overlap of crystal growth with shearing was observed for higher strains. Parallel-polar transmission intensity measurements confirmed the faster crystallization (the results are not presented here).

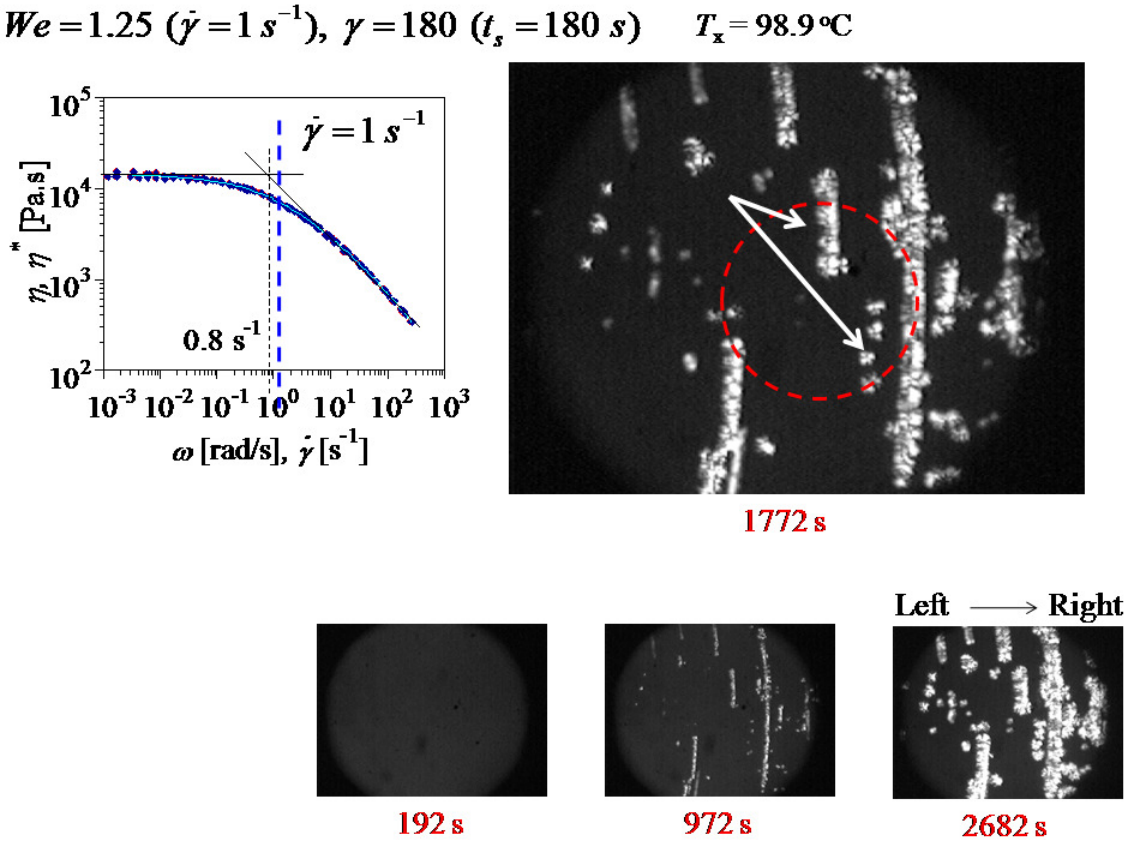

Figure 3.9 Cross polar optical micrographs at different times for *We* = 1.25 ($\dot{\gamma} = 1\ s^{-1}$) and shear strain of 180 units during crystallization of iPB at 98.8 °C. The circular dashed ring in the micrograph shows the size and position of the laser beam used for transmission and SALS measurements. Shear thinning plot is shown with a bold dashed line representing the *We* =1.25.

From optical micrographs, fig.3.9, we can state that there is still sufficient material available to further the nucleation density even after shearing the melt for 180 strain units at *We*=1.25. Steady state for the flow is reached in 2-3 strain units (fig.3.8), however strain effects on nucleation density and so on the rate of crystallization are realized for strains up to 180 and larger.

We number is precisely 1.25 at the center of the circular ring and increases as one moves from left to right across the image, fig.3.9. A higher shear rate at the right end of the image results in higher strain (shearing duration remains same) and so the higher

nucleation density and more orientation than rest of the window. A few oriented structures were observed around the center though not a lot. A careful observation even reveals that the oriented structures are the collections of growing and impinged spherulites that are nucleated along a row in the flow direction. Arrows in the image at t=1772 shows the rows of spherulites. One of the rows is composed of impinged spherulites and the spherulitic curvature is clearly visible. For the other row, spherulites are still away from the impingement at 1772 s, though they impinge and form an elongated structure that is seen in image at 2682 s.

For quiescent crystallization and the experiments at We=1.25, we did not have enough nucleation density to give us a good average signal for transmission and SALS measurements and variation in different runs was found due to the statistical nature of nucleation.

3.4.3 Shear-induced Crystallization in Shear-thinning region ($We >> 1$)

A set of SALS images under cross-polars (HV) and parallel-polars (VV) modes are shown in fig.3.10. Images were corrected for the excess scattering from the melt and the stage windows and correspond to the We=8.75 ($\dot{\gamma} = 7\ s^{-1}$) and strain units of 210. Sample reached to a temperature of 98.9 ^{o}C (T_x) at t=0 and was sheared for a duration of 30s. Shearing direction was at 45^{o} to both polarizer and analyzer, and is shown in fig.3.10. Light scattering images just after shearing (t_s^+) showed a very little scattering. An anisotropic scattering pattern, perpendicular to the flow direction, was observed at 610 s under cross-polars. Scattering in the direction perpendicular to the flow corresponds to the development of oriented shish-like structure in the flow direction.

Cross-polar micrograph at this time, fig.3.11, confirmed the presence of oriented structures in the flow direction. VV image at this time also had anisotropic scattering perpendicular to the flow, though the development of shish-type structures was more clearly visible under HV mode of scattering.

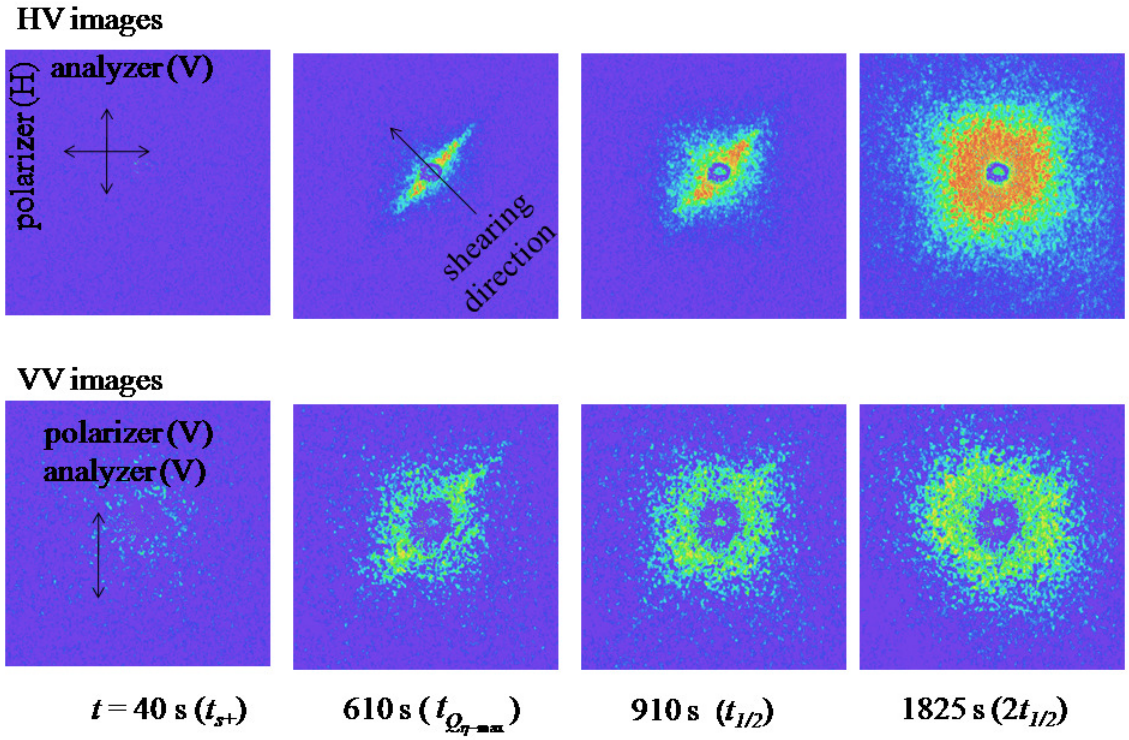

Figure 3.10 Cross-polar (HV) and parallel-polar (VV) images from SALS during crystallization of iPB at 98.9 °C after shearing at *We* = 8.75 ($\dot{\gamma} = 7\ s^{-1}$) for 30 s.

SALS HV images showed the enhanced scattering in the flow directions at the later stages and a transformation from anisotropic scattering to isotropic scattering. Enhanced scattering in the flow direction is attributed to structure growth perpendicular to the flow and thus it was due to the lamellar kebab growth on the existing shish. Crystallization in the absence of flow would give rise to mix of lamellar kebab growth on existing shish structures with the spherulitic growth in the relaxed melt, which would lead to isotropic scattering. Micrographs in fig.3.11 further confirmed this observation.

Micrograph at $t = t_{Q_{\eta-\max}}$ has distinct oriented structure with almost no spherulitic growth. Further crystallization, micrographs at $t=t_{1/2}$ and $2t_{1/2}$, show the unoriented growth as well.

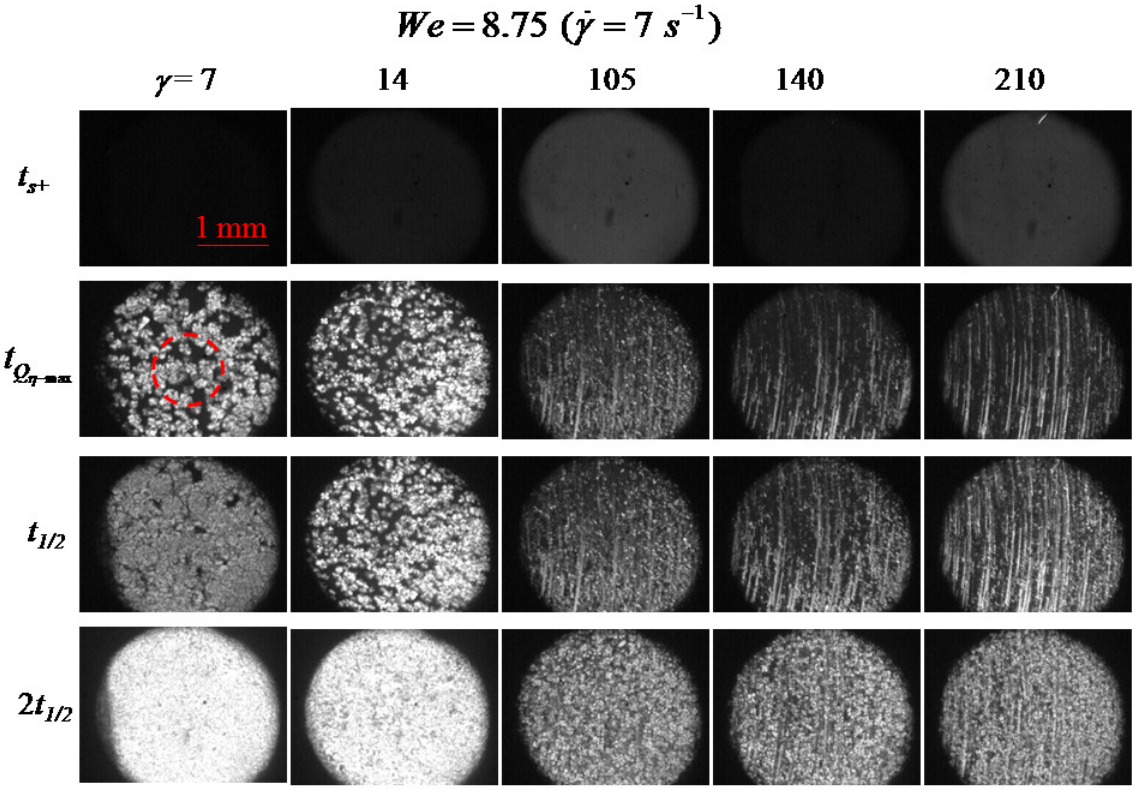

Figure 3.11 Optical micrographs under cross-polars for crystallizing iPB at 98.9 °C for *We* = 8.75 ($\dot{\gamma} = 7\ s^{-1}$) at different shear strains.

Similar optical measurements were made for strains from 7 to 280 units for *We* =8.75 ($\dot{\gamma} = 7\ s^{-1}$) and *We* =12.5 ($\dot{\gamma} = 10\ s^{-1}$). Light scattering invariants along with parallel polar transmission intensity measurements are shown in fig.3.12 for *We* =8.75. A steady viscosity plot is added with a thick dashed line representing the *We* =8.75 in shear-thinning region. Even a small strain of seven accelerated the crystallization significantly compared to the quiescent case. Parallel polar transmission intensity dropped off much faster at higher strains. Density fluctuation invariants (Q_η) leveled off faster as well at

larger strains. Time corresponding to the maximum in density fluctuation invariant ($t_{Q_{\eta-\max}}$) moved to lower values at larger strains and so were in line with the parallel polar transmission intensity measurements. Orientation fluctuation invariants (Q_δ) are a measure of growing crystallinity in the sample. The invariants, Q_δs, increased with time and leveled off at late stages during crystallization.

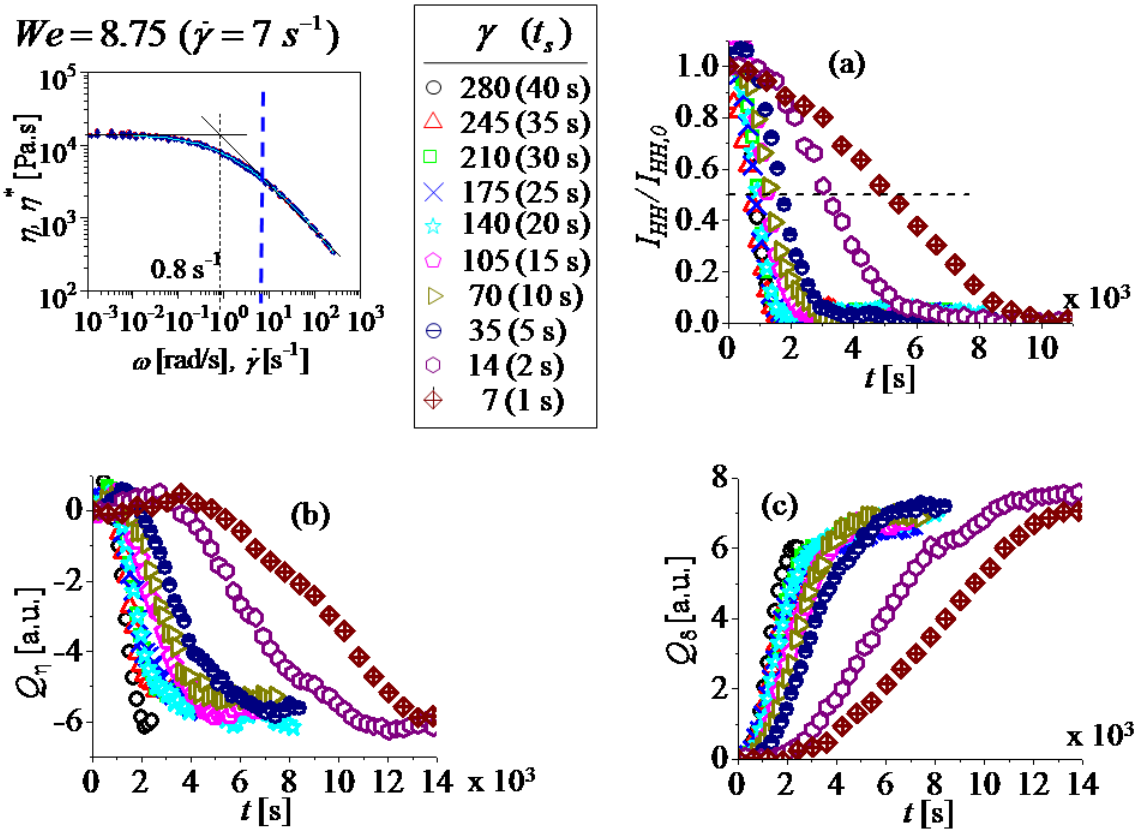

Figure 3.12 Shear-induced crystallization of iPB at *We* = 8.75 ($\dot{\gamma}$ = 7 s^{-1}) for varying strains and shearing durations (a) Normalized parallel-polar transmission intensity (b) density fluctuation invariants (c) orientation fluctuation invariants. A shear-thinning plot is added with a thick dashed line representing the *We* = 8.75.

Density fluctuation invariants and parallel-polar transmission intensity measurements provided us characteristic timescales for crystallization $t_{Q_{\eta-\max}}$ and $t_{1/2}$, respectively. These timescales are plotted in fig.3.13 for *We* =8.75 and 12.5 against the

applied strains and specific mechanical work. Both the characteristic time scales decreased with increasing strain and attained a steady value for a strain of 140 in the case of *We* =8.75. In addition, the difference between two characteristic time scales diminished with increasing strain.

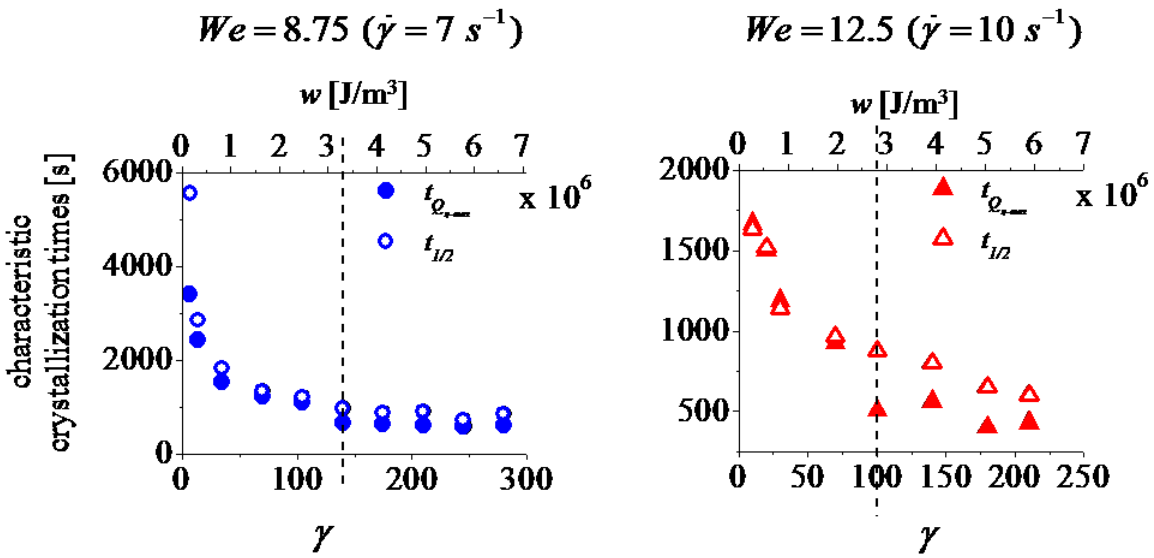

Figure 3.13 Characteristic crystallization time scales obtained from transmission intensity and SALS measurements for iPB at 98.9 °C. Crystallization times are plotted against strain and the specific mechanical work for *We* numbers in shear thinning region.

At this juncture, it should be noted that for *We* =1.25, we were not able to get to a steady state for the rate of crystallization (by looking at nucleation density in optical micrographs in fig.3.9) even up to the strain of 180 units. Whereas at larger *We* of 8.75, we were able to attain steady state for strain of 140. Thus large strain requirements for rate of crystallization moved to lower strains at higher *We* numbers. Measurements at *We* =12.5 were in agreement with this trend as well. A leveling off for the rate of crystallization was observed at a strain of about 100 for *We* =12.5.

For *We* =8.75 and 12.5, steady state for the flow was reached within 7-10 strain units, fig.3.8, though the flow effects on the rate of crystallization were observed up to

much larger strains. Thus the large strain requirements that were earlier observed for iPP [4] and PE [29] were also found for iPB. In addition, the large strain requirements decrease upon increasing the *We* number.

Dependence of the rate of crystallization on strain and *We* pointed toward the presence of a criterion based on specific mechanical work. The characteristic crystallization time scales leveled off around a specific mechanical work of 3 MJ/m^3 for the *We* numbers of 8.75 and 12.5. It was not possible to obtain such reproducible measurements for *We* =1.25 due to low nucleation density. More experiments are needed along these lines to reinforce the criterion of specific mechanical work for the rate of crystallization.

Application of flow fastens the rate of crystallization by enhancing the nucleation density. Flow effects on the growth rate are presumably small to alter the rate of crystallization significantly. A consequence of interplay between flow and material relaxation process is the morphological transition to the oriented growth from spherulitic growth. Figure 3.11 shows the cross-polar micrographs for *We* = 8.75 at different strains. Smaller strains of 7 and 14 at this *We* number resulted in spherulitic growth with significantly higher nucleation density compared to quiescent crystallization. It was surprising to see a huge effect for even small strains of 7 at *We* =8.75 in increasing the nucleation density dramatically since for *We* =1.25, we did not observe such a striking increment in nucleation density even for the strains up to 180 units. The observation reinforces the critical role of *We* in influencing the nucleation density and so the rate of crystallization.

Much larger strains at *We* =8.75, fig.3.11, resulted in oriented structures. We did not observe significant oriented growth for *We* =1.25 up to strains of 180 units. At higher *We* number of 8.75 in the shear-thinning regime, we were able to obtain oriented growth at large enough strains. So *We* >>1 along with large enough critical strains are needed for morphological transition from spherulitic growth to oriented growth. We observed a mixed growth for a strain of 105 at *We* =8.75 at $t = t_{Q_{\eta-\max}}$ whereas the growth was mostly oriented for strains of 140 and 210 at this time. For longer times a mixed growth was observed even for the strains of 140and 210. Certainly it is the consequence of orientation relaxation after melt shearing. Although we realized that a critical strain was required to attain oriented growth even for *We*>>1, it was hard to pin point the critical strain from the optical micrographs, fig.3.11. Strong enough flow could even result in fully oriented growth with minimal kebab-type lamellar growth [6, 54].

3.5 Discussion

3.5.1 Criteria for Flow-induced Crystallization

Chai [29] and Elmoumni [4] found it necessary to apply very high strains (~100) to affect polymer crystallization to its fullest. Elmoumni et al. observed a high limiting strain of 700 for iPP for the *We* =1. The present studies on flow-induced crystallization (FIC) for *We* ranging from 1.25 to 12.5 confirmed the presence of large strain requirements for iPB as well. Steady state for the viscosity was reached within 3-10 strain units (fig. 3.8), though much larger strains in the order of 100 were required to attain the steady state for the rate of crystallization. We speculate that such leveling off for the rate of crystallization is associated with the saturation in the nucleation density with

increasing strain. Although the oriented growth was observed for *We* >>1, yet large strains were needed to obtain oriented morphologies. Thus large strain, compared to the strain units needed to attain steady state of flow, were required not only to attain a leveling off for the rate of crystallization but also for the morphological transition from spherulitic growth to elongated growth.

The large strain requirements for the leveling off of the rate of crystallization go to lower strain values for higher *We* numbers. *We* is used as a criterion here since *We*=1 denotes the onset of non-linear shear. Polymer chains retain their equilibrium conformation for *We*<1, but above *We*=1, they adopt non-equilibrium conformations. A distinctive behavior for *We* >> 1 might be due to the different chain conformations. As far as leveling off is concerned, we speculate that it could be achieved at large strains at all *We* numbers. Flow-induced crystallization experiments on low molecular weight polyolefins (linear alkanes) might be able to confirm this speculation. In such experiments, nucleation density can be increased without attaining any micro or macro oriented structures. Thus the application of the large strains is a requirement to get the steady state of the rate of crystallization, where as *We* is not a necessary criterion. Comparing fig.3.9 (*We* =1.25 and γ= 180) and fig.3.11 (*We*=8.75 and γ= 7) reveals the catalytic effect of the *We* in increasing the nucleation density and thus lowering the large strain requirements for the rate of crystallization. On the other hand, strain and *We*, both form the criteria for the morphological transition. Large strains at *We* >>1 are essential to form oriented structures. In this study, *We* was defined using a material relaxation time from plot, η Vs $\dot{\gamma}$, fig. 3.4.

The catalytic role of the *We* for the leveling off of the rate of crystallization and the required role for the oriented growth indicated the presence of a criterion based on specific mechanical work. The leveling off for the rate of crystallization occurred at a specific mechanical work of about 3 MJ/m^3 for *We* numbers of 8.75 and 12.5. Dependence of crystallization rate was highly nonlinear with mechanical work, fig.3.13. Parallel trends were observed for iPP by Janeschitz-Kriegl's group at Linz. They observed nonlinear dependence of rate of nucleation with mechanical work and also a transition to shish-kebab morphology at ~ 7 MPa [2]. More experiments in the range of $1.25 \le We \le 12.5$ would be helpful in establishing this criterion. Thus the nucleation density which depends on the applied strain and specific mechanical work would govern the leveling off of the rate of crystallization and a combination of strain and *We* would control the morphological transition to oriented growth.

Crystallization rate leveled off at very large values of strains and optical microscopy indicated that morphological transition from spherulitic growth to elongated growth is dependent on strain as well as the *We*. Both these phenomena can be explained using the fact that strain accelerates the crystallization by increasing nucleation density as well as by inducing orientation by stretching the polymer chain/ chain segments and bringing them closer to their lattice conformation. Orientated stretched molecules have low entropy and so the low free energy that in turn speeds up the crystallization. Thus, the rate of crystallization can be enhanced by increasing the nucleation density or by inducing order or by combining both. On the other hand, for morphological transition ordering/stretching seems to be a necessary criterion.

3.5.2 Mechanism for the Oriented Growth

In the optical micrographs at *We* =1.25 and strain of 180, fig.3.8, we observed aligned growing crystals in the flow direction which eventually impinge and form an oriented structure. The elongated structures grew laterally as well as at the ends. Growth at the ends was more like spherulitic and had a curvature to it. We speculate that it's due to the unobstructed nature of the growth at the ends compared to the highly hindered growth within an elongated structure due to large number of nuclei arranged on a row. The aligned crystals and the lateral curvature of the oriented structures are shown by an arrow in the image at t = 1772 s. The curvature on the sides of an oriented structure indicates that the crystal growth is not strictly perpendicular to the flow; rather it is more like spherulitic radial growth on nucleation sites that are aligned in a row and are far apart, fig. 3.14(a). Whether the connectivity exist among such aligned nuclei, is not clear from the images. However possible connectivity mechanisms of spherulite-crossing and tie molecules that are described for spherulites might as well exist for oriented structures [36]. Janeschitz observed [2, 8] when the distance between the spherulites was shorter than the size of spherulites, they combined together to give rise to an elongated structure. Han and coworkers [55] also saw similar elongated structures for iPP, fig.3.15 (a) and (b). For iPP such structures were obtained with a shear rate of 0.5 s^{-1} for duration of 5 s.

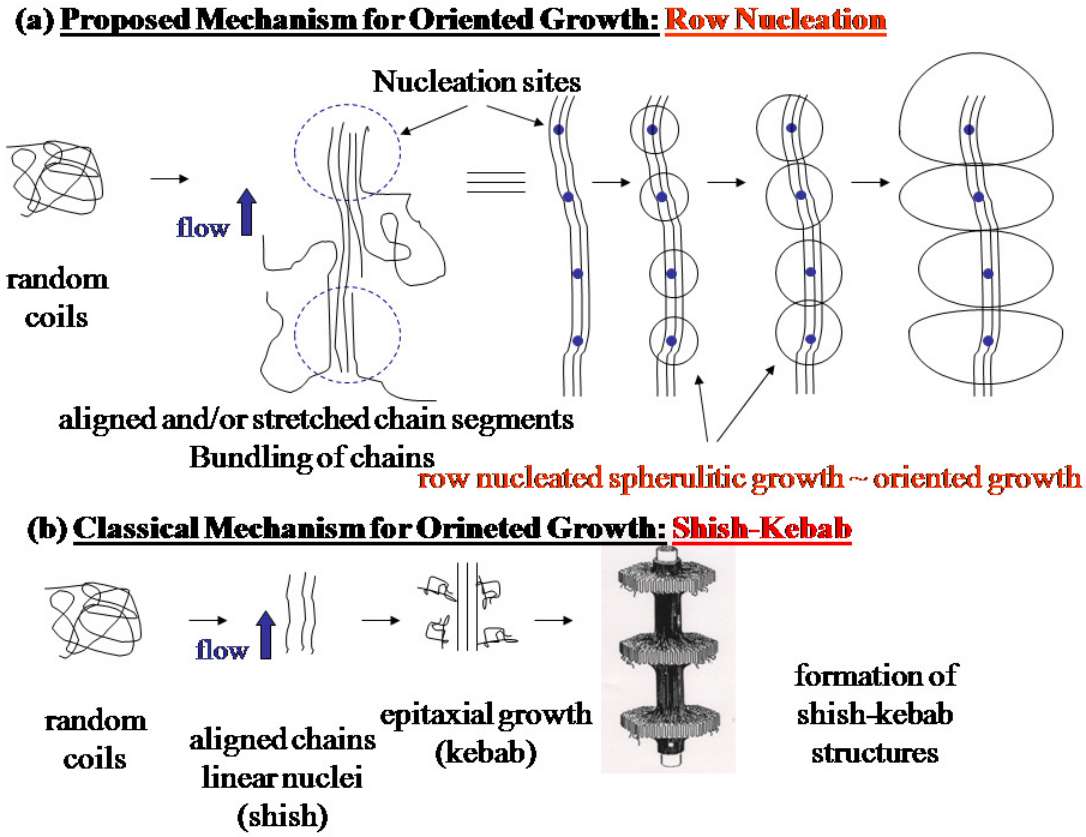

Figure 3.14 Flow dependent mechanisms for oriented growth (a) Proposed mechanism: impingement of aligned and connected spherulites (b) Classical mechanism: formation of Shish-kebabs by lamellar growth perpendicular to the core (Shish).

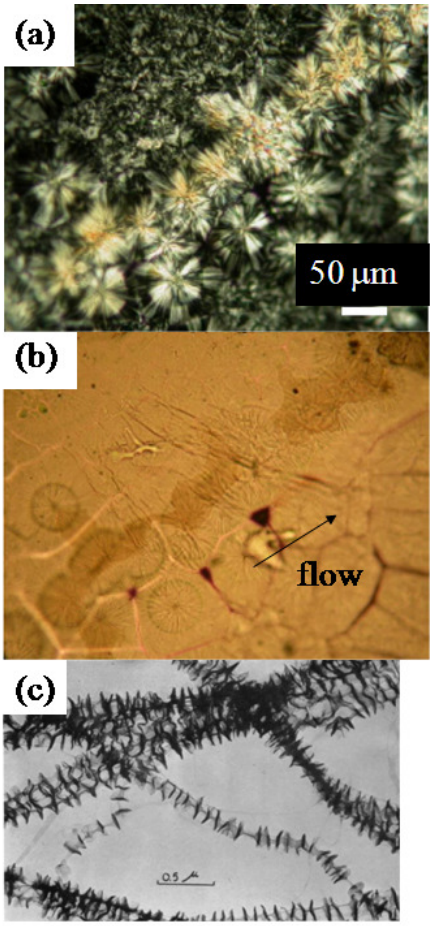

Figure 3.15 (a) and (b) Optical micrographs of Isothermally crystallized iPP at 140 ^{o}C for shear rate of 0.5 s^{-1} and shearing duration of 5 s [55] (c) Electron micrograph of shish-kebabs of polyethylene grown in an agitated xylene solution at 100 ^{o}C [56].

Classical work by Keller [6] and Pennings [56] on solution crystallization showed highly oriented structures (shish) with strictly perpendicular growth (lamellar kebab) on them, fig. 3.15 (c). It was shown conclusively that the core (shish) was most stable towards melting, following by micro and macro kebabs. Micro kebabs were exposed by treating shish-kebab structures with fuming nitric acid.

Based on these observations, we propose that the nature of oriented morphologies and so the mechanism to form them depends on the flow conditions. Mild shearing will give rise to oriented structures that are formed by impingement of spherulites that grow

from aligned nuclei. Application of flow aligns the polymer chain segments in the flow direction and brings them together. This gives rise to oriented bundles of chain segments in the flow direction. When the size of these bundles reaches a critical size, they act as nuclei as is the case for spherulitic growth as well. Thus the nucleation event encompasses point nuclei instead of linear nuclei. Features that differ in oriented growth compared to spherulitic growth are the alignment of these nuclei in a row due to the chain orientation and their dense population along the row. Growth from these nuclei is spherulitic until they touch each other. After the impingement of spherulites, they tend to grow faster in the lateral direction (direction perpendicular to the flow) than the flow direction and this leads to elongated structures that look like row-nucleated structures. Mild shearing would orient the tubes/ chains followed by radial lamellar growth by relaxed chains in the melt. Strong flow would give rise to highly oriented core formed of highly strained chains and the growth of strictly perpendicular lamellar kebabs from mildly strained chains, fig.3.14 (b).

3.6 Conclusion

Flow-induced crystallization studies for *We* ranging from 1.25 to 12.5 at varying strains up to 280 confirmed the presence of large strain requirements for iPB for the rate of crystallization as well as the morphological transition. Similar observations were made earlier for iPP [4] and PE [29]. Large strain requirements for the rate of crystallization go to lower strain values for higher *We*. Weissenberg number plays a catalytic role in increasing nucleation density and thus lowering the large strain requirements for the rate of crystallization. Strain and specific mechanical work seem to govern the leveling off of the rate of crystallization whereas $We >> 1$ seems to be a necessary criterion to obtain

oriented growth. Atleast two different mechanisms exist for row nucleated growth – shish-kebab mechanism and coalescence of spherulites. An alternative mechanism based on coalescence of spherulites is proposed.

3.7 References

[1] Janeschitz-Kriegel H: Crystallization modalities in polymer melt procesing, Fundmental Aspects of Structure Formation, Springer, NewYork (2010).

[2] Janeschitz-Kriegl H, Ratajski E, Stadlbauer M: Flow as an effective promotor of nucleation in polymer melts: A quantitative evaluation, Rheologica Acta 42 (2003) 355-364.

[3] Huo H, Meng YF, Li HF, Jiang SC, An LJ: Influence of shear on polypropylene crystallization kinetics, European Physical Journal E 15 (2004) 167-175.

[4] Elmoumni A, Winter HH: Large strain requirements for shear-induced crystallization of isotactic polypropylene, Rheologica Acta 45 (2006) 793-801.

[5] Strobl GR: Metastable partially crystalline states, The physics of polymers, Berlin (1997).

[6] Keller A: Polymer crystals, Reports on Progress in Physics 31 (1968) 623-704.

[7] Muthukumar M: Commentary on theories of polymer crystallization, European Physical Journal E 3 (2000) 199-202.

[8] Janeschitz-Kriegl H: Phases of flow-induced crystallization of i-pp: How remote pieces of the puzzle appear to fit, Macromolecules 39 (2006) 4448-4454.

[9] Janeschitz-Kriegl H, Eder G, Stadlbauer M, Ratajski E: A thermodynamic frame for the kinetics of polymer crystallization under processing conditions, Monatshefte fur Chemie 136 (2005) 1119-1137.

[10] Patki RP, Phillips PJ: Crystallization kinetics of linear polyethylene: The maximum in crystal growth rate-temperature dependence, European Polymer Journal 44 (2008) 534-541.

[11] Hsiao BS, Yang L, Somani RH, Avila-Orta CA, Zhu L: Unexpected shish-kebab structure in a sheared polyethylene melt, Physical Review Letters 94 (2005) 1-4.

[12] Gedde UW: Crystalline polymers, Polymer physics, London (1995).

[13] Hobbs JK, Humphris ADL, Miles MJ: In-situ atomic force microscopy of polyethylene crystallization. 1. Crystallization from an oriented backbone, Macromolecules 34 (2001) 5508-5519.

[14] Manzione L, Jameel H, Wilkes GL: Small-angle light-scattering from shish-kebab structures, Journal of Polymer Science Part C-Polymer Letters 16 (1978) 237-243.

[15] Somani RH, Yang L, Sics I, Hsiao BS, Pogodina NV, Winter HH, Agarwal P, Fruitwala H, Tsou A: Orientation-induced crystallization in isotactic polypropylene melt by shear deformation, Macromolecular Symposia 185 (2002) 105-117.

[16] Keller A, Kolnaar HW: Flow induced orientation and structure formation, Processing of polymers, New York (1997).

[17] Janeschitz-Kriegl H, Ratajski E, Wippel H: The physics of athermal nuclei in polymer crystallization, Colloid and Polymer Science 277 (1999) 217-226.

[18] Yang L, Somani RH, Sics I, Hsiao BS, Kolb R, Lohse D: The role of high molecular weight chains in flow-induced crystallization precursor structures, Journal of Physics-Condensed Matter 18 (2006) 2421-2436.

[19] Kimata S, Sakurai T, Nozue Y, Kasahara T, Yamaguchi N, Karino T, Shibayama M, Kornfield JA: Molecular basis of the shish-kebab morphology in polymer crystallization, Science 316 (2007) 1014-1017.

[20] Kumaraswamy G: Crystallization of polymers from stressed melts, Journal of Macromolecular Science-Polymer Reviews C45 (2005) 375-397.

[21] Dukovski I, Muthukumar M: Langevin dynamics simulations of early stage shish-kebab crystallization of polymers in extensional flow, Journal of Chemical Physics 118 (2003) 6648-6655.

[22] van Meerveld J, Peters GWM, Hutter M: Towards a rheological classification of flow induced crystallization experiments of polymer melts, Rheologica Acta 44 (2004) 119-134.

[23] Peters GWM, Swartjes FHM, Meijer HEH: A recoverable strain-based model for flow-induced crystallization, Macromolecular Symposia 185 (2002) 277-292.

[24] Hobbs JK, Miles MJ: Direct observation of polyethylene shish-kebab crystallization using in-situ atomic force microscopy, Macromolecules 34 (2001) 353-355.

[25] Vleeshouwers S, Meijer HEH: A rheological study of shear induced crystallization, Rheologica Acta 35 (1996) 391-399.

[26] Hadinata C, Gabriel C, Ruellman M, Laun HM: Comparison of shear-induced crystallization behavior of pb-1 samples with different molecular weight distribution, Journal of Rheology 49 (2005) 327-349.

[27] Kornfield JA, Kumaraswamy G, Issaian AM: Recent advances in understanding flow effects on polymer crystallization, Industrial & Engineering Chemistry Research 41 (2002) 6383-6392.

[28] Janeschitz-Kriegl H: How to understand nucleation in crystallizing polymer melts under real processing conditions, Colloid and Polymer Science 281 (2003) 1157-1171.

[29] Chai CK, Auzoux Q, Randrianatoandro H, Navard P, Haudin JM: Influence of pre-shearing on the crystallisation of conventional and metallocene polyethylenes, Polymer 44 (2003) 773-782.

[30] Elmoumni A, Fruitwala H, Winter HH: Correlation of material and processing time scales with structure development in isotactic polypropylene crystallization, 225th National Meeting of the American-Chemical-Society (2003) 6-7.

[31] Ishikiriyama K, Boller A, Wunderlich B: Melting of indium by temperature-modulated differential scanning calorimetry, Journal of Thermal Analysis 50 (1997) 547-558.

[32] Kalay G, Kalay CR: Structure and physical property relationships in processed polybutene-1, Journal of Applied Polymer Science 88 (2003) 814-824.

[33] Kaszonyiova M, Rybnikar K, Geil PH: Polymorphism of isotactic poly(butene-1), Journal of Macromolecular Science-Physics B44 (2005) 377-396.

[34] Azzurri F, Gomez MA, Alfonso GC, Ellis G, Marco C: Time-resolved saxs/waxs studies of the polymorphic transformation of 1-butene/ethylene copolymers, Conference on Synchrotron Radiation in Polymer Science II (2002) 177-189.

[35] Azzurri F, Flores A, Alfonso GC, Calleja FJB: Polymorphism of isotactic poly(1-butene) as revealed by microindentation hardness. 1. Kinetics of the transformation, Macromolecules 35 (2002) 9069-9073.

[36] Arora D, Winter HH: Network formation in a semicrystalline polymer at the early crystallization stages: From nucleation to percolation (Unpublished work).

[37] Mours M, Winter HH: Time-resolved rheometry, Rheologica Acta 33 (1994) 385-397.

[38] Booij HC, Leblans P, Palmen J, Tiemersmathoone G: Non-linear viscoelasticity and the cox-merz relations for polymeric fluids, Journal of Polymer Science Part B-Polymer Physics 21 (1983) 1703-1711.

[39] Yasuda K, Armstrong RC, Cohen RE: Shear-flow properties of concentrated-solutions of linear and star branched polystyrenes, Rheologica Acta 20 (1981) 163-178.

[40] Pogodina NV, Siddiquee SK, van Egmond JW, Winter HH: Correlation of rheology and light scattering in isotactic polypropylene during early stages of crystallization, Macromolecules 32 (1999) 1167-1174.

[41] Pogodina NV, Lavrenko VP, Srinivas S, Winter HH: Rheology and structure of isotactic polypropylene near the gel point: Quiescent and shear-induced crystallization, Polymer 42 (2001) 9031-9043.

[42] Elmoumni A, Gonzalez-Ruiz RA, Coughlin EB, Winter HH: Isotactic poly(propylene) crystallization: Role of small fractions of high or low molecular weight polymer, Macromolecular Chemistry and Physics 206 (2005) 125-134.

[43] Koberstein J, Russell TP, Stein RS: Total integrated light-scattering intensity from polymeric solids, Journal of Polymer Science Part B-Polymer Physics 17 (1979) 1719-1730.

[44] Akpalu Y, Kielhorn L, Hsiao BS, Stein RS, Russell TP, van Egmond J, Muthukumar M: Structure development during crystallization of homogeneous copolymers of ethene and 1-octene: Time-resolved synchrotron x-ray and sals measurements, Macromolecules 32 (1999) 765-770.

[45] Stein RS: Recent advances in rheo-optical studies of polymers in the solid-state, Polymer Journal 17 (1985) 289-305.

[46] Milner ST, McLeish TCB: Reptation and contour-length fluctuations in melts of linear polymers, Physical Review Letters 81 (1998) 725-728.

[47] McKinley GH, Sridhar T: Filament-stretching rheometry of complex fluids, Annual Review of Fluid Mechanics 34 (2002) 375-415.

[48] Rothstein JP, McKinley GH: A comparison of the stress and birefringence growth of dilute, semi-dilute and concentrated polymer solutions in uniaxial extensional flows, Journal of Non-Newtonian Fluid Mechanics 108 (2002) 275-290.

[49] Coppola S, Grizzuti N, Maffettone PL: Microrheological modeling of flow-induced crystallization, Macromolecules 34 (2001) 5030-5036.

[50] McLeish TCB, Allgaier J, Bick DK, Bishko G, Biswas P, Blackwell R, Blottiere B, Clarke N, Gibbs B, Groves DJ, Hakiki A, Heenan RK, Johnson JM, Kant R, Read DJ, Young RN: Dynamics of entangled h-polymers: Theory, rheology, and neutron-scattering, Macromolecules 32 (1999) 6734-6758.

[51] Baumgaertel M, Derosa ME, Machado J, Masse M, Winter HH: The relaxation-time spectrum of nearly monodisperse polybutadiene melts, Rheologica Acta 31 (1992) 75-82.

[52] Doi M, Edwards SF: The theory of polymer dynamics, Oxford (1994).

[53] Wagner MH, Yamaguchi M, Takahashi M: Quantitative assessment of strain hardening of low-density polyethylene melts by the molecular stress function model, Journal of Rheology 47 (2003) 779-793.

[54] Phillips PJ: Polymer crystals, Reports on Progress in Physics 53 (1990) 549-604.

[55] Zhang CG, Hu HQ, Wang XH, Yao YH, Dong X, Wang DJ, Wang ZG, Han CC: Formation of cylindrite structures in shear-induced crystallization of isotactic polypropylene at low shear rate, Polymer 48 (2007) 1105-1115.

[56] Pennings AJ, Kiel AM: Fractionation of polymers by crystallization from solution .3. On morphology of fibrillar polyethylene crystals grown in solution, Kolloid-Zeitschrift and Zeitschrift Fur Polymere 205 (1965) 160-173.

CHAPTER 4

A NEW GENERATION OF LIGHT SCATTERING DEVICE WITH REAL TIME DATA ANALYSIS FOR RHEO-OPTICAL MEASUREMENTS

4.1 Summary

An apparatus for small angle light scattering (SALS) and light transmission measurements under shear was built and tested at the University of Massachusetts Amherst. As a new development, the polarization direction can be rotated by a liquid crystal polarization rotator (LCPR) with a short response time of 20 ms. The experiments were controlled and analyzed with a LabVIEW^{TM} based code (LabVIEW^{TM} 7.1) in real time. Quiescent and flow-induced crystallization experiments on isotactic poly-1-butene (iPB) were conducted to demonstrate the instrument and software capabilities. Software was designed with a modular approach, so that further modules can be added to investigate other systems such as polymer blends, colloidal suspensions, solutions with droplets etc. The SALS apparatus was custom built for ExxonMobil Research in Clinton NJ.

4.2 Introduction

Small angle light scattering (SALS) is gaining ample popularity in material industries as a preferred technique to perform real time structural analysis especially as a combinatorial tool with rheometry [1-5]. The fast data acquisition, easy handling, robustness and the ease of integrating with variety of other techniques such as X-ray, optical microscopy (OM) and differential scanning calorimetry (DSC) make SALS an attractive sensor [6, 7] even for incorporating with industrial film extruders and injection

molding machines. Here we present a house-built device that can perform light scattering and transmission intensity measurements simultaneously while analyzing the data in real time. The device grew out of an earlier apparatus at the University of Massachusetts Amherst [8, 9] and incorporated a liquid crystal based device to control the polarization direction of a linearly polarized laser beam Crystallization of isotactic poly-1-butene with and without flow was studied to validate the device [10, 11]. The material response was captured under cross and parallel polars while unpolarized light did not provide any characteristic scattering for polyethylene films.

In their seminal work in light scattering of polymers, Stein and coworkers laid the theoretical foundation for relating structure to the measured SALS [12]. The analysis was further extended to polymer films with orientation fluctuations [13], random assembly of truncated spherulites [14] and oriented films [15]. The Stein-Wilson theory provides the light scattering invariants for random orientation correlations [16].

$$Q_\delta = \int_{q_1}^{q_2} I_{HV}(q) q^2 dq \propto \left\langle \delta^2 \right\rangle, Q_\eta = \int_{q_1}^{q_2} \left(I_{VV}(q) - \frac{4}{3} I_{HV}(q) \right) q^2 dq \propto \left\langle \eta^2 \right\rangle \quad \text{and} \quad q = \frac{4\pi}{\lambda} \sin\frac{\theta}{2} \tag{1}$$

Q_δ, Q_η, q, δ, η, θ, and λ are the orientation fluctuation invariant, density fluctuation invariant, wave vector, orientation fluctuations, density fluctuations, scattering angle and wavelength of the light source, respectively. These invariants are the measure of mean square fluctuations.

Mean square density fluctuations, $\left\langle \eta^2 \right\rangle$, are related to the volume fraction of anisotropic aggregates (ϕ_A) as,

$$\left\langle \eta^2 \right\rangle = \phi_A (1 - \phi_A)(\bar{\alpha}_A - \alpha_s)^2 \tag{2}$$

$\bar{\alpha}_A$ and α_s are the average polarizability of the aggregate and the surrounding, respectively. For a crystallizing polymer, spherulites can be treated as anisotropic aggregates of crystals in an isotropic melt. Mean square orientation fluctuations, $\langle \delta^2 \rangle$, offer an estimate of the crystal volume fraction in the sample.

$$\langle \delta^2 \rangle = \phi_A \delta_A^{\,2} + (1-\phi_A)\delta_s^{\,2} \qquad (3)$$

δ_A and δ_s define the anisotropy of the aggregate and surrounding, respectively. For a melt, δ_s can be assumed to be zero. For semicrystalline aggregates, their anisotropy can be expressed as a function of their crystal content, eq. 4.

$$\delta_A = \phi_{cry,A}\delta^0_{cry} f_{cry,A} + (1-\phi_{cry,A})\delta^0_{amo} f_{amo,A} + \delta_F \qquad (4)$$

$\phi_{cry,A}, \delta^0_{cry}, \delta^0_{amo}, \delta_F, f_{cry,A}$, and $f_{amo,A}$, are the volume fraction of the crystal in the aggregate, intrinsic anisotropy of the crystal, anisotropy of the amorphous region, form anisotropy, orientation function for the crystals in aggregate and orientation function for the amorphous regions in the aggregate, respectively. The assumptions are that all crystals reside within the aggregates,

$$\phi_{cry} = \phi_A \phi_{cry,A} \qquad (5),$$

that form and amorphous anisotropies can be neglected. Then, eqs. 3, 4 and 5 combined predict the mean square anisotropy for a volume-filling sample,

$$\langle \delta^2 \rangle = \phi_{cry}^{\,2} \delta^{0\,2}_{cry} f_{cry,A}^{\,2} \propto Q_\delta \qquad (6).$$

The crystal volume fraction in the sample is predicted to be proportional to the square root of the mean square orientation fluctuation invariant

$$\phi_{cry}(t) \propto \sqrt{Q_\delta(t)} \qquad (7)$$

under the assumption that δ^0_{cry} and $f_{cry,A}$ remain constant during crystallization.

The transmission intensity under parallel-polars (I_{HH}) defines the evolving turbidity, $\mu = -(1/h)\ln(I_{HH}/I_0)$, of the sample due to crystallization. h and I_0 are sample thickness and laser source intensity, respectively [8, 17].

4.3 Instrument Description

In the SALS experiment, linearly polarized light from a 5 mW He-Ne laser (632.8 nm wave length) passes through a linear polarizer followed by a beam splitter where the source intensity, I_0, is measured by a photodiode, Fig.4.1. The transmitted beam then passes through a liquid crystal polarization rotator (LCPR). The polymer sample, held in a shearing device, is placed in the path of the polarized light to obtain the scattering pattern. Scattered light from the polymer sample generates an image on a polarizing screen under a CCD camera. HV and VV patterns are recorded, digitized, and analyzed during the experiment. The scattering patterns are corrected for image distortions, which arise from the distance and angle of the camera. The main beam of the transmitted light passes through the center hole in the screen and gets split for cross polar and parallel polar transmission intensity measurements.

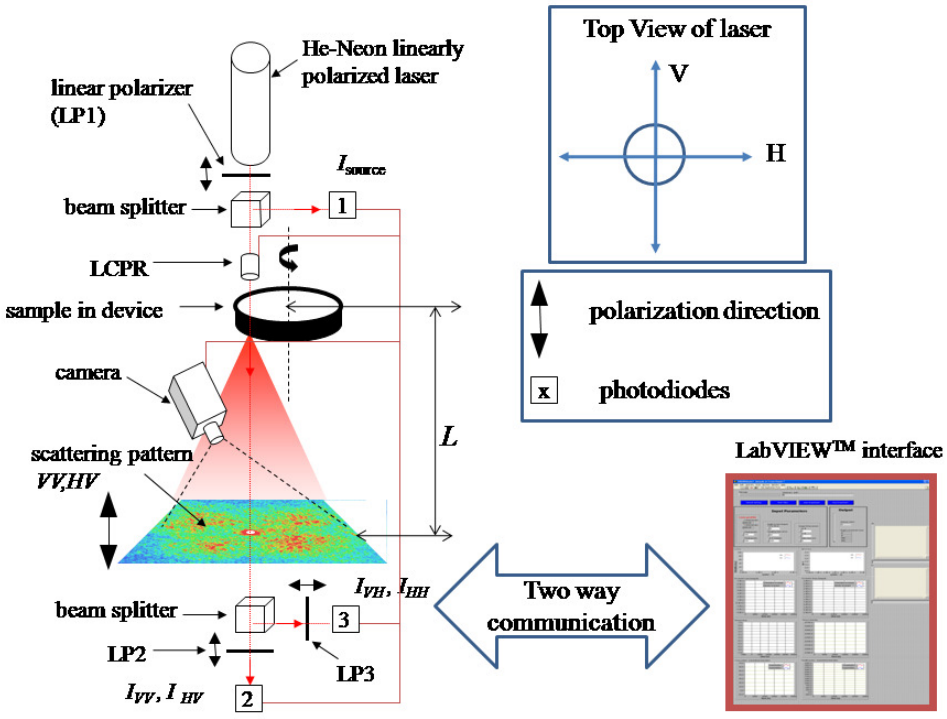

Figure 4.1 Schematic for the small angle light scattering device. Transmission measurements are performed along with scattering measurements. Double sided arrows represent the direction of polarization.

The experimental set-up is shown in Fig.4.1. Its components are:

- A 5 mW linearly polarized Helium-Neon (He-Ne) laser is held vertically on an optical bench that passes through a linear polarizer followed by a beam splitter. The polarization of the laser beam and the linear polarizer are inside-out and are termed as V (Vertical). The beam diameter is $\approx$1mm.
- About half of the beam is used to measure the source intensity in order to track the fluctuations in laser intensity and the other half is transmitted through the beam splitter for scattering and further transmission measurements.
- For control of the polarization direction, the beam passes through a liquid-crystal polarization rotator (LCPR) driven by a dedicated low-voltage controller. Depending on the

applied voltage across the LCPR, the incoming linearly polarized beam can be rotated by a fixed angle from 0 to 180 ^{o}.

- A sample holder is placed on the bench that can be moved vertically to change the scattering angle range and the distance between sample and screen (L).
- A polarization screen (analyzer) with an opaque background is placed below the sample holder to obtain the scattered image. The analyzer has the same polarization as the source i.e. V. The analyzing screen has a hole in the center to measure transmitted intensities.
- A CCD camera is placed at an angle above the polarization screen to capture the images. CCD camera is placed on a different optical bench in order to keep the optical alignment undisturbed from the camera adjustments.
- A beam splitter is placed below the analyzing screen and two photodiodes measure the transmitted intensities at orthogonal polarization directions simultaneously. The photodiode 2 and photodiode 3 have linear polarizers in front of them with V and H orientations, respectively.

4.4 Liquid Crystal Polarization Rotator (LCPR)

The LCPR device (meadowlark optics) is designed for an input wavelength of 632.8 nm. It combines a liquid crystal variable retarder with a zero-order polymer quarter wave retarder. It can rotate the polarization direction of the incoming monochromatic linearly polarized beam from 0 to 180^{o} depending on the applied voltage. The retarder material is a birefringent nematic liquid crystal polymer which is sandwiched between two optically flat fused silica windows coated with transparent indium tin oxide (ITO). The working principle of the device is explained in the schematic, Fig.4.2. The incoming

laser beam to the LCPR is linearly polarized with a polarization of V. The polarization direction of the output beam changes as different voltages are applied in the increments of 0.01 volts across the LCPR. The voltage increment and the range of applied voltage are controlled via a LabVIEW^{TM} written code. The changed state of polarization is detected using a photodiode with a linear polarizer (V) in front of it, Fig.4.2 (a). If the polarization direction of the output beam is same as input i.e. V, then the photodiode measures maximum intensity and provides us a voltage necessary for 0^{o} rotation of input beam. The intensity measured by the photodiode is minimum (close to zero) for a rotation of 90^{o}, Fig.4.2 (b). The schematic shown in Fig.4.2 (a) is a part of the whole light scattering train, Fig.4.1. The intensities measured by the photodiodes are normalized by the source intensity to correct of fluctuating laser intensity.

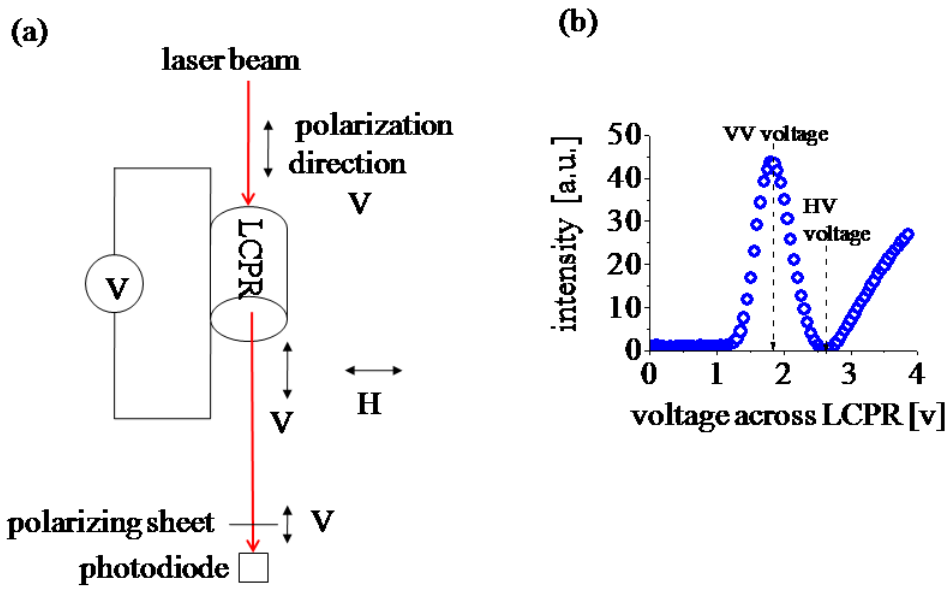

Figure 4.2 (a) Working principle of LCPR. A dedicated low voltage controller applies different voltages across the LCPR and the intensity of the output beam is measured using a photodiode. (b) A characteristic LCPR curve. Maximum and the minimum intensities correspond to the voltages for VV and HV scattering.

4.5 Nomenclature for Scattering Images and Transmission Intensities

The polarization direction for the analyzing screen and the source is chosen to be always V. When the leaving beam from LCPR has same polarization direction as the source and the analyzing screen i.e. V, we obtain a VV scattering pattern with transmission intensities being VV (photodiode 2) and VH (photodiode 3). When the leaving beam has a polarization direction of H, we get a HV scattering pattern with transmission intensities being HV (photodiode 2) and HH (photodiode 3).

4.6 Image Correction for CCD Camera Tilt

The analyzing screen for the SALS images is aligned normal to the incident beam while the detector, a charge-coupled device (CCD) camera, records these images at an angle to the analyzing screen, see Fig.4.1. The angular position of the CCD results in

perspective distortion of the captured images. An example of such distortion is shown in Fig.4.3 (a). For Calibration, a reference image with a regular pattern of equal size circular dots was placed on the screen and its image was taken using the CCD camera. The laser was switched off for this part of the experiment and a white light source was used to illuminate the pattern. The captured image, Fig 4.3(a), shows dots that are distorted from their true shape. The image was then corrected using a mathematical scheme in LabVIEW^{TM}, Fig.4.3 (b). The correction parameters were saved and used for following SALS experiments.

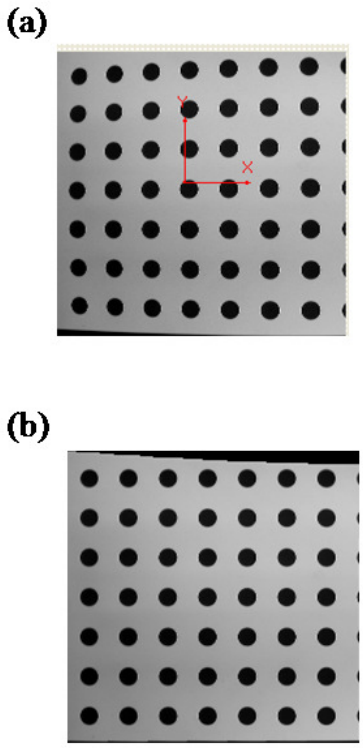

Figure 4.3 Image correction for CCD camera tilt: An image with equally spaced circular dots was printed on a piece of paper and was used as a template to correct for the image distortion from camera angle and distance (a) image captured from the CCD camera before correction shows distorted circular dots. The distortion is along the X-axis as well as the Y-axis. (b) Corrected image after applying the necessary mathematical scheme.

4.7 Scattering Wave Vector (q) Calculations

The momentum change upon elastic scattering is described by the wave vector, q, which is related to the length scales (d) that scatter light of wavelength, λ at scattering angle of θ, see Fig.4.4. The wave vector is given as $q = (4\pi / \lambda)\sin(\theta / 2) = 2\pi / d$. The Scattering angle depends on the camera length (L), the distance between sample and analyzing screen, and the distance of an image point from the center of the screen, x, as $\tan\theta = x / L$. The q- range can be altered by varying L or the size of the screen.

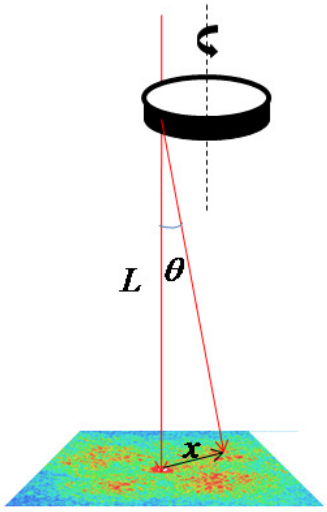

Figure 4.4 Scattering wave vector (q) calculation: Scattering angle from camera length L and distance of a point on the scattering image, x.

4.8 Software for Real Time Data Acquisition and Analysis

The input parameters to the SALS analysis software are the sample distance from the analyzing screen (L), angle of analyzing screen, Image size in pixels, HV and VV voltages to the LCPR, number of samples and sampling interval. The tilt angle for analyzing screen was zero for the experimental data presented in Figs.4.6, 4.7 and 4.8. Users can add multiple images for HV and VV patterns to improve the signal quality for

slowly varying structures. Software combines source intensity (photodiode1) and transmission intensities (photodiodes 2 and 3) measurements and calculates the light scattering invariants in real time. Line integrals (1-Dimentional) as well as areal integrals (2-Dimentional) are obtained by analyzing HV and VV patterns in real time according to eq.1. For the line integrals, user can control the initial and final pixel coordinates of a line during the experiments and can precisely center it with the acquired images. Intensity (I) Vs q and Iq^2 Vs q curves are also plotted in real time during the experiment.

4.9 Example: Crystallization of Isotactic Poly-1-Butene

4.9.1 Material and Sample Preparation

Isotactic poly-1-butene (iPB), from Basell, with M_w = 176000 g/mol and M_w/M_n of 5.7, served as test material. Pellets of iPB (as obtained from Basell) were compression molded into thick sheets, from which samples were cut for Differential Scanning Calorimetry (DSC) and optical measurements. The iPB was used without a nucleating agent.

Differential scanning calorimetry (DSC) was carried out under nitrogen in a DSC Q1000 (TA Instruments) using standard aluminum pans (from TA instruments) 6 mm in diameter and weighing about 24 mg. A thin sample (about 12 mg) was pressed into a DSC pan and heated above melting temperature to establish uniform contact between polymer and pan. For the DSC measurements, samples were heated as well as cooled at 10K/min. First melting, second melting, and crystallization peaks were observed at 120 ^oC (100-130 ^oC), 110 ^oC (100-120 ^oC), and 54 ^oC, respectively (Fig. 4.5). First melting belongs to the crystal FormI of iPB, which has a density of 950 Kg/m^3 and is a

thermodynamically stable form. Second melting belongs to FormII that is less dense (907 Kg/m^3) than FormI and is a kinetically favored crystal form. FormII transforms into FormI within 7-12 days at room temperature and atmospheric pressure [18-21].

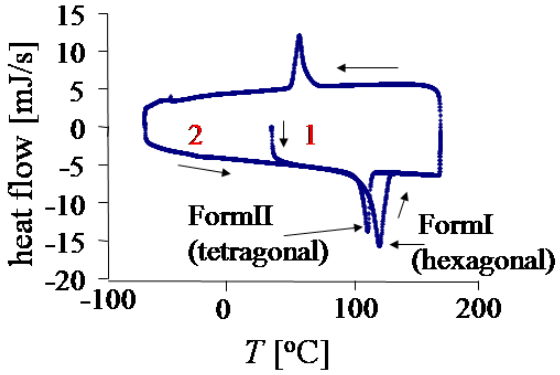

1 – first heating cycle

2 – second heating cycle

$T_{m\text{-}I}$=120.0 °C (100-130 °C)
$T_{m\text{-}II}$=110.7 °C (100-120 °C)
T_c=54.7 °C (70-50 °C) at 10 K/min

Figure 4.5 Differential scanning calorimetry for iPB for heating and cooling rates of 10 K/min. Two polymorphs of iPB, FormI and FormII, were observed during first and second heating, respectively.

4.9.2 Temperature and Shearing Protocol

For all experiments, samples were heated to 174 °C, kept there for about 15 minutes. Such a high temperature (about 50 K above melting) was used to erase the thermo-mechanical history and to melt all the crystallites present in the sample as recommended by Hadinata *et al.* [22]. Then the sample was cooled down to T_x, the temperature for isothermal crystallization. Time t = 0 was assigned to the instant at which the experimental temperature T_x was reached. Sample was sheared for a duration of t_s from t=0 and then crystallized isothermally without any further shearing. Cooling was performed fast enough to avoid any crystallization during cooling. The main purpose of

adopting Janeschitz-Kriegl protocol [23, 24] was to isolate shearing action from crystal growth. This way dynamics of flow was governed by the melt dynamics instead of suspension dynamics (solid crystal suspended in melt).

4.9.3 Quiescent Crystallization of iPB

The development of four-clover light scattering patterns (HV images), a characteristic of spherulitic morphology, is presented in Fig. 4.6. Crystallization was performed isothermally at 88.9 ^{o}C without any preshearing. The maximum scattering angle was 5.8 ^{o}, corresponding to a maximum q value of 1 μm^{-1} and the minimum length scale of 6.3 μm. Scattering images under parallel-polars are shown as well. Images are corrected for the excess scattering (due to melt and stage windows) as well as the fluctuations in source intensity. Light scattering invariants were calculated according to the areal integrals of eq. 1. The measured density fluctuation invariant goes through a maximum at about t = 250-400 s for six different measurements (Fig. 4.7). For a system consisting of anisotropic scatterers in an isotropic matrix with random orientation fluctuations, this maximum characterizes the instant when half of the sample volume is occupied by the scattering aggregates [16]. The normalized orientation fluctuation invariant ($Q_\delta(t)/Q_{\delta-\infty}$) grows with time and reaches a steady value within about 1600-2400 s. Due to growing inhomogeneities, the normalized parallel polar transmission intensity ($I_{HH}(t)/I_{HH-\infty}$) decreases and reaches a plateau in about 1600-1700 s. The HV pattern loses its four clover shape and becomes isotropic after this.

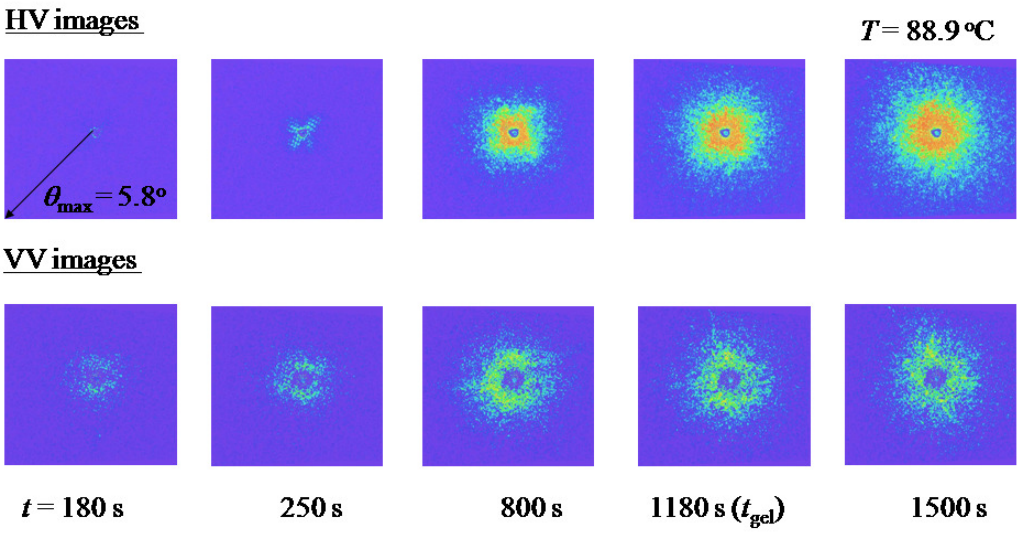

Figure 4.6 Small angle light scattering (SALS) images under cross-polars and parallel-polars for crystallizing isotactic poly-1-butene at 88.9 °C. Crystallization was performed without applying any flow.

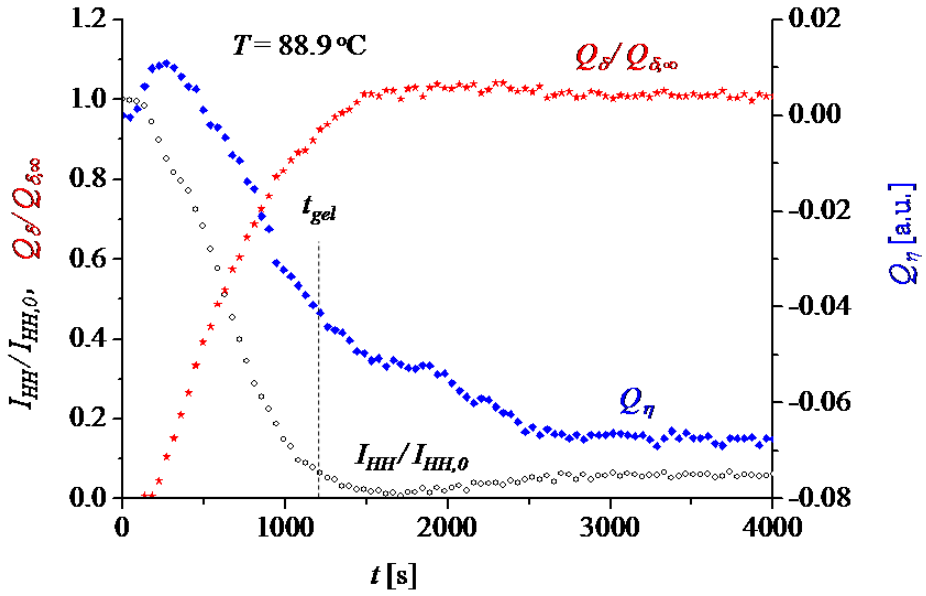

Figure 4.7 SALS and transmission measurements for crystallizing isotactic poly-1-butene at 88.9 °C. Invariants were obtained by analyzing the images in Fig.4.6.

4.9.4 Shear-induced Crystallization of iPB

Figure 4.8 shows a set of SALS images under cross-polars (HV) and parallel-polars (VV) modes for crystallization of iPB at 98.9 °C with $\dot{\gamma} = 7\ s^{-1}$ and strain units of

210. Sample reached to a temperature of 98.9 ^{o}C (T_x) at t=0 and was sheared for a duration of 30s. Shearing direction was at 45^{o} to both polarizer and analyzer, and is shown in Fig.4.8. Light scattering images just after shearing (t_s^+) showed a very little scattering. An anisotropic scattering pattern, perpendicular to the flow direction, was observed at 610 s under cross-polars. Scattering in the direction perpendicular to the flow corresponds to the development of oriented shish-like structure in the flow direction. VV image at this time also had anisotropic scattering perpendicular to the flow, though the development of shish-type structures was more clearly visible under HV mode of scattering. HV images showed the enhanced scattering in the flow directions at the later stages and a transformation from anisotropic scattering to isotropic scattering. Enhanced scattering in the flow direction is attributed to structure growth perpendicular to the flow and thus it was due to the lamellar kebab growth on the existing shish. Crystallization in the absence of flow would give rise to mix of lamellar kebab growth on existing shish structures with the spherulitic growth in the relaxed melt, which would lead to isotropic scattering.

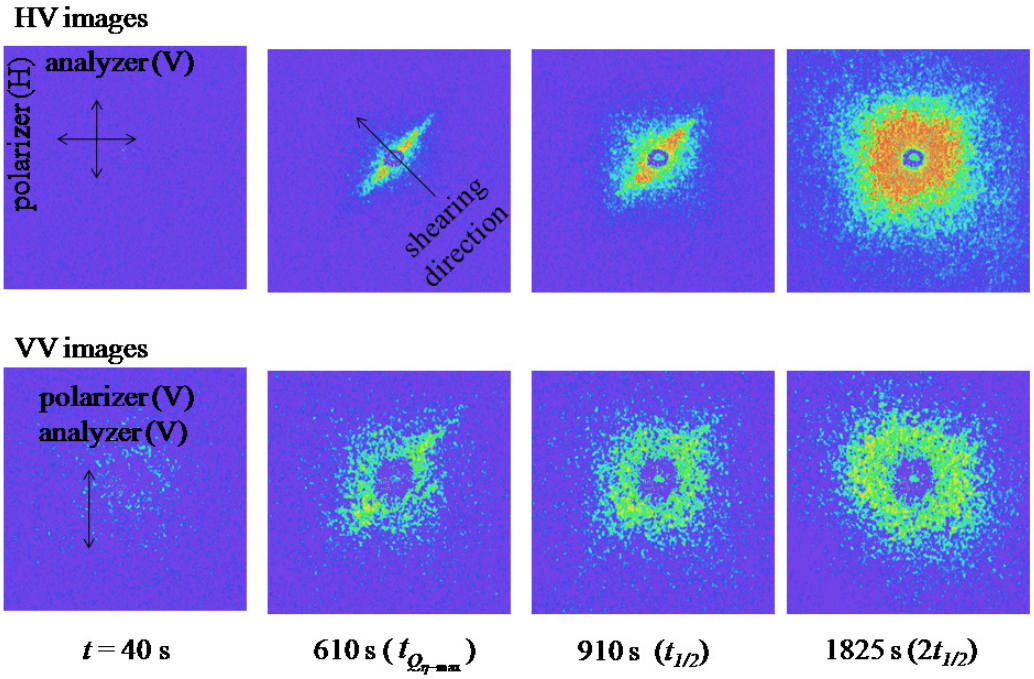

Figure 4.8 Cross-polar (HV) and parallel-polar (VV) images from SALS during crystallization of iPB at 98.9 °C after shearing with $\dot{\gamma} = 7\ s^{-1}$ for 30 s.

4.10 Linear Rheometer with an Inverted Light Scattering Set-up

The SALS apparatus described above has a vertical configuration with the laser source being at the top. The similar set-up has been combined with a house-built linear parallel plate rheometer and a customized optical microscope, Fig.4.7. A program is being developed in LabVIEW™ to synchronize rheometry with image acquisition in optical microscopy and SALS.

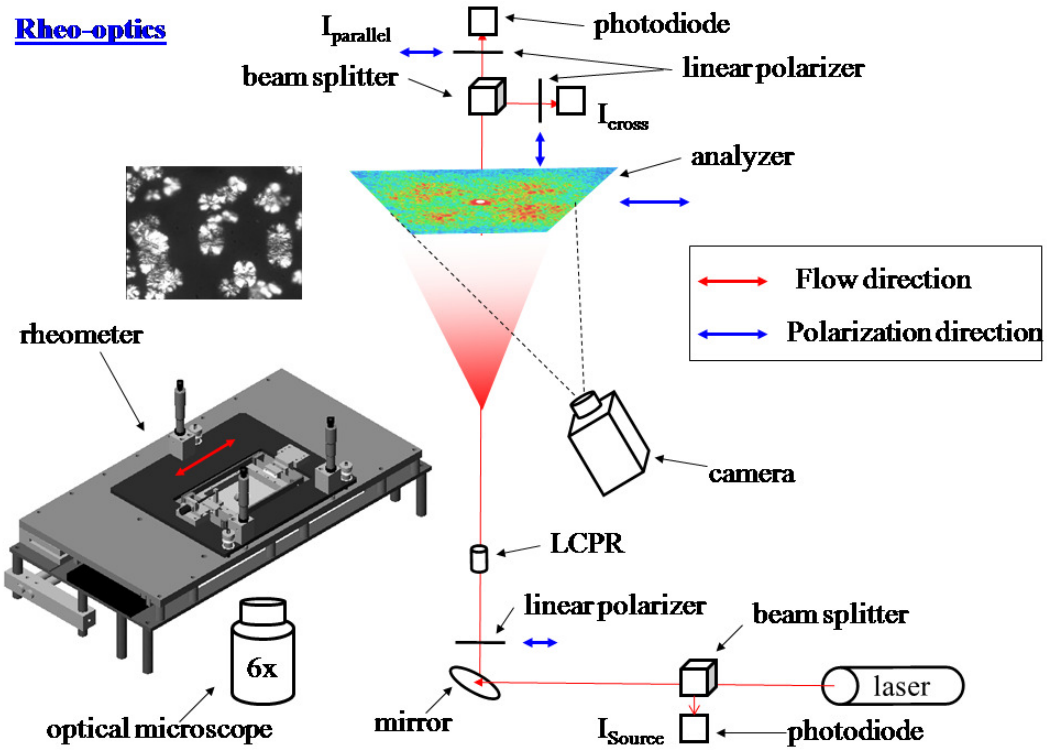

Figure 4.9 An inverted SALS set-up combined with a rheometer and an optical microscope to follow the evolution of mechanical and optical properties simultaneously along with the morphology from scattering and optical microscopy images.

4.11 Conclusions

The device at UMass Amherst was developed to investigate the crystallization of thermoplastic semicrystalline polymers though it can readily be extended to polymer blends, concentrated suspensions, micellar solutions, crude oil and to variety of other materials [1, 25-28]. A LabVIEW^{TM} based platform provides flexibility to add new modules to the existing code. The house-built small angle light scattering apparatus is able to perform following in real time:

- Transmission intensity measurements under cross and parallel polars
- Record scattering images under cross and parallel polars and their real time analysis to obtain light scattering invariants

- Source intensity measurements
- Controlling polarization direction using a liquid crystal based device for fast response time

As a novel addition a liquid crystal based device is incorporated as a superior substitute of quarter wave plate to control the polarization direction of a linearly polarized laser. The LCPR unit not only provides faster rotation of light but also is less bulky than the traditional quarter wave plate set-up which requires a motor to rotate the plate. The set-up is being combined with a rheometer and an optical microscope.

4.12 References

[1] Elmoumni A, Franck AJ, Helgeson ME, Reichert MD, McMullan JM, Wagner NJ: Simultaneous light scattering-rheology measurements for studying stress induced phase transitions, 15th International Congress on Rheology/80th Annual Meeting of the Society-of-Rheology (2008) 1147-1149.

[2] Lauger J, Gronski W: A melt rheometer with integrated small-angle light-scattering, Rheologica Acta 34 (1995) 70-79.

[3] Hou YY, Kassim HO: Instrument techniques for rheometry, Review of Scientific Instruments 76 (2005) 1-19.

[4] Acierno S, Palomba B, Winter HH, Grizzuti N: Effect of molecular weight on the flow-induced crystallization of isotactic poly(1-butene), Rheologica Acta 42 (2003) 243-250.

[5] Klein C, Venema P, Sagis L, van Dusschoten D, Wilhelm M, Spiess HW, van der Linden E, Rogers SS, Donald AM: Optimized rheo-optical measurements using fast fourier transform and oversampling, Applied Rheology 17 (2007)

[6] Wutz C, Bark M, Cronauer J, Dohrmann R, Zachmann HG: Simultaneous measurements of small-angle x-ray-scattering, wide-angle x-ray-scattering, and light-scattering during phase-transitions in polymers, Review of Scientific Instruments 66 (1995) 1303-1307.

[7] Wurm A, Minakov AA, Schick C: Combining x-ray scattering with dielectric and calorimetric experiments for monitoring polymer crystallization, European Polymer Journal 45 (2009) 3280-3289.

[8] Pogodina NV, Lavrenko VP, Srinivas S, Winter HH: Rheology and structure of isotactic polypropylene near the gel point: Quiescent and shear-induced crystallization, Polymer 42 (2001) 9031-9043.

[9] Pogodina NV, Siddiquee SK, van Egmond JW, Winter HH: Correlation of rheology and light scattering in isotactic polypropylene during early stages of crystallization, Macromolecules 32 (1999) 1167-1174.

[10] Arora D, Rothstein JP, Winter HH: Criteria for shear-induced crystallization: Strain and Weissenberg number (Unpublished work).

[11] Arora D, Winter HH: Network formation in a semicrystalline polymer at the early crystallization stages: From nucleation to percolation (Unpublished work).

[12] Stein RS, Rhodes MB: Photographic light scattering by polyethylene films, Journal of Applied Physics 31 (1960) 1873-1884.

[13] Stein RS, Wilson PR: Scattering of light by polymer films possessing correlated orientation fluctuations, Journal of Applied Physics 33 (1962) 1914-1922.
[14] Stein RS, Chu W: Scattering of light by disordered spherulites, Journal of Polymer Science Part A-2-Polymer Physics 8 (1970) 1137-1157.

[15] Stein RS, Hashimoto.T: Scattering of light from oriented polymer films .2, Journal of Polymer Science Part A-2-Polymer Physics 8 (1970) 1503-1519.

[16] Koberstein J, Russell TP, Stein RS: Total integrated light-scattering intensity from polymeric solids, Journal of Polymer Science Part B-Polymer Physics 17 (1979) 1719-1730.

[17] Elmoumni A, Gonzalez-Ruiz RA, Coughlin EB, Winter HH: Isotactic poly(propylene) crystallization: Role of small fractions of high or low molecular weight polymer, Macromolecular Chemistry and Physics 206 (2005) 125-134.

[18] Kalay G, Kalay CR: Structure and physical property relationships in processed polybutene-1, Journal of Applied Polymer Science 88 (2003) 814-824.

[19] Kaszonyiova M, Rybnikar K, Geil PH: Polymorphism of isotactic poly(butene-1), Journal of Macromolecular Science-Physics B44 (2005) 377-396.

[20] Azzurri F, Gomez MA, Alfonso GC, Ellis G, Marco C: Time-resolved saxs/waxs studies of the polymorphic transformation of 1-butene/ethylene copolymers, Conference on Synchrotron Radiation in Polymer Science II (2002) 177-189.

[21] Azzurri F, Flores A, Alfonso GC, Calleja FJB: Polymorphism of isotactic poly(1-butene) as revealed by microindentation hardness. 1. Kinetics of the transformation, Macromolecules 35 (2002) 9069-9073.
[22] Hadinata C, Gabriel C, Ruellman M, Laun HM: Comparison of shear-induced crystallization behavior of pb-1 samples with different molecular weight distribution, Journal of Rheology 49 (2005) 327-349.

[23] Janeschitz-Kriegel H: Crystallization modalities in polymer melt procesing, Fundmental Aspects of Structure Formation, Springer, NewYork (2010).

[24] Janeschitz-Kriegl H: Phases of flow-induced crystallization of i-pp: How remote pieces of the puzzle appear to fit, Macromolecules 39 (2006) 4448-4454.

[25] Vanegmond JW, Werner DE, Fuller GG: Time-dependent small-angle light-scattering of shear-induced concentration fluctuations in polymer-solutions, Journal of Chemical Physics 96 (1992) 7742-7757.

[26] Stein RS: Recent advances in rheo-optical studies of polymers in the solid-state, Polymer Journal 17 (1985) 289-305.

[27] Versmold H: Scattering from shear-ordered dispersions, Applied Rheology 17 (2007) 11412-11418.

[28] Glass JE, Schulz DN, Zukoski CF: Polymers as rheology modifiers - an overview, ACS Symposium Series 462 (1991) 2-17.

CHAPTER 5

FINAL COMMENTS AND FUTURE WORK

We have investigated the structure-property evolution in real-time during crystallization of a commercial semicrystalline thermoplastic polyolefin, isotactic poly-1-butene. The polymer was chosen due to its slow crystallization dynamics and the lower tendency for surface induced crystallization compared to polypropylene and polyethylene [1-3]. Variety of techniques including rheometry, small angle light scattering, transmission intensity measurements, differential scanning calorimetry and optical microscopy were implemented to follow the mechanical and optical properties along with the crystallinity and the morphology. Synchronization among various techniques was achieved by using the same probe for temperature calibration for different instruments. However different instruments have different degree of surface induced crystallization due to varying surfaces as well as variation in the overall applied temperature profiles. It would be valuable to combine these techniques into a single apparatus where when can perform optical microscopy, DSC, light scattering, transmission intensity measurements and rheology simultaneously. It will eliminate any concerns regarding the variation in crystallization conditions.

For quiescent crystallization, it will be useful to perform such experiments in a closed device with a blanket of heated nitrogen. An apparatus like this will be instrumental in extending such studies to variety of other semicrystalline polymers such as PET, PEO and PLA that are more sensitive to thermal degradation than iPB. A closed set up will have uniform temperature profile as well.

In Chapter 2, we have reported on the mechanism of network formation for crystallizing isotactic poly-1-butene and have performed detailed studies capturing evolution in mechanical and optical properties along with the crystallinity. Complex moduli from rheometry, orientation fluctuation invariants from light scattering and crystallinity from DSC grow in a sigmoidal fashion and can be described by Weibull functions with different exponents and characteristic times. It would be interesting to carry out such measurements for varying temperatures and establish a correlation among such exponents and time scales. Such correlations will help up predict one property from another and build predictive tools for structure-property relations.

In the same Chapter 2, an initiative is taken to model the process of sample volume filling by spherulites based on experimental information of kinetics of nucleation. A simple set of experiments and data analysis provide us with an analytical expression for the growing volume fraction of spherulites. The randomness of nucleation is not addressed adequately in the literature. Some of the earlier work was initiated by Stein and coworkers [4]. A set of experiments performed isothermally at different temperatures with above mentioned approach will give us wealth of information. Such experiments will also help us understand the effect of spherulite size distribution and grain boundaries on mechanical properties.

Flow effects on crystallization are reported in Chapter 3. Optical measurements are carried out in a quest to establish criteria that govern flow-induced crystallization. The shear rates chosen were too large to perform rheometry in the existing instruments. A set of experiments can be designed based on the current work to perform mechanical

measurements at small shear rates along with the optical measurements. It would be interesting to learn the flow effects on gelation and crystallization.

5.1 References

[1] Chatterjee AM, Price FP, Newman S: Heterogeneous nucleation of crystallization of high polymers from melt .1. Substrate-induced morphologies, Journal of Polymer Science Part B-Polymer Physics 13 (1975) 2369-2383.

[2] Chatterjee AM, Price FP, Newman S: Heterogeneous nucleation of crystallization of high polymers from melt .2. Aspects of transcrystallinity and nucleation density, Journal of Polymer Science Part B-Polymer Physics 13 (1975) 2385-2390.

[3] Chatterjee AM: Heterogeneous nucleation in the crystallization of high polymers from the melt, Polymer Science and Engineering Ph.D. (1974) 157.

[4] Misra A, Prudhomm.Re, Stein RS: Distribution of spherulites in a polyethylene sample, Journal of Polymer Science Part B-Polymer Physics 12 (1974) 1235-1238.

BIBLIOGRAPHY

Acierno S, Grizzuti N, Winter HH: Effects of molecular weight on the isothermal crystallization of poly(1-butene), Macromolecules 35 (2002) 5043-5048.

Acierno S, Palomba B, Winter HH, Grizzuti N: Effect of molecular weight on the flow-induced crystallization of isotactic poly(1-butene), Rheologica Acta 42 (2003) 243-250.

Akpalu Y, Kielhorn L, Hsiao BS, Stein RS, Russell TP, van Egmond J, Muthukumar M: Structure development during crystallization of homogeneous copolymers of ethene and 1-octene: Time-resolved synchrotron x-ray and sals measurements, Macromolecules 32 (1999) 765-770.

Arora D, Rothstein JP, Winter HH: Criteria for shear-induced crystallization: Strain and Weissenberg number (Unpublished work).

Arora D, Winter HH: Network formation in a semicrystalline polymer at the early crystallization stages: From nucleation to percolation (Unpublished work).

Arora D, Winter HH: Network formation in a semicrystalline polymer at the early crystallization stages: From nucleation to percolation (Unpublished work).

Azzurri F, Flores A, Alfonso GC, Calleja FJB: Polymorphism of isotactic poly(1-butene) as revealed by microindentation hardness. 1. Kinetics of the transformation, Macromolecules 35 (2002) 9069-9073.

Azzurri F, Gomez MA, Alfonso GC, Ellis G, Marco C: Time-resolved saxs/waxs studies of the polymorphic transformation of 1-butene/ethylene copolymers, Conference on Synchrotron Radiation in Polymer Science II (2002) 177-189.

Baumgaertel M, Derosa ME, Machado J, Masse M, Winter HH: The relaxation-time spectrum of nearly monodisperse polybutadiene melts, Rheologica Acta 31 (1992) 75-82.
Bonn D, Coussot P, Huynh HT, Bertrand F, Debregeas G: Rheology of soft glassy materials, Europhysics Letters 59 (2002) 786-792.

Booij HC, Leblans P, Palmen J, Tiemersmathoone G: Non-linear viscoelasticity and the cox-merz relations for polymeric fluids, Journal of Polymer Science Part B-Polymer Physics 21 (1983) 1703-1711.

Chai CK, Auzoux Q, Randrianatoandro H, Navard P, Haudin JM: Influence of pre-shearing on the crystallisation of conventional and metallocene polyethylenes, Polymer 44 (2003) 773-782.

Chen Q, Fan YR, Li WC, Zheng Q: Rheological properties of liquid-solid transition in isothermal crystallization for high-density polyethylene, Chemical Journal of Chinese Universities-Chinese 27 (2006) 365-368.

Coppola S, Grizzuti N, Maffettone PL: Microrheological modeling of flow-induced crystallization, Macromolecules 34 (2001) 5030-5036.

Doi M, Edwards SF: The theory of polymer dynamics, (1994).

Dukovski I, Muthukumar M: Langevin dynamics simulations of early stage shish-kebab crystallization of polymers in extensional flow, Journal of Chemical Physics 118 (2003) 6648-6655.

Elmoumni A, Franck AJ, Helgeson ME, Reichert MD, McMullan JM, Wagner NJ: Simultaneous light scattering-rheology measurements for studying stress induced phase transitions, 15th International Congress on Rheology/80th Annual Meeting of the Society-of-Rheology (2008) 1147-1149.

Elmoumni A, Fruitwala H, Winter HH: Correlation of material and processing time scales with structure development in isotactic polypropylene crystallization, 225th National Meeting of the American-Chemical-Society (2003) 6-7.

Elmoumni A, Gonzalez-Ruiz RA, Coughlin EB, Winter HH: Isotactic poly(propylene) crystallization: Role of small fractions of high or low molecular weight polymer, Macromolecular Chemistry and Physics 206 (2005) 125-134.

Elmoumni A, Winter HH: Large strain requirements for shear-induced crystallization of isotactic polypropylene, Rheologica Acta 45 (2006) 793-801.

Filippone G, Netti PA, Acierno D: Microstructural evolutions of ldpe/pa6 blends by rheological and rheo-optical analyses: Influence of flow and compatibilizer on break-up and coalescence processes, Polymer 48 (2007) 564-573.

Gedde UW: Crystalline polymers, Polymer physics, London (1995).

Gedde UW: Crystallization kinetics, Polymer physics, London (1995).

Gelfer M, Horst RH, Winter HH, Heintz AM, Hsu SL: Physical gelation of crystallizing metallocene and ziegler-natta ethylene-hexene copolymers, Polymer 44 (2003) 2363-2371.

Glass JE, Schulz DN, Zukoski CF: Polymers as rheology modifiers - an overview, ACS Symposium Series 462 (1991) 2-17.

Hadinata C, Gabriel C, Ruellman M, Laun HM: Comparison of shear-induced crystallization behavior of pb-1 samples with different molecular weight distribution, Journal of Rheology 49 (2005) 327-349.

Hadinata C, Gabriel C, Ruellman M, Laun HM: Comparison of shear-induced crystallization behavior of pb-1 samples with different molecular weight distribution, Journal of Rheology 49 (2005) 327-349.

Hadinata C, Gabriel C, Ruellman M, Laun HM: Comparison of shear-induced crystallization behavior of pb-1 samples with different molecular weight distribution, Journal of Rheology 49 (2005) 327-349.

Heeley EL, Maidens AV, Olmsted PD, Bras W, Dolbnya IP, Fairclough JPA, Terrill NJ, Ryan AJ: Early stages of crystallization in isotactic polypropylene, Macromolecules 36 (2003) 3656-3665.

Hikosaka M, Amano K, Rastogi S, Keller A: Lamellar thickening growth of an extended chain single crystal of polyethylene .1. Pointers to a new crystallization mechanism of polymers, Macromolecules 30 (1997) 2067-2074.

Hobbs JK, Humphris ADL, Miles MJ: In-situ atomic force microscopy of polyethylene crystallization. 1. Crystallization from an oriented backbone, Macromolecules 34 (2001) 5508-5519.

Hobbs JK, Miles MJ: Direct observation of polyethylene shish-kebab crystallization using in-situ atomic force microscopy, Macromolecules 34 (2001) 353-355.

Hoffman JD, Frolen LJ, Ross GS, Lauritzen JI: Growth-rate of spherulites and axialites from melt in polyethylene fractions - regime-1 and regime-2 crystallization, Journal of Research of the National Bureau of Standards Section a-Physics and Chemistry 79 (1975) 671-699.

Hoffman JD, Lauritzen JI: Crystallization of bulk polymers with chain folding - theory of growth of lamellar spherulites, Journal of Research of the National Bureau of Standards A 65 (1961) 297-336.

Hoffman JD, Miller RL: Kinetics of crystallization from the melt and chain folding in polyethylene fractions revisited: Theory and experiment, Polymer 38 (1997) 3151-3212.

Horst RH, Winter HH: Stable critical gels of a copolymer of ethene and 1-butene achieved by partial melting and recrystallization, Macromolecules 33 (2000) 7538-7543.

Hou YY, Kassim HO: Instrument techniques for rheometry, Review of Scientific Instruments 76 (2005) 1-19.

Hsiao BS, Yang L, Somani RH, Avila-Orta CA, Zhu L: Unexpected shish-kebab structure in a sheared polyethylene melt, Physical Review Letters 94 (2005) 1-4.

Huo H, Meng YF, Li HF, Jiang SC, An LJ: Influence of shear on polypropylene crystallization kinetics, European Physical Journal E 15 (2004) 167-175.

Ishikiriyama K, Boller A, Wunderlich B: Melting of indium by temperature-modulated differential scanning calorimetry, Journal of Thermal Analysis 50 (1997) 547-558.

Janeschitz-Kriegel H: Crystallization modalities in polymer melt procesing, Fundmental Aspects of Structure Formation, Springer, NewYork (2010).

Janeschitz-Kriegel H: Crystallization modalities in polymer melt procesing, Fundmental Aspects of Structure Formation, Springer, NewYork (2010).

Janeschitz-Kriegl H, Eder G, Stadlbauer M, Ratajski E: A thermodynamic frame for the kinetics of polymer crystallization under processing conditions, Monatshefte fur Chemie 136 (2005) 1119-1137.

Janeschitz-Kriegl H, Ratajski E, Stadlbauer M: Flow as an effective promotor of nucleation in polymer melts: A quantitative evaluation, Rheologica Acta 42 (2003) 355-364.

Janeschitz-Kriegl H, Ratajski E, Wippel H: The physics of athermal nuclei in polymer crystallization, Colloid and Polymer Science 277 (1999) 217-226.

Janeschitz-Kriegl H: How to understand nucleation in crystallizing polymer melts under real processing conditions, Colloid and Polymer Science 281 (2003) 1157-1171.

Janeschitz-Kriegl H: Phases of flow-induced crystallization of i-pp: How remote pieces of the puzzle appear to fit, Macromolecules 39 (2006) 4448-4454.

Kalay G, Kalay CR: Structure and physical property relationships in processed polybutene-1, Journal of Applied Polymer Science 88 (2003) 814-824.

Kaszonyiova M, Rybnikar K, Geil PH: Polymorphism of isotactic poly(butene-1), Journal of Macromolecular Science-Physics B44 (2005) 377-396.

Keller A, Kolnaar HW: Flow induced orientation and structure formation, Processing of polymers, New York (1997).

Keller A: Polymer crystals, Reports on Progress in Physics 31 (1968) 623-704.

Keller A: Reminiscences on the discovery of chain folded single crystals, Polymer 41 (2000) 8751-8754.

Kimata S, Sakurai T, Nozue Y, Kasahara T, Yamaguchi N, Karino T, Shibayama M, Kornfield JA: Molecular basis of the shish-kebab morphology in polymer crystallization, Science 316 (2007) 1014-1017.

Klein C, Venema P, Sagis L, van Dusschoten D, Wilhelm M, Spiess HW, van der Linden E, Rogers SS, Donald AM: Optimized rheo-optical measurements using fast fourier transform and oversampling, Applied Rheology 17 (2007)

Koberstein J, Russell TP, Stein RS: Total integrated light-scattering intensity from polymeric solids, Journal of Polymer Science Part B-Polymer Physics 17 (1979) 1719-1730.

Kolb R, Wutz C, Stribeck N, von Krosigk G, Riekel C: Investigation of secondary crystallization of polymers by means of microbeam x-ray scattering, Polymer 42 (2001) 5257-5266.

Kornfield JA, Kumaraswamy G, Issaian AM: Recent advances in understanding flow effects on polymer crystallization, Industrial & Engineering Chemistry Research 41 (2002) 6383-6392.

Kumaraswamy G: Crystallization of polymers from stressed melts, Journal of Macromolecular Science-Polymer Reviews C45 (2005) 375-397.

Lauger J, Gronski W: A melt rheometer with integrated small-angle light-scattering, Rheologica Acta 34 (1995) 70-79.

Lauritzen JI, Hoffman JD: Theory of formation of polymer crystals with folded chains in dilute solution, Journal of Research of the National Bureau of Standards Section a-Physics and Chemistry 64 (1960) 73-102.

Lazcano S, Fatou JG, Marco C, Bello A: Crystallization regimes in poly(3,3-dimethylthietane) fractions, Polymer 29 (1988) 2076-2080.

Lima MD, Andrade MJ, Skakalova V, Bergmann CP, Roth S: Dynamic percolation of carbon nanotubes in liquid medium, Journal of Materials Chemistry 17 (2007) 4846-4853.

Lin YG, Mallin DT, Chien JCW, Winter HH: Dynamic mechanical measurement of crystallization-induced gelation in thermoplastic elastomeric poly(propylene), Macromolecules 24 (1991) 850-854.

Manzione L, Jameel H, Wilkes GL: Small-angle light-scattering from shish-kebab structures, Journal of Polymer Science Part C-Polymer Letters 16 (1978) 237-243.

McKinley GH, Sridhar T: Filament-stretching rheometry of complex fluids, Annual Review of Fluid Mechanics 34 (2002) 375-415.

McLeish TCB, Allgaier J, Bick DK, Bishko G, Biswas P, Blackwell R, Blottiere B, Clarke N, Gibbs B, Groves DJ, Hakiki A, Heenan RK, Johnson JM, Kant R, Read DJ, Young RN: Dynamics of entangled h-polymers: Theory, rheology, and neutron-scattering, Macromolecules 32 (1999) 6734-6758.

Milner ST, McLeish TCB: Reptation and contour-length fluctuations in melts of linear polymers, Physical Review Letters 81 (1998) 725-728.

Misra A, Prudhomm.Re, Stein RS: Distribution of spherulites in a polyethylene sample, Journal of Polymer Science Part B-Polymer Physics 12 (1974) 1235-1238.

Mours M, Winter HH: Relaxation patterns of nearly critical gels, Macromolecules 29 (1996) 7221-7229.

Mours M, Winter HH: Time-resolved rheometry, Rheologica Acta 33 (1994) 385-397.

Muthukumar M: Commentary on theories of polymer crystallization, European Physical Journal E 3 (2000) 199-202.

Nishida K, Kaji K, Kanaya T, Matsuba G, Konishi T: Spinodal patterns indicating unstable regime of polymer crystallization, Journal of Polymer Science Part B-Polymer Physics 42 (2004) 1817-1822.

Olmsted PD, Poon WCK, McLeish TCB, Terrill NJ, Ryan AJ: Spinodal-assisted crystallization in polymer melts, Physical Review Letters 81 (1998) 373-376.

Organ SJ, Keller A: Fast growth-rates of polyethylene single-crystals grown at high-temperatures and their relevance to crystallization theories, Journal of Polymer Science Part B-Polymer Physics 24 (1986) 2319-2335.

Panine P, Di Cola E, Sztucki M, Narayanan T: Early stages of polymer melt crystallization, Polymer 49 (2008) 676-680.

Patki RP, Phillips PJ: Crystallization kinetics of linear polyethylene: The maximum in crystal growth rate-temperature dependence, European Polymer Journal 44 (2008) 534-541.

Pennings AJ, Kiel AM: Fractionation of polymers by crystallization from solution .3. On morphology of fibrillar polyethylene crystals grown in solution, Kolloid-Zeitschrift and Zeitschrift Fur Polymere 205 (1965) 160-173.

Peters GWM, Swartjes FHM, Meijer HEH: A recoverable strain-based model for flow-induced crystallization, Macromolecular Symposia 185 (2002) 277-292.

Phillips PJ, Tseng HT: Influence of pressure on crystallization in poly(ethylene-terephthalate), Macromolecules 22 (1989) 1649-1655.

Phillips PJ, Vatansever N: Regime transitions in fractions of cis-polyisoprene, Macromolecules 20 (1987) 2138-2146.

Phillips PJ: Polymer crystals, Reports on Progress in Physics 53 (1990) 549-604.

Pogodina NV, Lavrenko VP, Srinivas S, Winter HH: Rheology and structure of isotactic polypropylene near the gel point: Quiescent and shear-induced crystallization, Polymer 42 (2001) 9031-9043.

Pogodina NV, Siddiquee SK, van Egmond JW, Winter HH: Correlation of rheology and light scattering in isotactic polypropylene during early stages of crystallization, Macromolecules 32 (1999) 1167-1174.

Pogodina NV, Winter HH: Polypropylene crystallization as a physical gelation process, Macromolecules 31 (1998) 8164-8172.

Raimo M: "Kinematic" Analysis of growth and coalescence of spherulites for predictions on spherulitic morphology and on the crystallization mechanism, Progress in Polymer Science 32 (2007) 597-622.

Rothstein JP, McKinley GH: A comparison of the stress and birefringence growth of dilute, semi-dilute and concentrated polymer solutions in uniaxial extensional flows, Journal of Non-Newtonian Fluid Mechanics 108 (2002) 275-290.

Sadler DM, Gilmer GH: A model for chain folding in polymer crystals - rough growth faces are consistent with the observed growth-rates, Polymer 25 (1984) 1446-1452.

Sadler DM, Gilmer GH: Rate-theory model of polymer crystallization, Physical Review Letters 56 (1986) 2708-2711.

Sadler DM, Gilmer GH: Selection of lamellar thickness in polymer crystal-growth - a rate-theory model, Physical Review B 38 (1988) 5684-5693.

Sadler DM, Keller A: Neutron-scattering studies on molecular trajectory in polyethylene crystallized from solution and melt, Macromolecules 10 (1977) 1128-1140.

Sadler DM, Spells SJ: A neutron-scattering study of slowly crystallized bulk polyethylene, Polymer 25 (1984) 1219-1226.

Sadler DM: New explanation for chain folding in polymers, Nature 326 (1987) 174-177.

Schwittay C, Mours M, Winter HH: Rheological expression of physical gelation in polymers, General Discussion on Gels (1995) 93-104.

Shangguan YG, Song YH, Zheng Q: A query on crystallization temperature-dependent cooling function under nonisothermal condition, Journal of Polymer Science Part B-Polymer Physics 44 (2006) 795-800.

Soccio M, Nogales A, Lotti N, Munari A, Ezquerra TA: Evidence of early stage precursors of polymer crystals by dielectric spectroscopy, Physical Review Letters 98 (2007) 1-4.

Somani RH, Yang L, Sics I, Hsiao BS, Pogodina NV, Winter HH, Agarwal P, Fruitwala H, Tsou A: Orientation-induced crystallization in isotactic polypropylene melt by shear deformation, Macromolecular Symposia 185 (2002) 105-117.

Stein RS, Chu W: Scattering of light by disordered spherulites, Journal of Polymer Science Part A-2-Polymer Physics 8 (1970) 1137-1157.

Stein RS, Hashimoto.T: Scattering of light from oriented polymer films .2, Journal of Polymer Science Part A-2-Polymer Physics 8 (1970) 1503-1519.

Stein RS, Rhodes MB: Photographic light scattering by polyethylene films, Journal of Applied Physics 31 (1960) 1873-1884.

Stein RS, Wilson PR: Scattering of light by polymer films possessing correlated orientation fluctuations, Journal of Applied Physics 33 (1962) 1914-1922.

Stein RS: Recent advances in rheo-optical studies of polymers in the solid-state, Polymer Journal 17 (1985) 289-305.

Stein RS: Recent advances in rheo-optical studies of polymers in the solid-state, Polymer Journal 17 (1985) 289-305.

Strobl GR: Metastable partially crystalline states, The physics of polymers, Berlin (1997).

Surve M, Pryamitsyn V, Ganesan V: Polymer-bridged gels of nanoparticles in solutions of adsorbing polymers, Journal of Chemical Physics 125 (2006) 1-12.

Turnbull D, Fisher JC: Rate of nucleation in condensed systems, Journal of Chemical Physics 17 (1949) 71-73.

van Meerveld J, Peters GWM, Hutter M: Towards a rheological classification of flow induced crystallization experiments of polymer melts, Rheologica Acta 44 (2004) 119-134.

Vanegmond JW, Werner DE, Fuller GG: Time-dependent small-angle light-scattering of shear-induced concentration fluctuations in polymer-solutions, Journal of Chemical Physics 96 (1992) 7742-7757.

Versmold H: Scattering from shear-ordered dispersions, Applied Rheology 17 (2007) 11412-11418.

Wagner MH, Yamaguchi M, Takahashi M: Quantitative assessment of strain hardening of low-density polyethylene melts by the molecular stress function model, Journal of Rheology 47 (2003) 779-793.

Wang ZG, Hsiao BS, Sirota EB, Agarwal P, Srinivas S: Probing the early stages of melt crystallization in polypropylene by simultaneous small- and wide-angle x-ray scattering and laser light scattering, Macromolecules 33 (2000) 978-989.

Wilkins GMH, Spicer PT, Solomon MJ: Colloidal system to explore structural and dynamical transitions in rod networks, gels, and glasses, Langmuir 25 (2009) 8951-8959.

Winter HH, Mours M: Rheology of polymers near liquid-solid transitions, Neutron spin echo spectroscopy viscoelasticity rheology, Berlin (1997).

Winter HH: Polymer gels, materials that combine liquid and solid properties, MRS Bulletin 16 (1991) 44-47.

Winter HH: Sharing the world's advanced rheology knowledge through rheo-hub, 15th International Congress on Rheology/80th Annual Meeting of the Society-of-Rheology (2008) 1387-1389.

Wurm A, Minakov AA, Schick C: Combining x-ray scattering with dielectric and calorimetric experiments for monitoring polymer crystallization, European Polymer Journal 45 (2009) 3280-3289.

Wurm A, Soliman R, Schick C: Early stages of polymer crystallization - a dielectric study, Polymer 44 (2003) 7467-7476.

Wutz C, Bark M, Cronauer J, Dohrmann R, Zachmann HG: Simultaneous measurements of small-angle x-ray-scattering, wide-angle x-ray-scattering, and light-scattering during phase-transitions in polymers, Review of Scientific Instruments 66 (1995) 1303-1307.

Xu XM, Tao XL, Gao CH, Zheng Q: Studies on the steady and dynamic rheological properties of poly(dimethyl-siloxane) filled with calcium carbonate based on superposition of its relative functions, Journal of Applied Polymer Science 107 (2008) 1590-1597.

Yang L, Somani RH, Sics I, Hsiao BS, Kolb R, Lohse D: The role of high molecular weight chains in flow-induced crystallization precursor structures, Journal of Physics-Condensed Matter 18 (2006) 2421-2436.

Yasuda K, Armstrong RC, Cohen RE: Shear-flow properties of concentrated-solutions of linear and star branched polystyrenes, Rheologica Acta 20 (1981) 163-178.

Zhang CG, Hu HQ, Wang XH, Yao YH, Dong X, Wang DJ, Wang ZG, Han CC: Formation of cylindrite structures in shear-induced crystallization of isotactic polypropylene at low shear rate, Polymer 48 (2007) 1105-1115.